

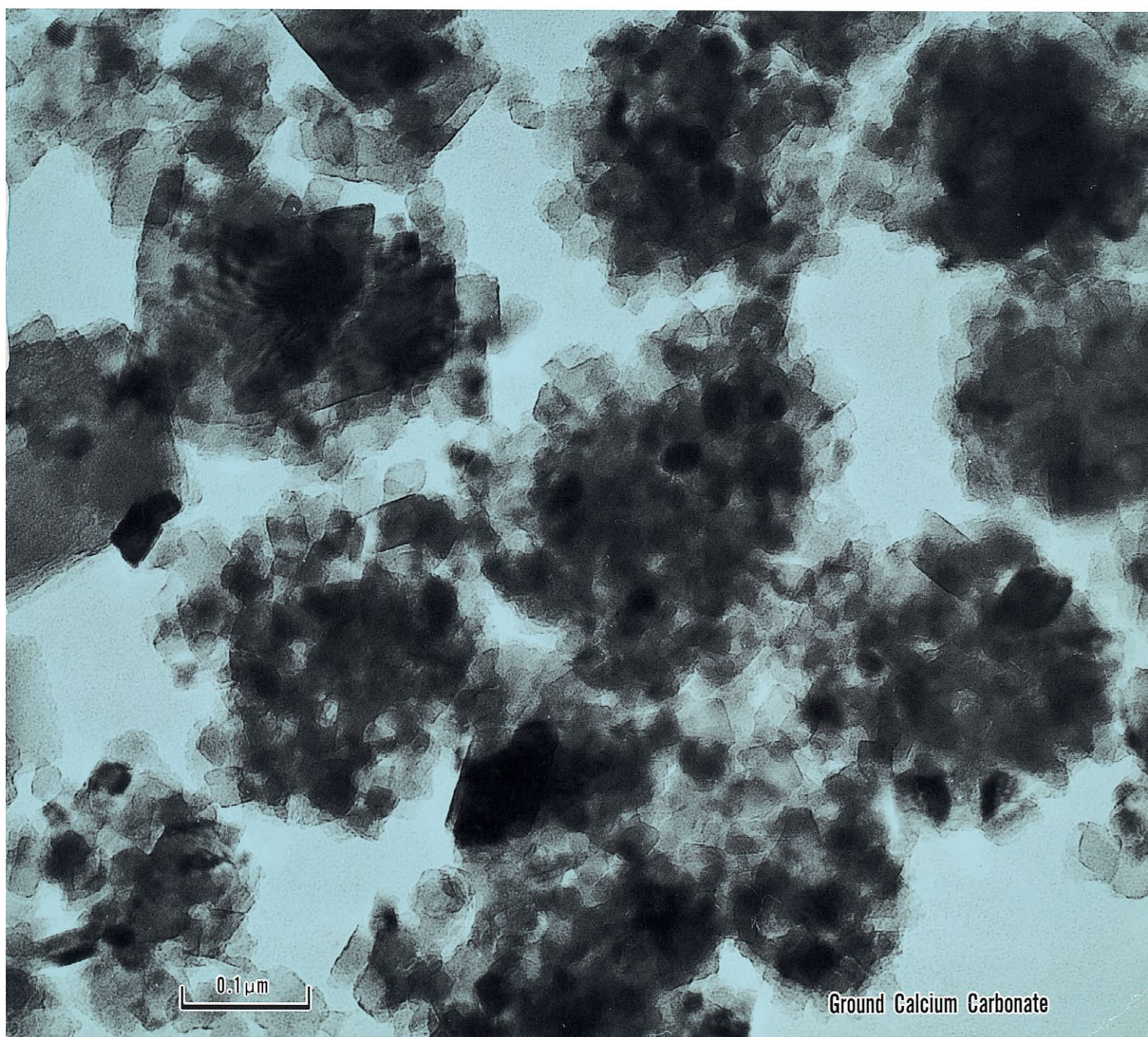
粉

KONA

**POWDER SCIENCE AND
TECHNOLOGY IN JAPAN**

No. 1 (1983)

Published by The Party of Powder Technology (JAPAN)



Ground Calcium Carbonate

Explanation of the Cover

“粉”; This Chinese character is pronounced as “KONA” in Japanese and means “Powder”

“粉” on the front page was written by the late Mr. Eiichi Hosokawa, founder of Hosokawa Micron Corporation.

See page 53 for description of the cover photograph.

Editorial Board

Naoya Yoshioka	(Kyoto University) Editor in Chief.
Masuo Hosokawa	(Hosokawa Micron Corp.)
Koichi Inoya	(Aichi Institute of Technology)
Genji Jimbo	(Nagoya University)
Takeshi Kano	(Shizuoka University)
Yasuo Kousaka	(University of Osaka Prefecture)
Kei Miyanami	(University of Osaka Prefecture)
Takeo Yano	(Yano Technical Institute)
Tetsuo Yoshida	(Chubu Institute of Technology)
Tohei Yokoyama	(Hosokawa Micromeritics Laboratory)

Editorial Assistants

Shigesumi Kobayashi	(Hosokawa International Inc.)
Toyokazu Yokoyama	(Hosokawa Micromeritics Laboratory)
Kenji Fujii	(Hosokawa Micromeritics Laboratory)
Tomoyuki Yamaguchi	(Hosokawa Micromeritics Laboratory)

Publication Office

The Party of Powder Technology (Japan)
c/o Hosokawa Micromeritics Laboratory
9, Shodai-tajika 1-chome, Hirakata, Osaka, 573 JAPAN
(Complimentary Copy)

Copyright © 1983, The Party of Powder Technology (Japan)
Printed by Naniwa Printing Co., Ltd. in Osaka, Japan

Contents

Message from the Editor	<i>Naoya Yoshioka</i>	2
Theoretical Approach to Dust Explosion	<i>Tatsuo Tanaka</i>	4
Bulk Density Measurement by a New Tapping System	<i>Akira Suganuma, Takashi Sugawara and Ryuichi Aoki</i>	14
Some Problems in Size Measurement of Submicron Particles	<i>Yasuo Kousaka</i>	19
Direct Shear Test of Powder Beds	<i>Kei Miyanami, Keiji Terashita and Takeo Yano</i>	28
The Development and Evaluation of New Measuring Methods of the Adhesion Force of Single Particles	<i>Genji Jimbo and Ryohei Yamazaki</i>	40
Criteria of Activation of Powdery Materials by a Preliminary Mechanical Treatment	<i>Mamoru Senna</i>	48
Ultra-Fine Grinding and Consequent Changes of Powder Characteristics	<i>Tohei Yokoyama, Kiyoshi Urayama and Toyokazu Yokoyama</i>	53
Musical Sand	<i>Shigeo Miwa, Jusuke Hidaka and Atsuko Shimosaka</i>	64
< Review >		
Some Technical Views of Recent Drying Processes in Japan	<i>Tetsuo Yoshida</i>	73
Survey of Recent Advances in Research on Powder Mixing in Japan	<i>Munetake Satoh and Keiji Terashita</i>	82
Recent Status of Bulk-Solids Transportation in Japan	<i>Takeshi Kano</i>	90
Informational Articles		97

Message from the Editor



It is a great pleasure and honour for us, the members of the Party of Powder Technology (Japan), to declare our new annual publication of "KONA" and to present its first issue to you.

"KONA" is the Japanese word that means "powder". Our publication of "KONA" is aimed, as its sub-title indicates, to introduce annually Powder Science and Technology in Japan to the interested parties in the world.

Powder is a very universal form of existence of substances and materials. It is seen in each part of the natural and industrial worlds. Thus the knowledge on the properties and behaviours of powders is of fundamental importance for understanding of the natural phenomena as well as for the industrial progress. Further, there are great many people in widely spread fields, who have interest in powders, who handle powders day to day, and who try to solve the problem relating to powders.

In recent years, the world-wide institutions or societies have been organized by those people under the banner of Powder Technology and Powder Science. Special periodicals are now being published. Also the abstracts of powder-related reports are often introduced in the various information papers. In Japan, too, research and development have been actively and earnestly carried out, and their fruits are being distributed through the world as the high-technology products. However, the information written in Japanese seldom catch the eyes of foreigners due to the language barrier.

We will publish "KONA" with the aim to introduce in the English language and free of fee, the latest research on powders and technological development made in Japan, in a manner as original as possible, although we shall be restricted for the time being to annual publication with 60-80 pages and 500 copies of circulation.

Launching of the Japanese industry is being welcomed in some places of the world, and is causing serious problems in other parts. In the case of our "KONA", however, it will produce no friction on the part of its "receiver", but there exist certain problems on the side of "supplier". One is the financial problem and the other is the selection of the theses for introduction in the limited pages from a great many research results. Also we have to work out to whom we should present the limited number of copies.

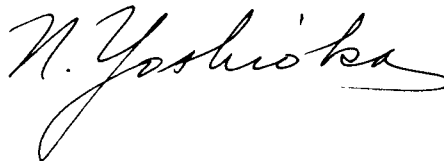
The Chinese character appearing on the cover page of "KONA" means powder, and it is a reproduction of the original writing by the late Mr. Eiichi Hosokawa. He was the founder and the former president of Hosokawa Micron Corporation, who will sponsor our publication. Mr. E. Hosokawa was the inventor of the prototype of the

Micron Mill which has been well known among the industries as a high-efficiency size reduction equipment. In 1957 he established a separate organization of Hosokawa Micromeritics Laboratory, and at the time of its opening Mr. E. Hosokawa stated that the Laboratory was founded not for the sake of seeking the direct profit but for the purpose of contribution to the technological societies through research and development of powder technology and powder science. The spirit was taken over by Mr. Masuo Hosokawa, president of the Company and it has been decided that "KONA" would be published as a part of the activities of Hosokawa Micromeritics Laboratory. Thus the first financial problem has been solved.

"KONA" is edited by us, the members of the Party of Powder Technology. We are the group of academic society who desire to extend cooperation for the advance of powder technology. Amongst us are the distinguished authorities in the field of powder technology in Japan. We will take responsibility for proper selection of the theses to be introduced and for determination of the circulation recipients. We will carry out these tasks with best for solution of the above-mentioned second problem.

No. 1 of "KONA" is the first fruit of our small trials. In presenting it to you as one of the selected readers, we sincerely ask you to warmly accept it and hope to receive your advice and cooperation hereafter, so that "KONA" will grow into a more significant publication.

Yours truly,

A handwritten signature in black ink, reading "N. Yoshioka".

Naoya Yoshioka
Editor in chief

Theoretical Approach to Dust Explosion

Tatsuo Tanaka*

Department of Chemical Process Engineering,
Hokkaido University

Abstract

A number of experimental researches on dust explosion have been published with measured data of the explosive characteristics such as the ignition temperature, the flame propagation velocity, the upper and lower limit explosible concentrations and the rate of pressure rise.

In this study the above-mentioned explosive characteristics are dealt with systematically based on a simple model of uniformly dispersed dust cloud consisting of particles of the same size, from the viewpoint of heat transfer process.

Comparing the computed results with the empirical law and the experimental data, it is assured that the explosive characteristics can be predicted theoretically. In addition, the analysis of the area for the pressure relief venting is conducted to minimize the damage, leading to a new dimensionless vent ratio.

1. Prediction of ignition temperature

1. 1 Definition of ignition temperature¹⁾

The ignition temperature is defined as the gas temperature at which a mass of particles begin to burn, when they are heated in an oven with a certain shape and size. It has been measured with a great number of materials. In Fig. 1, the surface temperature of solid T_s is displayed on the abscissa and the heat of reaction q_1 and

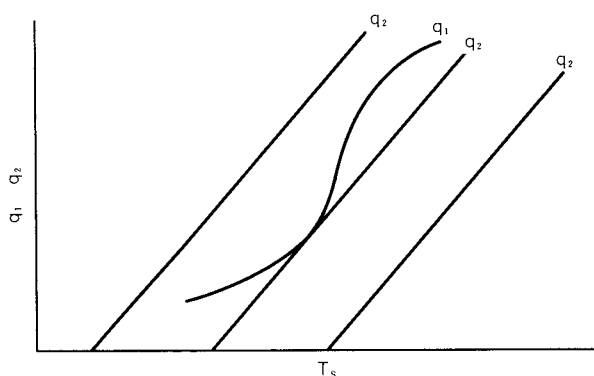


Fig. 1 Definition of ignition temperature

the heat emitting from the solid surface into the atmosphere by convection q_2 are taken on the ordinate. When q_1 is less than q_2 , the reaction is always kept at the level of oxidation. On the other hand, when q_1 is more than q_2 , the reaction of combustion makes continuous progress. A steady state can be kept only on the conditions of $q_1 = q_2$ and $dq_1/dT_s = dq_2/dT_s$. The reading of the horizontal axis T (surrounding temperature) on this condition is experimentally defined as the ignition temperature.

1. 2 Ignition temperature of dust cloud^{4,6)}

The reaction rate of oxidation of a single spherical particle with a diameter of D_p is given by Hottel *et al.*⁵⁾ as follows:

$$-\frac{dm}{dt} = \frac{k_s}{\sqrt{T_s}} \exp\left(-\frac{E}{RT_s}\right) C_g \pi D_p^2 \quad (1)$$

where m is mass of the particle, t time, k_s rate constant of reaction, E activation energy and C_g concentration of oxygen. The number of the particles n in the dust cloud with a diameter l and the dust concentration C_d is

$$n = C_d l^3 / \rho_s D_p^3 \quad (2)$$

for the particle of a density ρ_s . The generated heat G in the lump of the particles and the emitted heat U from them are calculated in the

* Nishi 8-chome, Kita 13-jo, Kita-ku, Sapporo, 060
TEL. 011 (711) 2111

Received January 31, 1983

following equations:

$$G = nQ\left(-\frac{dm}{dt}\right) = n\pi D_p^2 \frac{A}{\sqrt{T_s}} \exp\left(-\frac{E}{RT_s}\right) \quad (3)$$

$$U = n\pi D_p^2 h(T_s - T) + n\pi D_p^2 (\epsilon_p a_G \sigma T_s^4 - a_p \epsilon_G \sigma T^4) + \pi l^2 (\epsilon_p a_w \sigma T_s^4 - a_p \epsilon_w \sigma T_w^4) \quad (4)$$

Symbols A , ϵ , a , σ and h are a constant, blackness, absorptivity, Stefan - Boltzmann's con-

stant and film coefficient of heat transfer, respectively. The suffixes P , G and W represent particle, gas and wall respectively. The solution of T of the simultaneous equations

$$G = U \quad \text{and} \quad \frac{dG}{dT_s} = \frac{dU}{dT_s} \quad (5)$$

is compared with the empirical ignition temperature^{2,3} in Fig. 2. The value of A is plotted against the activation energy in Fig. 3.

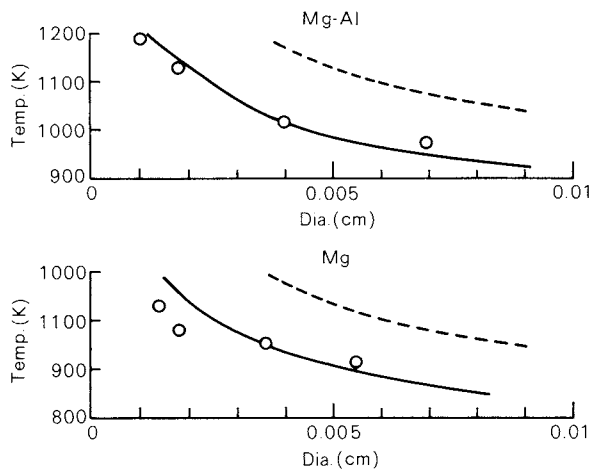


Fig. 2A Comparison of empirical ignition point of some metals with predicted values

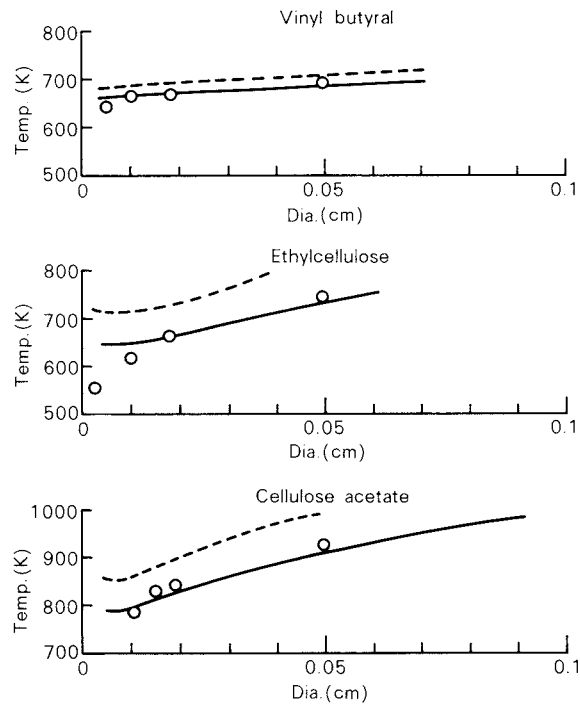


Fig. 2B Comparison of empirical ignition point of some plastics with predicted values

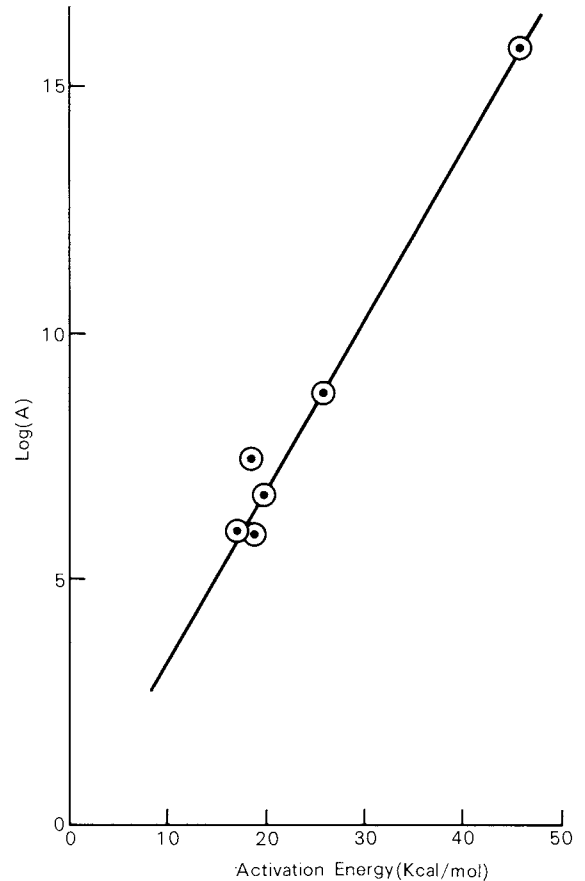


Fig. 3 Relationship between A value and activation energy

2. Prediction of flame propagation velocity.¹⁶⁾

2. 1 Model of propagation

Let us consider a cloud of dust in the vast space where a series of particles can be regarded to line up in the direction of flame propagation

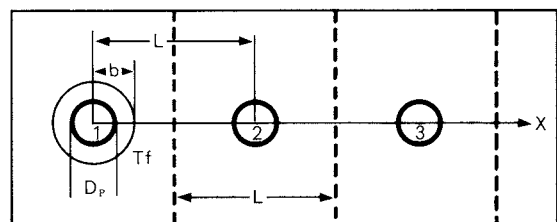


Fig. 4 Model of propagation with notation

excluding the case of a long pipe of small diameter. The average distance L between each particle with a diameter D_p is calculated as

$$L = \left(\frac{\pi}{6} D_p^3 \rho_s / C_d \right)^{1/3} \quad (6)$$

with the dust concentration C_d and the solid density ρ_s . The time interval Δt_n between the ignition of the n th particle and that of the $(n+1)$ th is the time required for the flame propagation. From these values, the so-called burning velocity is calculated. Meanwhile, if the left end of a vessel is closed and the right end is open, the particles in the second and the following sections will be pushed toward right owing to the pressure rise by the generated gas from the combustion of the 1st particle. The successive particles start burning one after another and cause the expansion of gas. In this way the expansion velocity is calculated as the sum of the transportation effect by the simultaneously burning particles.

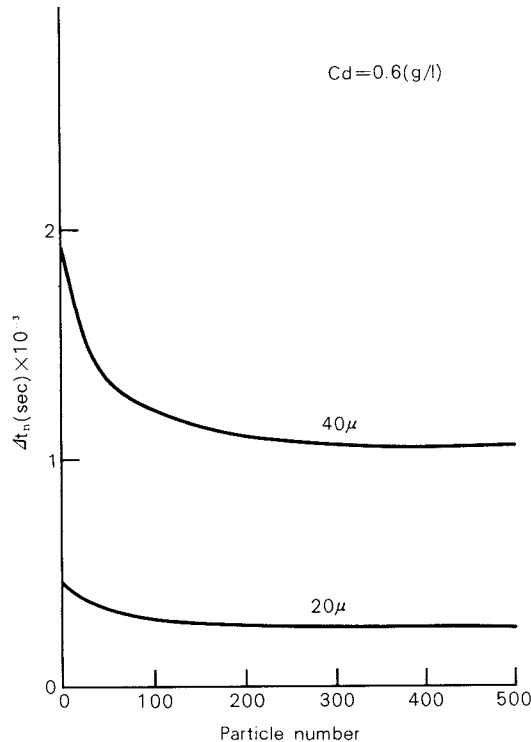


Fig. 5 Flame propagation time from n -th particle to $(n+1)$ th particle

2. 2 Burning velocity

The equation of one-dimensional thermal diffusion and its solution with the boundary conditions of $T = T_f = \text{constant}$ flame temperature, and $T = T_o$ at $t = 0$ are:

$$\frac{\partial T(x, t)}{\partial t} = \kappa \frac{\partial^2 T(x, t)}{\partial x^2} \quad (7)$$

$$T(x, t) = (T_f - T_o) \operatorname{erfc} \left(\frac{x}{2\sqrt{\kappa t}} \right) + T_o \quad (8)$$

where T is the gas temperature with the suffix f for the flame and 0 for the initial stage and κ represents the coefficient of thermal diffusion. The radius R_b of the flame is given as

$$R_b = (D_p/4) [1 + \sqrt{1 + (2k^*/D_p)}] \quad (9)$$

for a liquid droplet with a diameter D_p and equilibrium constant k^* ($k^* = 1 \sim 10 \text{ cm}^2$). Taking dynamic heat balance of a particle,

$$\begin{aligned} \frac{\pi}{6} D_p^3 \rho_s C_{ps} \frac{dT_{dL}}{dt} \\ = \pi D_p^2 h (T_{gL} - T_{dL}) + \frac{\pi}{2} D_p^2 (a_p \epsilon_f F \sigma T_f^4 \\ + a_p \epsilon_G \sigma T_G^4) - \pi D_p^2 \epsilon_p \sigma T_{dL}^4 \end{aligned} \quad (10)$$

The suffixes gL and dL represent the gas and the particle at the point of L respectively. The time required for the complete combustion of a single particle τ is given as

$$\tau = K_D D_p^2 \quad (11)$$

with the burning constant $K_D = 100 \sim 1000 \text{ (sec/cm}^2 \text{)}^8$.

2. 3 Expansion velocity, overall flame propagation velocity

The mass of a single particle m changes with time θ as follows:

$$m(\theta) = m_o \left[1 - \left(\frac{D_p(\theta)}{D_{po}} \right)^3 \right] \quad (12)$$

therefore

$$\frac{dm(\theta)}{d\theta} = \frac{3m_o}{\tau} \left(1 - \frac{\theta}{\tau} \right)^2 \quad (13)$$

When net n_C moles of gas is generated by the combustion of one mole of the particles, the volume increases at the same pressure P and the temperature T_G from $V_1 (= n_N RT_o/P)$ to

$$V_2 = (n_N + n_C) RT_G / P \quad (14)$$

Where n_N is the number of mole of air per one mole of particle and n_C the number of mole of gas evolved by the combustion of one mole of the particle. The velocity due to this expansion $v(\theta)$ is

$$v(\theta) = \frac{R}{L^2 MP} [(n_N + n_C) T_G - n_N T_o] \frac{dm}{d\theta}$$

$$= \frac{3m_0 R}{L^2 MP\tau} [(n_N + n_C)T_G - n_N T_0] \left(1 - \frac{\theta}{\tau}\right)^2 \quad (15)$$

M is the molecular weight of the particle.

$$V(t) = \sum_{i=1}^{n-1} v(t - i\Delta t) \quad (16)$$

$V(t)$ is the overall propagation velocity (approximately equals the expansion velocity). As an example, $V(t)$ is calculated for cellulose acetate with density of 1.28 g/cc, $C_p = 0.35$, $\epsilon_p = 0.8$ and $M = 450$ as well as with the settings of $\epsilon = a$, $T_f = 1600\text{K}$ and $T_0 = 293\text{K}$ and depicted in Fig. 6. These predicted values show good agreement with the empirical values of deflagration¹⁰⁾.

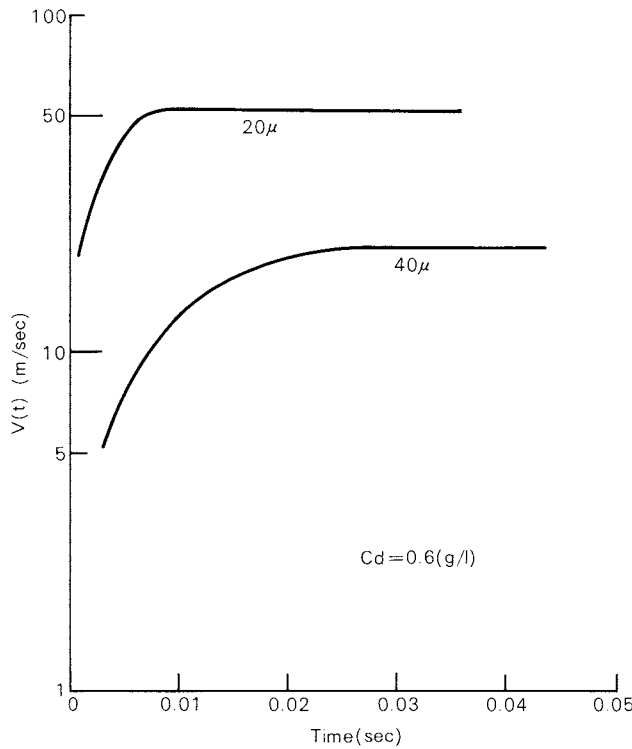


Fig. 6 Overall expansion velocity

3. Prediction of upper and lower limit explosible concentration

3. 1 Theory of lower limit explosible concentration⁹⁾

Dust cloud is regarded as a group of uniformly dispersed particles in the vast space with a constant mutual distance of L as shown in Fig. 7. The distance between each particle is given as

$$L = (\rho_s / C_d)^{1/3} D_p \quad (17)$$

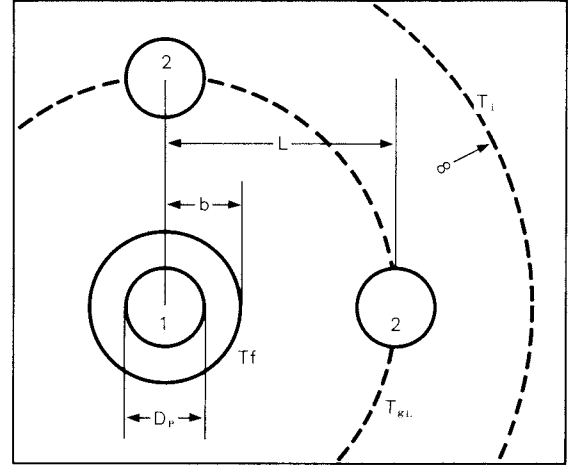


Fig. 7 Model of propagation with notation

Placing the dust cloud in the spherical coordination, first the particle in the center begins to burn and then the particles in the 2nd shell are heated by the emitted heat from the central particle. Supposing the particles in the 2nd shell reach the ignition temperature T_{ig} and ignite at the moment when the central particle has finished its combustion, gives the limit condition for the flame propagation to be possible. The limit concentration C_d is calculated from the L satisfying the above-mentioned condition and the equation (17). This is the theoretical lower limit explosible concentration. From the equation of heat conduction

$$\frac{\partial T(r, t)}{\partial t} = \kappa \left[\frac{\partial^2 T(r, t)}{\partial r^2} + \frac{2}{r} \frac{\partial T(r, t)}{\partial r} \right] \quad (18)$$

and the boundary conditions of $T = T_f$ at $r = R_b$ and $T = T_i$ at $t = 0$, the solution is

$$T(r, t) = (T_f - T_i) \frac{R_b}{r} \operatorname{erfc} \left(\frac{r - R_b}{2\sqrt{\kappa t}} \right) + T_i \quad (19)$$

From the heat balance of the particles,

$$\begin{aligned} \frac{\pi}{6} D_p^3 \rho_s \frac{dT_{dL}}{dt} &= \pi D_p^2 h (T_{gL} - T_{dL}) \\ &+ \frac{\pi}{2} D_p^2 a_p \epsilon_f F \sigma T_f^4 - \pi D_p^2 \epsilon_p \sigma T_d^4 \end{aligned} \quad (20)$$

Assuming the relations $\eta = t/\tau$ (21)

and $\tau = K_D D_p^2$ (22)

$$\begin{aligned} T_{gL}(\eta) &= (T_f - T_i) \frac{R_b}{L} \operatorname{erfc} \left(\frac{L - R_b}{2\sqrt{\kappa K_D D_p^2 \eta}} \right) \\ &+ T_i \end{aligned} \quad (23)$$

The predicted C_d with $\eta = 1$ (lower limit explosible concentration) is compared with the

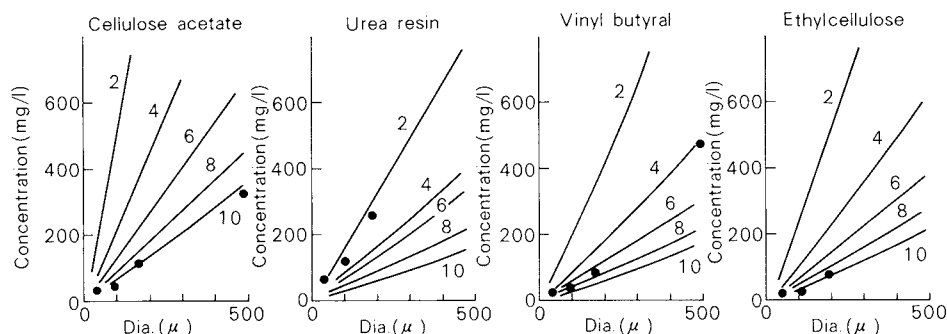


Fig. 8 Comparison of empirical minimum explosible concentration of dust with the present theory

experimental values in Fig. 8. As for the cellulose compounds both values agree well when k^* is 10cm^{11} .

3. 2 Theoretical consideration on upper limit explosible concentration¹²⁾

Oxygen in a limited area must diffuse to catch up with the combustion of some particles in the dust cloud for the continuous burning. First the total amount of oxygen in the considered space is shared evenly among all the particles in it. Each particle must get enough heat for ignition from the adjoining burning particle, by the time when it consumes its assigned oxygen. The upper limit explosible dust

concentration is clearly defined as the one at the state where all the particles at least begin to burn, not to say have finished burning. The equations are developed in the same way as in the last section except the consideration on the quantity of oxygen. An example of the comparison of the predicted values and the experimental data^{13,14)} is shown in Fig. 9. In this case explosion cannot take place with the oxygen concentration under 10%. Thus it is possible to conduct the fundamental calculation for "inerting".

4. Maximum rate of pressure rise²⁰⁾

4. 1 Cubical law

The pressure and the rate of pressure rise of dust explosion in a closed vessel are most immediate characteristics to show the degree of hazard.

$$V_0^{1/3} \left. \frac{dP}{dt} \right|_{\max} = K_{GC} \quad (24)$$

where V_0 is the volume of a spherical vessel and dP/dt is the rate of pressure rise.

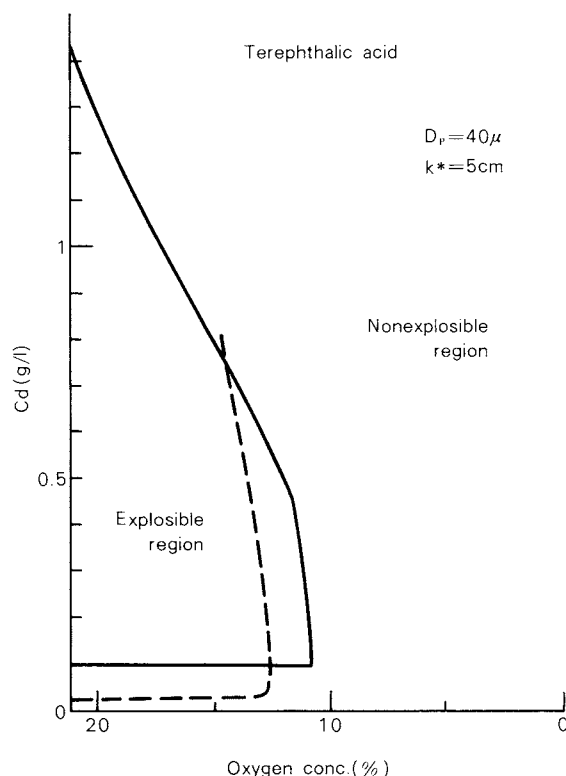


Fig. 9 Upper and lower explosible limits of dust concentration of terephthalic acid in relation to oxygen concentration

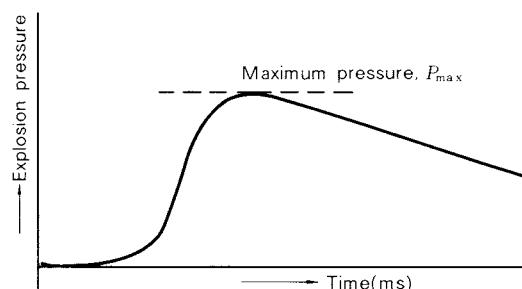


Fig. 10 Pressure against time

Recently the above equation has become agreed empirically¹⁵⁾. K_{GC} has been found to be a constant for each dust, but to differ depending on the kind of material, particle size, dust concentration and so on, although the details of it still remain unknown. In the present

report it will be discussed to understand the meaning of the constant K_{GC} and to enable to predict it for unknown materials and under any condition. Besides the effect on scale-up by the extension to the case of unspherical vessels and the possibility of comparing experimental data obtained with the testers of different size and shape will be also discussed in the followings.

4. 2 Modeling of dust cloud in vessel

When the particles are dispersed as shown in Fig. 11,

$$L = (\rho_s / C_d)^{1/3} D_p \quad (25)$$

$$N(n) = 24n^2 - 48n + 26 \quad (26)$$

N is the number of the particles on the n th spherical surface from the center ($n \geq 2$).

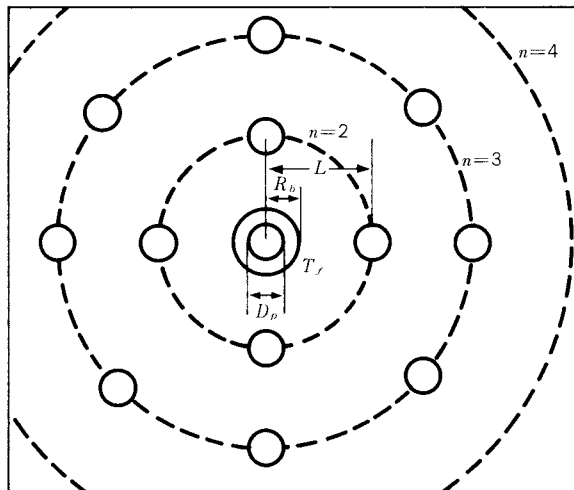


Fig. 11 Model of dust particles with notation

4. 3 Flame propagation time

The equation of heat conduction is as shown formerly

$$\frac{\partial T_g}{\partial t} = \kappa \left(\frac{\partial^2 T_g}{\partial r^2} + \frac{2}{r} \frac{\partial T_g}{\partial r} \right) \quad (27)$$

When solved with the previous boundary conditions,

$$T_g(r, t) = (T_f - T_{io}) \frac{R_b}{r} \operatorname{erfc} \left(\frac{r - R_b}{2\sqrt{\kappa t}} \right) + T_{io} \quad (28)$$

From the heat balance,

$$\frac{\pi}{6} D_p^3 \rho_s C_{ps} \frac{dT_d}{dt} = \pi D_p^2 \left(\frac{2k}{D_p} \right) (T_g - T_d)$$

$$+ \frac{\pi}{2} D_p^2 F a_p \epsilon_f \sigma T_f^4 \quad (29)$$

The solution is

$$T_d(\Delta t) = e^{-A \Delta t} \left[A \int_0^{\Delta t} e^{A \Delta t} T_g(nL, \Delta t) dt + \frac{B}{A} (e^{A \Delta t} - 1) + T_{do} \right] \quad (30)$$

where

$$A = 12k / \rho_s C_{ps} D_p^2$$

$$B = 3F a_p \epsilon_f \sigma T_f^4 / \rho_s C_{ps} D_p$$

k : thermal conductivity of gas

Δt : propagation time

T_{io} : initial temperature

T_g, T_d : temperature of gas and particle respectively

T_f : temperature of flame

R_b : radius of flame

κ : thermal diffusion coefficient

F : shape factor

σ : Stefan - Boltzmann's constant

L : distance between particles

The time Δt when $T_d(\Delta t) = T_{ig}$ (ignition temperature) in the equation (30) is the one required for the flame to transfer from the $(n-1)$ th surface to the n th, namely the flame propagation time. When the vessel is spherical and n is large enough, the propagation velocity v is

$$v = L / \Delta t$$

4. 4 Quantity of burned out dust

As $\theta / \tau \approx 1 - D_p(\theta) / D_{po}$ where the combustion completing time $\tau = K_D D_{po}^2$, the quantity of the burned out dust by the time θ is

$$m(\theta) = m_o [1 - (1 - \theta / \tau)^3]$$

$$m_o = (\pi/6) D_{po}^3 \rho_s$$

Therefore, the total mass of the material which started burning at $t = 0$ and has burned out by the time t is

$$M(t) = m_o \sum_{i=1}^n N(i) \left[1 - \left\{ 1 - \frac{t - (i-1)\Delta t}{\tau} \right\}^3 \right] \approx 8m_o (t/\Delta t)^3 \quad (31)$$

In case the oxygen is enough, the maximum amount M_o of the burned out material in a vessel of volume V_o and with the concentration C_d is

$$M_o = C_d V_o$$

If C_d is rather large and the oxygen is not

enough,

$$M_o = aV_o = n_o (t_o / \Delta t)^3$$

$$t_o = \left(\frac{aV_o}{8m_o} \right)^{1/3} \Delta t$$

Where a is equal to C_d , when C_d is smaller than a definite value.

4. 5 Pressure inside a vessel and maximum rate of pressure rise

$$P = RT_G (n_C / V) \quad (32)$$

$$\frac{dP}{P} + \frac{dV}{V} = \frac{dn_C}{n_C} + \frac{dT_G}{T_G} \quad (33)$$

For the adiabatic system

$$P^{(1-\gamma)/\gamma} T_G = \text{constant} \quad (34)$$

Combining the above equations,

$$\frac{dP}{dt} = \frac{\gamma dM(t)/dt}{M_o} P^{1-1/\gamma} [P_{\max}^{1/\gamma} - P_o^{1/\gamma}] \quad (35)$$

therefore

$$P(t) = [(P_{\max}^{1/\gamma} - P_o^{1/\gamma}) \frac{M(t)}{M_o} + P_o^{1/\gamma}] \quad (36)$$

$$\left. \frac{dP}{dt} \right|_{\max} = \gamma P_{\max} \left[1 - \left(\frac{P_o}{P_{\max}} \right)^{1/\gamma} \right] \frac{dM(t)/dt|_{t=t_o}}{M_o} \quad (37)$$

where

$$\left. \frac{dM(t)}{dt} \right|_{t=t_o} = \frac{24m_o}{(\Delta t)^3} t_o^2 = \frac{24m_o}{(\Delta t)^3} \left(\frac{aV_o}{8m_o} \right)^{2/3} \Delta t^2$$

$$= \frac{6}{\Delta t} m_o^{1/3} (aV_o)^{2/3} \quad (38)$$

therefore

$$V_o^{1/3} \left. \frac{dP}{dt} \right|_{\max} = \frac{\gamma D_p}{\Delta t} \left(\frac{36\pi\rho_s}{a} \right)^{1/3} P_{\max} \left[1 - \left(\frac{P_o}{P_{\max}} \right)^{1/\gamma} \right] \quad (39)$$

This equation shows that the empirical cubical law has been deduced theoretically and that when the properties of the dust (chemical formula, concentration, particle size) are known, the value K_{GC} in the equation (24), namely the right hand side of the equation (39) is apparently constant. Though a spherical vessel has been dealt with here, the cubical law including a shape factor can be adaptable also for vessels of approximately cylindrical shape, which suggests the possibility of exchanging data with vessels of various shapes. **Figs. 13 and 14** show the predicted value by the equation (39) and (35) respectively and **Fig. 15** displays the comparison of the theoretical and experimental values^{18,19}.

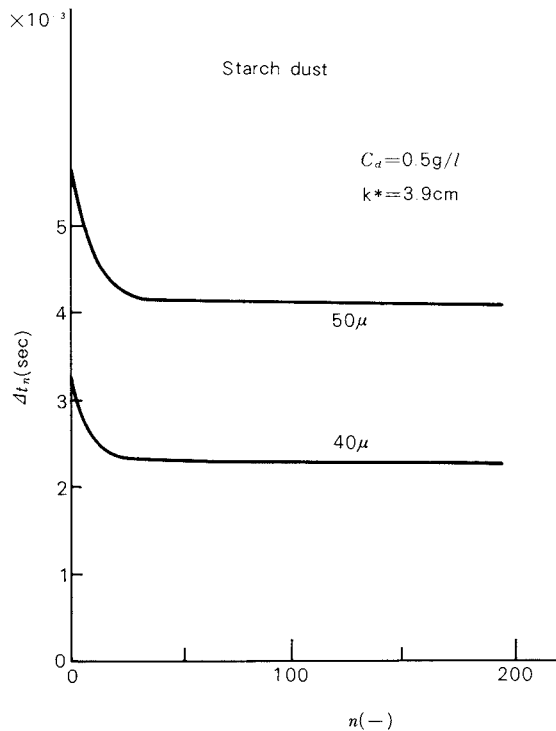


Fig. 12 Variation of Δt_n with n

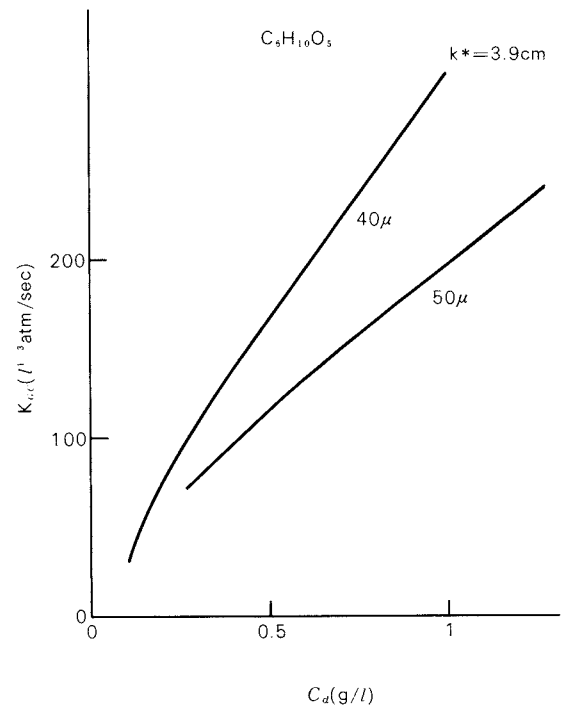


Fig. 13 Relation between K_{GC} value and dust concentration

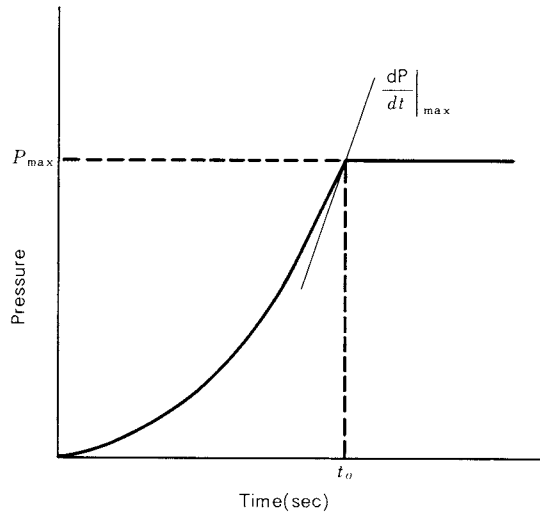


Fig. 14 Relation between pressure and time in a closed spherical vessel

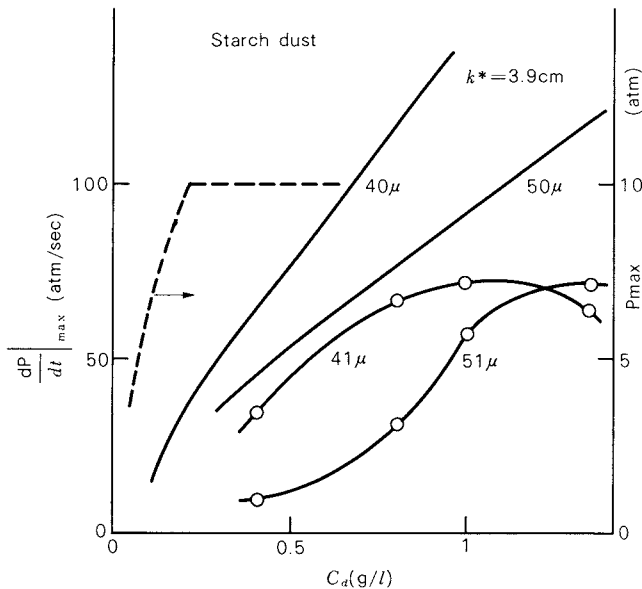


Fig. 15 Comparison of empirical maximum rate of pressure rise of starch dust with the predicted values vs. dust concentration in a spherical vessel

5. Design of pressure relief vent⁽²¹⁾

5. 1 Vent ratio

The vent ratio is defined conventionally as the one of the area S of the pressure relief vent to the volume V_o of the vessel. Empirically it is used for designing pressure relief vent but not sound because it is not dimensionless.

5. 2 Pressure rise at explosion relief venting

From the equation of dynamics for pressure rise,

$$\frac{dP}{dt} = \gamma P^{1-1/\gamma} (P_m^{1/\gamma} - 1) \frac{dM(t)}{dt} - \gamma P^{1-1/\gamma} (P_m^{1/\gamma} \frac{W_b}{\rho_m V_o} + \frac{W_u}{\rho_o V_o}) \quad (40)$$

For $P < 1/0.53$

$$W = C_s S \left[\left(\frac{2\gamma}{\gamma-1} \right) g_c P \rho (P^{-2/\gamma} - P^{-(\gamma+1)/\gamma}) \right]^{1/2}$$

and for $P > 1/0.53$

$$W = C_s S \left[\gamma \left(\frac{2}{\gamma+1} \right)^{(\gamma+1)/(\gamma-1)} g_c P \rho \right]^{1/2} \quad (41)$$

If P in the equation (40) reaches the maximum achievable pressure $P_v (= P_v/P_o)$, dP/dt must become 0. The area of the relief vent should be designed in such a way that the P_v is kept under the strength of the material constructing the vessel. The value C_s is called coefficient of discharge.

Using the above-mentioned K_{GC}

$$[S/V_o^{2/3}]^{-1} = \frac{P_o}{K_{GC}} \left(\frac{g_c P_o}{\rho_o} \right)^{1/2} f(\gamma) g(P_v) \quad (42)$$

Here for $P_v < 1/0.53$

$$f(\gamma) = \gamma \left(\frac{2\gamma}{\gamma-1} \right)^{1/2},$$

$$g(P_v) = P_v^{1-1/\gamma} (P_v^{1-1/\gamma} - 1)^{1/2} \quad (43)$$

and for $P_v > 1/0.53$

$$f(\gamma) = \gamma \left[\gamma \left(\frac{2}{\gamma+1} \right)^{(\gamma+1)/(\gamma-1)} \right]^{1/2},$$

$$g(P_v) = P_v^{(3\gamma-1)/2\gamma}$$

$$\frac{dP}{dt} \Big|_{\max} = V_o^{-1/3} P_o^{-1} K_{GC} \quad (44)$$

The theoretical values and the experimental ones^{18,22,23)} of $S/V_o^{2/3}$ are compared in Fig. 16 with different symbols for the various kinds of material. The theoretical values seem larger to some extent than the experimental ones, as the first term of rate of pressure rise in Eq. (40) is replaced by the maximum one to assure safety. But it is clearly understood from the figures that the tendency of the predicted values is in accordance with that of the experimental ones. Besides, the compared values range over the second power of 10, which suggests the theoretical equation can be applied to the wide

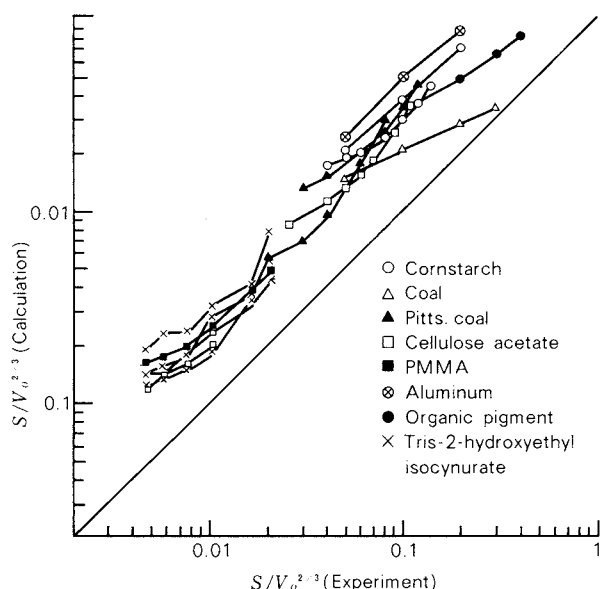


Fig. 16 Comparison of calculated $S/V_o^{2/3}$ with experimental $S/V_o^{2/3}$

range of design of relief vent.

Nomenclature

- A : constant
 a : a constant regarding dust concentration = C_d at a dilute dust concentration
 B : constant
 C_d : dust concentration
 C_g : concentration of oxygen
 C_s : coefficient of discharge
 C_{ps} : specific heat of solid
 D_p : particle diameter
 E : activation energy for oxidation
 F : view factor
 G : generated heat
 g_c : gravitation conversion factor
 h : heat transfer coefficient
 K_D : burning constant
 K_{GC} : constant for cubical law
 k_s : rate constant
 k^* : equilibrium constant
 L : average distance between two particles
 l : diameter of dust cloud
 M : molecular mass
 m : mass of particle
 $N(n)$: number of particles at n th spherical surface
 n : number of assumed spherical surface
 n : number of particles
 n_C : mole number of gas produced by combustion per one mole of particle
 n_N : mole number of air per one mole of particle
 P : pressure
 P : pressure ratio

- P_{\max} : maximum pressure
 P_v : maximum achievable pressure = strength of material
 Q : heat of reaction per gram
 q_1, q_2 : heat generated and emitted
 R : gas constant
 R_b : radius of flame
 r : distance for spherical co-ordinates
 S : vent area
 T : temperature of gas
 T_{GL} : gas temperature at a distance L
 T_f : flame temperature
 T_{dL} : solid temperature at a distance L
 T_s : temperature of solid surface
 T_i, T_o : initial temperature
 t : time
 Δt : time interval for propagation
 U : heat left
 V : overall expansion velocity
 V_o : volume of equipment
 v : velocity
 W : mass velocity of gas
 X : distance
 α : absorptivity
 γ : specific heat ratio
 ϵ : blackness
 ρ_s : density of solid
 κ : thermal diffusivity
 σ : Stefan - Boltzmann's constant
 τ : time for completing reaction
 θ : time
 η : t/τ

Subscripts

- G : gas
 p : particle
 w : wall
 b : burnt
 u : unburnt
 o : initial

References

- 1) Palmer K.N.: "Dust Explosion and Fire": Chapman, Lond. (1973).
- 2) Cassel H.M. and I. Liebman: *Combust. & Flame* **3**, 467 (1959).
- 3) Hartmann I. and J. Nagy: *US Bur. Mines R.I.* No. 3751 (1944).
- 4) Mitsui Y. and T. Tanaka: *I & EC. Proc. Des. Dev.* **12**, 384 (1973).
- 5) Parker A.S. and H.C. Hottel: *Ind. Eng. Chem.* **44**, 1095 (1952).
- 6) Nomura S. and T. Tanaka: *Kagaku-Kogaku Ronbun-shu* **4**, 634 (1978).
- 7) Miesse C.C.: 6th Symp. Combustion p.732 (1957).

- 8) Essenhigh R.H. and I. Fells: *Discuss. Faraday Soc.* **30**, 208 (1960).
- 9) Nomura S. and T. Tanaka: *Kagaku-Kogaku Ronbun-shu* **5**, 47 (1979).
- 10) Maesawa M.: "Intro. Safety Eng." (Kyoritsu) p.85 (1975).
- 11) Hartmann I. et al.: *US Bur. Mines R.I.* No. 5062 (1954).
- 12) Nomura S., M. Torimoto and T. Tanaka: *Chem. Eng.* **45**, 327 (1981).
- 13) Craven A.P. and M.G. Foster: *Com. Flame* **11**, 408 (1967).
- 14) Ishihama W. and H. Enomoto: 15th Symp. Combust. p.479 (1974).
- 15) Bartknecht W.: *V.D.I.-Berichte* Nr. 165, 24 (1971).
- 16) Nomura S. and T. Tanaka: *Kagaku-Kogaku Ronbun-shu* **5**, 601 (1979).
- 17) Ishihama W. and H. Enomoto: *Safety Eng.* **14**, 195, 243 (1975).
- 18) Donat C.: *C.E.P. Tech. Manual Loss Prevention* **11**, 87 (1977).
- 19) Jacobsen H.J. and R. Kowall: *V.D.I.-Berichte* Nr. 165, 53 (1971).
- 20) Nomura S. and T. Tanaka: *I & EC Proc. Des. Dev.* **19**, 451 (1980).
- 21) Nomura S. and T. Tanaka: *J. Chem. Eng. Japan* **13**, 309 (1980).
- 22) Hartmann I. and J. Nagy: *Ind. Eng. Chem.* **49**, 1734 (1957).
- 23) Schwab R.F. and D.F. Othmer: *Chem. Proc. Eng* **45**, 165 (1964).

Bulk Density Measurement by a New Tapping System

Akira Suganuma*, Takashi Sugawara*
and Ryuichi Aoki*

Department of Chemical Engineering,
University of Tokyo

Abstract

A new tapping system has been developed to measure bulk densities of powdery materials and to study their compaction characteristics. The new tapping system has an electronic monitor of impact acceleration to observe the peak value of impact acceleration, that is, the intensity of tapping action. The impact acceleration of a conventional tapping machine is not monitored quantitatively and generally higher than 200 G. The adjustable range of the new tapping system is from 3 to 500 G. Tapping height adjustment of a conventional tapping machine is done without any appropriate change of colliding materials. Such an adjustment causes very ambiguous covariation of tapping intensity and tapping energy quantity. Some confusions of these different factors have been making it difficult to analyse and discuss the effects of tapping height. The peak value of impact acceleration and the tapping energy quantity of the new tapping system can be varied independently through the combination of tapping height adjustment and cushioning material selection.

Four limestone powders, five white alundum powders and two Kanto loam powders were used as testing powders. Their specific surfaces, S_w , were measured by an air permeability method. Tapping tests were done for each powder under various tapping conditions.

Higher tapping energy in the sense of quantity causes faster compaction process but does not affect the terminal tapping density, ρ_∞ , which varies widely with S_w and tapping acceleration, A . The terminal tapping density of finer powder is lower than that of coarser powder. Higher impact acceleration causes higher terminal density, but the effect of A seems to be saturated when A becomes sufficiently high. The density difference owing to the size difference becomes smaller with an increase in A . Tapping tests with lower impact acceleration are much more informative than those with higher acceleration.

1. Introduction

Tapping of powdery materials is a well known and conventional technique of bulk density measurement, but it has remained in a native state with little sophistication. The tapping height or the falling height of a powder container is almost only one adjustable parameter of a conventional tapping machine. The

aim of tapping height adjustment is to control or to vary the intensity of tapping, but few quantitative correlations of intensity and height have been reported. Furthermore, the intensity of tapping depends not only on the tapping height but also on the combination of colliding materials. A conventional tapping test gives therefore very ambiguous and relative informations. Any quantitative comparison of a test result with another one by a different tapping machine is almost impossible and generally in vain.

A new tapping system developed in our lab-

* 7-3-1 Hongo, Bunkyo-ku, Tokyo, 113
TEL. 03 (812) 2111

Received April 11, 1983

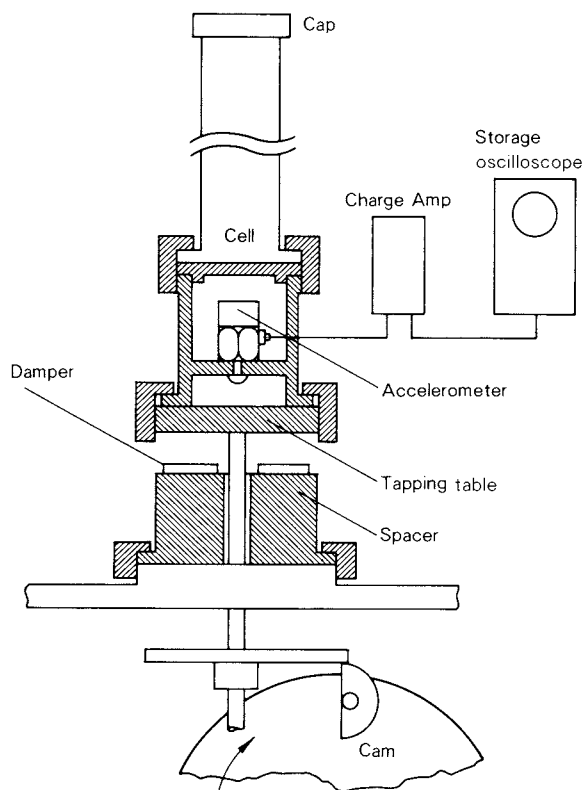


Fig. 1 Main part of new tapping system

oratory has an electronic monitor of impact acceleration. The acceleration and the energy of tapping are adjustable independently. The adjustable range of acceleration is from 3 to 500 G.

2. New tapping system

The main part of a new tapping system is schematically shown in Fig. 1. A 100 cm³ acrylic resin cylindrical cell is generally used as a powder container. Its ratio of depth to inner diameter is about 6. The cell is fixed to a tapping table by a screw and filled with powder to be tested. The powdery material is poured into the cell through a 24 mesh vibrating sieve. An impact accelerometer is attached to the tapping table to monitor the tapping acceleration. The tapping acceleration can be varied by tapping height adjustment and/or by selection of damper material and damper dimensions.

Fig. 2 is an example of tapping acceleration observed by a storage oscilloscope. The peak value of such observation is denoted by A and named impact acceleration of tapping in this paper. The adjustable range of A is from 3 to 500 G. The adjustable range of tapping height

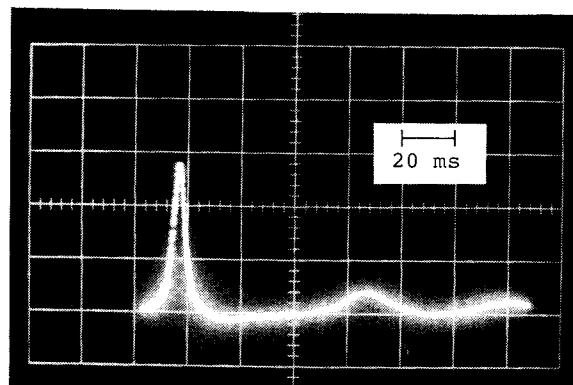


Fig. 2 Storage oscilloscopic observation of impact acceleration of tapping

of a conventional tapping machine is generally from several millimeters to a few centimeters. After our preliminary experiments, such tapping height range gives impact acceleration of tapping higher than 200 G when no special cushioning system is used. As described in the following chapters, tapping tests with such higher level of impact acceleration are less informative for many cases than those with lower impact acceleration. The new tapping system is, therefore, used mainly in the range of 3 to 100 G.

By the combination of appropriate cushioning system and tapping height, the impact acceleration of tapping and the energy of tapping are adjustable independently. Higher tapping height gives always more tapping energy but the peak value of impact acceleration of tapping can be reduced by cushioning.

An interval of tapping is 6 s. This interval is much longer than that of an ordinary tapping machine so that any motion or displacement of powder initiated by a tapping action is completed before the next tapping process.

3. Powders

Limestone powder (CaCO_3), white alundum (Al_2O_3) and Kanto loam dust were used as testing materials. Many samples with different particle size distribution were prepared. Their particle sizes were measured by an air permeability method and evaluated by specific surface, S_w [cm²/g]. In the following tables, ρ_p denotes true particle density and ρ_0 denotes the initial bulk density of each powdery sample poured into the 100 cm³ tapping cell before tapping. Table 1 is the list of powdery samples of limestone ground by a small ball mill. Particle sizes

Table 1 Limestone powder

	S_w [cm ² /g]	ρ_p [g/cm ³]	ρ_0 [g/cm ³]
CaCO I	2.22×10^3	2.72	1.035
CaCO II	3.94×10^3	2.72	0.845
CaCO III	5.26×10^3	2.72	0.770
CaCO IV	6.05×10^3	2.72	0.720

Table 2 White alundum powder

	S_w [cm ² /g]	ρ_p [g/cm ³]	ρ_0 [g/cm ³]
Al ₂ O ₃ #240	0.67×10^3	4.11	1.70
Al ₂ O ₃ #500	1.31×10^3	3.96	1.44
Al ₂ O ₃ #1000	2.53×10^3	3.91	0.973
Al ₂ O ₃ #2000	4.89×10^3	3.94	0.750
Al ₂ O ₃ #4000	9.23×10^3	3.94	0.527

Table 3 Kanto loam powder

	S_w [cm ² /g]	ρ_p [g/cm ³]	ρ_0 [g/cm ³]
Kanto loam No. 8	5.60×10^3	3.00	0.575
Kanto loam No. 11	20.97×10^3	3.07	0.462

were varied by grinding time adjustment. **Table 2** is the list of white alundum powders, which were manufactured and distributed as polishing powder. **Table 3** is the list of Kanto loam powders, which were prepared and supplied by APPIE (The Association of Powder Process Industry and Engineering, Japan) as a test dust after JIS Z 8901.

4. Experimental results

Tapping tests were done for each powdery sample described in the last chapter under various tapping conditions. Examples of compaction process by tapping are shown in **Fig. 3** for limestone powder. The tapping height, H , was 10 mm and the impact acceleration of tapping, A , was 3.4 G. n denotes number of tapping and ρ_n denotes bulk density of powder tapped n times. The compaction process starts from the initial bulk density, ρ_0 , which is defined as the bulk density of powder poured into the tapping cell before the tapping. The compaction proceeds monotonically to the terminal tapping density, ρ_∞ , which is defined as the bulk density of powder tapped sufficiently many times. In the case of **Fig. 3**, the terminal tapping density, ρ_∞ , varies remarkably with specific surface of powder, S_w .

Fig. 4 shows the effects of the impact accel-

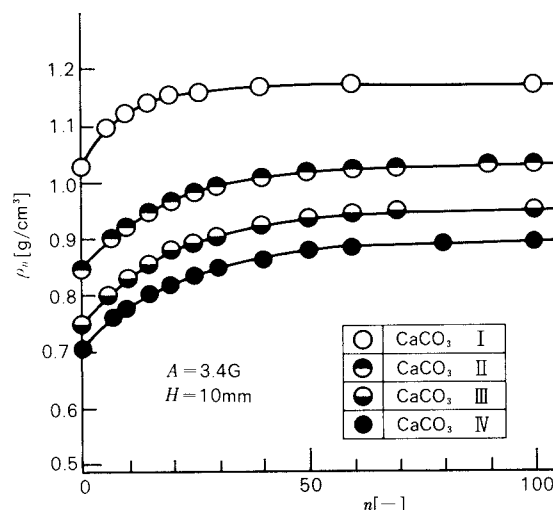


Fig. 3 Examples of limestone powder compaction process by tapping
(Effect of specific surface of powder, S_w)

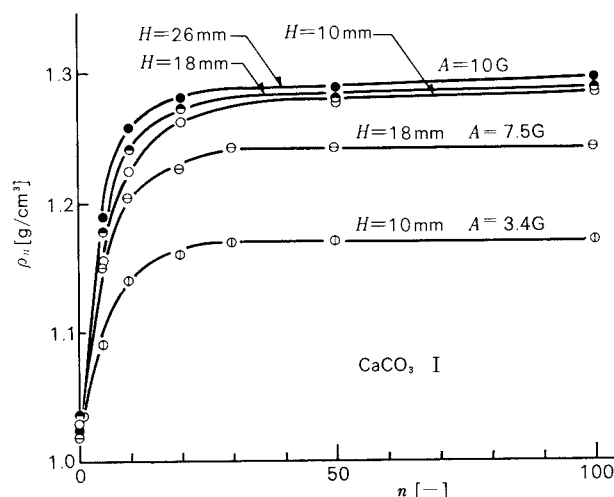


Fig. 4 Examples of limestone powder compaction process by tapping
(Effects of impact acceleration of tapping, A , and tapping height, H)

eration of tapping, A , and those of the tapping height, H , on the compaction process. The terminal tapping density, ρ_∞ , varies with the impact acceleration, A , but does not depend on the tapping height, H , as far as A is constant. Compaction proceeds faster by tapping of higher tapping height but the terminal density is the same. This means that the energy of tapping in the sense of quantity affects the rate of compaction but it has no effect on the terminal density. The terminal density of tapping seems to depend not on the quantity of tapping energy but on the intensity of each tapping action, that is, the impact acceleration of tapping. **Fig. 5** also shows the independency of terminal

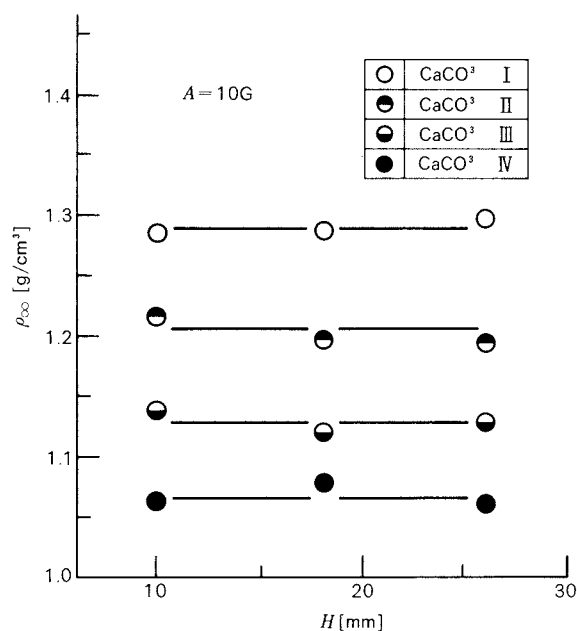


Fig. 5 Independence of terminal tapping density, ρ_{∞} , from tapping height, H

density from the tapping height.

The terminal density is also independent of any preliminary compaction by tapping with higher impact acceleration, as far as the density after the preliminary compaction does not exceed the terminal density of final tapping. The terminal density of limestone powder at 40 G tapping, for example, was not affected by 80 G nor 200 G preliminary tapping. This fact gives a very useful experimental technique to shorten the time required for the terminal density measurement.

If a combination of colliding materials is not changed, higher colliding velocity causes not only higher impact acceleration but also higher impact energy in the sense of quantity at the same time. The tapping height variation of a conventional tapping machine means therefore ambiguous covariation of the quantity of tapping energy and the intensity of tapping action. It may be said that some confusions of these different factors have been making it difficult to discuss and analyse the effects of tapping height clearly. For more successful discussions, the effects of tapping energy in the sense of quantity and the effects of tapping intensity should be distinguished clearly from each other and analysed separately. Descriptions and discussions in this paper are concentrated mainly on the influences of tapping intensity on the terminal tapping density. The other discussions

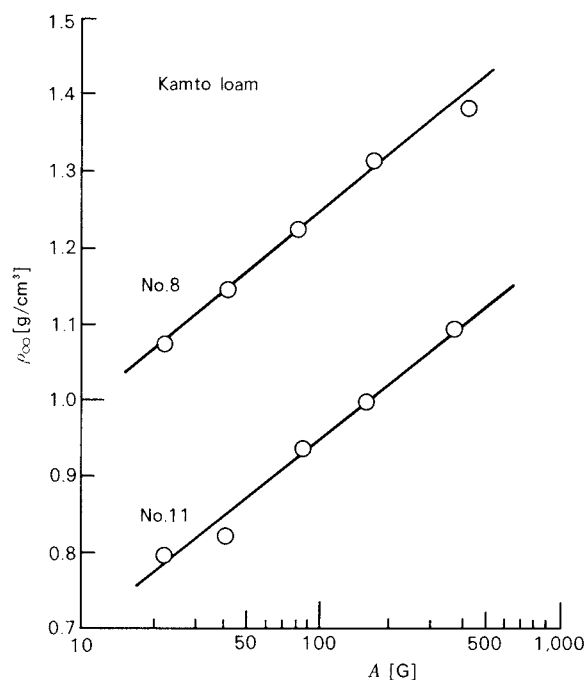


Fig. 6 Terminal tapping densities of Kanto loam powders

will be done in the near future.

In Fig. 6, the terminal tapping densities, ρ_{∞} , of Kanto loam powders are correlated to the impact acceleration of tapping, A . As already shown in Fig. 4, larger impact acceleration causes larger terminal tapping density. In the case of Fig. 6, the density difference between No. 8 and No. 11 does not vary with the impact acceleration. The terminal density of Kanto loam No. 11, of which specific surface is nearly 4 times larger than that of Kanto loam No. 8, is about 0.3 g/cm³ smaller than the density of No. 8. As shown also in the other figures, ρ_{∞} of finer powder is, in general, smaller than that of coarser one.

In Fig. 7, the terminal densities of white alundum powders are correlated to the acceleration of tapping. It is clear in Fig. 7 that the influence of A on ρ_{∞} is almost saturated when A becomes sufficiently high. The critical value of A , beyond which ρ_{∞} is almost independent of A , seems to depend on specific surface of powder, S_w . The critical value of A for coarser powder is lower than that for finer powder. The terminal tapping density of finer powder, which is smaller than that of coarser powder, becomes larger still in the range of A where the density of coarser powder is already independent of A . The density difference between

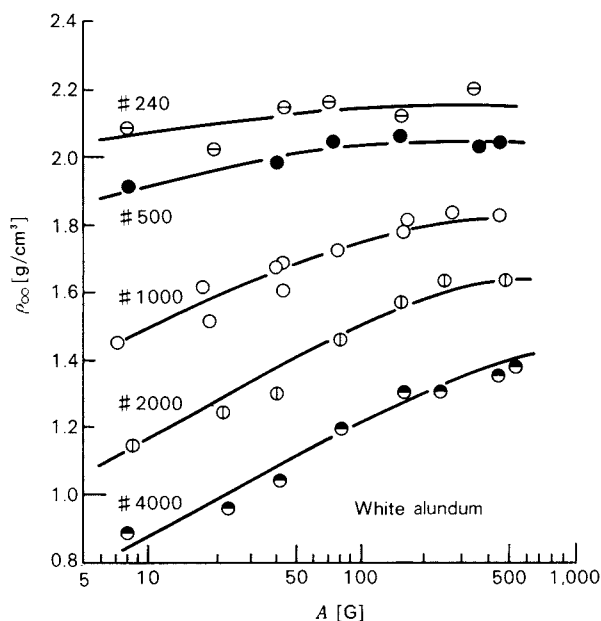


Fig. 7 Terminal tapping densities of white alundum powders

coarser and finer powders becomes therefore smaller in such a range of tapping acceleration. It may be estimated that the critical values of tapping acceleration for Kanto loam powders are larger than 500 G.

In Fig. 8, ρ_{∞} of limestone powders are correlated to A . When the impact acceleration of tapping becomes higher than about 150 G, the density differences among powders owing to their particle size differences are practically no more detectable. Tapping tests with lower impact acceleration are much more informative than those with higher impact acceleration.

5. Conclusion

Bulk densities of CaCO_3 , Al_2O_3 and Kanto loam powders were measured by a new tapping system with a electronic monitor of impact acceleration of tapping. The peak value of impact acceleration was varied from 3 to 500 G independently of tapping energy in the sense of quantity.

Experimental results were,

- 1) Energy quantity of a tapping action affected the rate of compaction but did not affect the terminal tapping density, ρ_{∞}
- 2) Higher tapping acceleration caused higher terminal density. This effect was saturated in the range of sufficiently high acceleration.
- 3) ρ_{∞} of finer powder was lower than that of coarser one. The density difference owing to

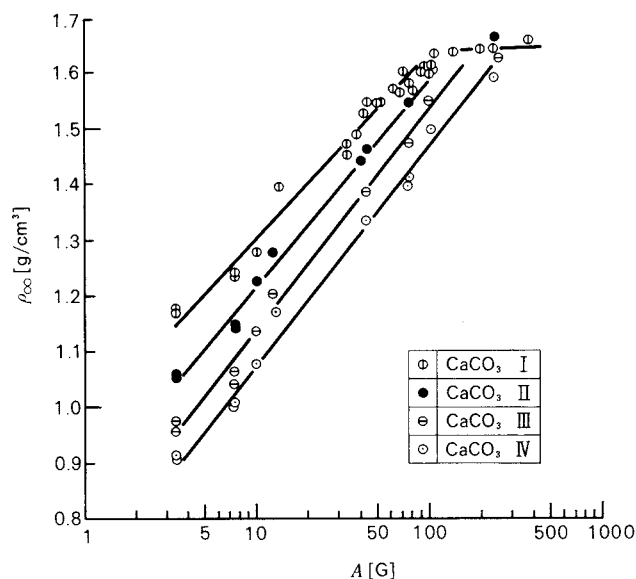


Fig. 8 Terminal tapping densities of limestone powders

particle size difference decreased with an increase in tapping acceleration.

It is very important to distinguish the effects of tapping energy in the sense of quantity and the intensity of tapping action. Tapping tests by the new tapping system are very informative especially with lower impact accelerations than a conventional tapping machine. Impact accelerations of a conventional tapping machine are generally higher than 200 G.

Acknowledgement

The authors are grateful to Dr. Hideo Yamamoto for his very useful comments and discussions. The authors are also very grateful to Mr. Masahiro Yoshida and Mr. Morimasa Katagiri for their intensive cooperation in tapping tests.

Nomenclature

- A : impact acceleration of tapping (peak value) [G]
 H : tapping height [mm]
 n : number of tapping [—]
 S_w : specific surface of powder [cm^2/g]
 ρ_0 : initial bulk density of powder [g/cm^3]
 ρ_n : bulk density of powder tapped n times [g/cm^3]
 ρ_p : true density of particle [g/cm^3]
 ρ_{∞} : terminal tapping density [g/cm^3]

Some Problems in Size Measurement of Submicron Particles

Yasuo Kousaka*

Department of Chemical Engineering
University of Osaka Prefecture

Abstract

Some problems that the author has encountered in size measurement of submicron particles in air and in water have been outlined. When particle size is smaller than around $0.5\mu\text{m}$, the mean velocity caused by Brownian motion of a particle, which cannot be repressed by any usual means, becomes comparable with the gravitational settling velocity in air and exceeds the velocity in water. When the number concentration of particles is higher than about 10^8 particles/ cm^3 , Brownian coagulation, which cannot be repressed in air and in water unless the use of appropriate dispersion agents becomes significant. Size measurement by sedimentation methods in one or both of these cases gives an erroneous result. Another difficulty arises in size measurement of aggregate particles composed of submicron primary particles. When one may want to know the size distribution of aggregates as they are, sedimentation in air is effective. For measurement of primary particle size composing aggregates, on the other hand, sedimentation in water is effective since deaggregation in water is much easier than in air. As to submicron liquid droplets there is a problem of stability. Even if they have low vapor pressure such as oil, they can easily evaporate to decrease in size by the Kelvin effect which becomes significant as the droplet size decreases.

1. Introduction

Particles in submicron range undergo the Brownian motion which results from the collision of surrounding gas or liquid molecules with the particles. Consequently such a motion causes deposition of particles on the wall of a size analyzer and Brownian coagulation under the condition of high number concentration, which have undesirable effects on size measurement.

Particle deposition is practically unavoidable in air or in water. Coagulation, on the other hand, can be prevented in water, although it is also unavoidable in air except under a sufficiently reduced number concentration. When an appropriate dispersion agent is added in suspension, electrical repulsion resulted from it would take place among the particles and pre-

vent coagulation.

Other phenomena causing problems in size measurement of small particles are evaporation and condensation. Evaporation takes place on the surface of liquid droplets suspended in air due to a vapor pressure rise on their surfaces having curvature by the Kelvin effect. A temperature drop within the system, on the other hand, causes condensation of a vapor on the particle surfaces, also producing problems in size measurement especially when very fine hygroscopic particles are kept suspended in air.

This paper summarizes some problems, such as not only those above stated but deaggregation and particle shape, which the author has encountered in size measurement for recent several years.

2. Brownian coagulation and deposition

The particle behavior in a small sedimentation cell as illustrated in Fig. 1 is discussed here so as to easily obtain an experimental verification. In this cell, a fluid is stationary and an ex-

* 4-804 Mozu-Umemachi, Sakai, Osaka, 591
TEL. 0722 (52) 1161

Received March 16, 1983

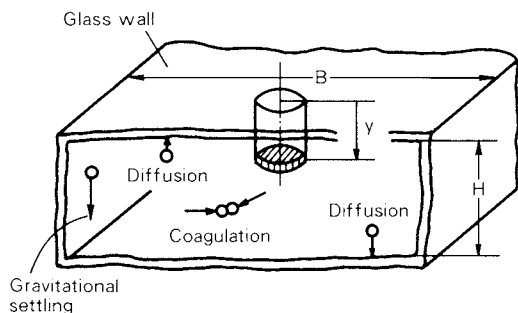


Fig. 1 Sedimentation cell

ternal force acting on particles is limited to the gravitational force. In addition horizontal particle diffusion is negligible because the cell width B is sufficiently large compared with the cell depth H . When particles of radius r exist in such a cell, the particle number concentration n at the point below the suspension surface y at the lapse of time t is given by the following population balance equation.

$$\begin{aligned} \frac{\partial n(r, t)}{\partial t} = & D(r) \frac{\partial^2 n(r, t)}{\partial y^2} - u_t(r) \frac{\partial n(r, t)}{\partial y} \\ & + \frac{1}{2} \int_{\rho=0}^{\rho=r} K_B(\sqrt[3]{r^3 - \rho^3}, \rho) n(\sqrt[3]{r^3 - \rho^3}, t) \\ & \times n(\rho, t) \left(\frac{r}{\sqrt[3]{r^3 - \rho^3}} \right)^2 d\rho \\ & - \int_{\rho=0}^{\rho=\infty} K_B(r, \rho) n(r, t) n(\rho, t) d\rho \end{aligned} \quad (1)$$

where $D(r)$ and $u_t(r)$ denote the diffusion coefficient and the terminal settling velocity of a particle having radius r respectively. The first term in the right hand side accounts for the Brownian diffusion, the second for the gravitational sedimentation, the third represents the number of newly formed particles with radius r by collision of two particles, while the last term represents the decrease in number of particles with radius r and density ρ by collision with other particles. In collision, it is assumed that two particles collided with each other form a new spherical particle whose mass is the same as the combined mass of two smaller particles. In addition, K_B is estimated by the following coagulation function.

$$K_B(r, \rho) = \frac{2kT}{3\mu} (r + \rho) \left\{ \frac{C_m(r)}{r} + \frac{C_m(\rho)}{\rho} \right\} \quad (2)$$

where $C_m(r)$ is the slip coefficient, k the Boltzmann's constant, μ the viscosity, and T the temperature. The numerical calculation of Eq. (1) in dimensionless form under various con-

ditions provides changes in the number concentration of particles of the radius r at the depth y with the time t . It is assumed that the initial size distribution of the particles introduced into the cell shown in Fig. 1 is regarded as a log-normal one in the calculation. This result estimates the effect of coagulation on a sedimentational size analysis, using the ratio of the coagulation rate to the gravitational settling velocity CG , as shown in the following equation.

$$CG = K_0 n_0 C_m(r_{g0}) H / u_t(r_{g0}) z, \quad K_0 = \frac{2kT}{3\mu} \quad (3)$$

In the similar manner it also estimates an effect of the diffusion on the analysis, using the ratio of the diffusion rate to the gravitational settling velocity DG , as given by the following equation.

$$DG = D(r_{g0}) / H u_t(r_{g0}) z \quad (4)$$

where n_0 , r_{g0} , H , and Z are an initial particle number concentration, an initial geometric mean radius, a sedimentation cell depth, and a centrifugal effect (centrifugal acceleration divided by gravitational acceleration) respectively. Z is unity in the gravitational field.

2. 1 Brownian coagulation

The sedimentational size analysis is discussed here to determine cumulative size distributions by observing time-dependent changes in the particle number concentration at the depth y shown in Fig. 1. Fig. 2 indicates a calculated result obtained from Eq. (1) when the first term due to diffusion is negligible.¹⁾ The abscissa represents a dimensionless radius \bar{r} (r divided by r_{g0}) modified by the slip coefficient, and the ordinate indicates a cumulative under-size. The broken line in this figure shows either a true particle size distribution when the number concentration is sufficiently low ($CG \cdot \bar{y} \approx 0$, $\bar{y} = y/H$) or the initial size distribution of the particles introduced into the cell illustrated in Fig. 1 when the concentration is high ($CG \cdot \bar{y} \neq 0$). In the case of high concentration, the change in number concentration of the particles in the cell depends on the Brownian coagulation as well as the gravitational settling. Accordingly these two effects cause faster decrease in the number concentration at the depth y in Fig. 1 than that of the gravitational

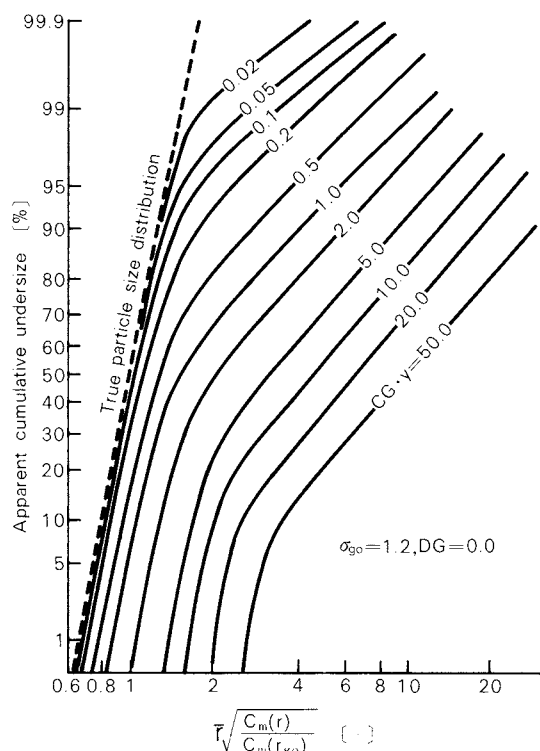


Fig. 2 Apparent size distribution when coagulation occurs

settling alone, and provide the same result as would be obtained from the analysis of larger particles. Hence the particle size distribution shown in Fig. 2 shifts to the larger side as $CG \cdot \bar{y}$ increases. The author experimentally verified that such phenomena could actually happen as follows.

A microscopic sedimentation analyzer (Shimadzu SA-MID) was used for the experiment, which converts the time-dependent changes of the particle number at the depth y in Fig. 1 into the particle size distribution by observing from the top using a TV camera and an ultra-microscope.²⁾ In order to calibrate this analyzer, standard particles of polystyrene latex whose size was known (geometric mean radius $r_{g0} = 2.85\mu\text{m}$, geometric standard deviation $a_g = 1.16$), were used being sufficiently diluted and dispersed in water. Consequently the good result could be obtained as shown in Fig. 3.

Fig. 4, ① indicates an experimental result of cigarette smoke which was diluted 100 times in clean air just after smoke generation. Fig. 4, ③ represents one under the highly concentrated condition without dilution. These results show the Brownian coagulation would cause remarkable changes in particle sizes of cigarette smoke. Fig. 4, ② shows, on the other hand,

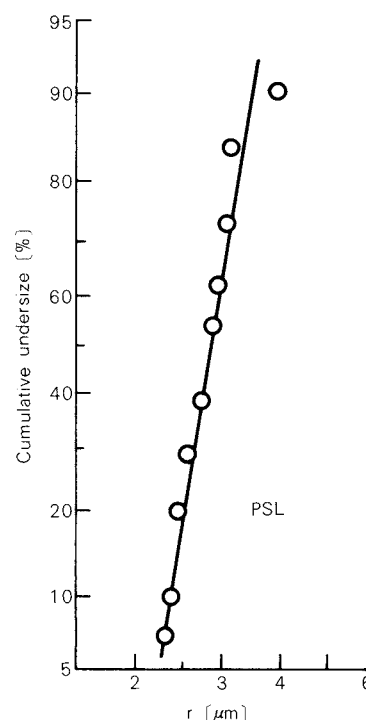


Fig. 3 Calibration of size analyzer

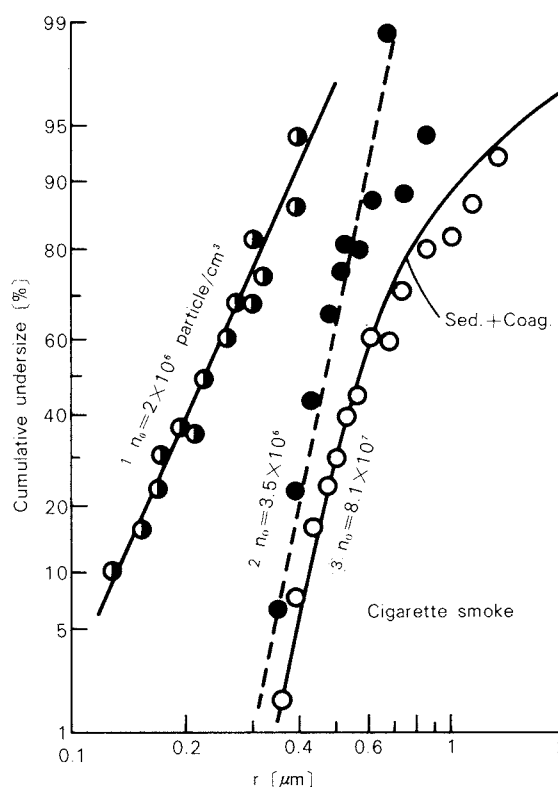


Fig. 4 Coagulation of cigarette smoke (in air)

the case where the smoke was diluted by small amounts of clean air before its introduction into the cell so as not to cause coagulation in the cell. The comparison between the result of ② and that of ③, therefore, estimates the

effect of coagulation in the cell. The solid line in Fig. 4, ③, which is theoretically obtained, shows good agreement with experimental results.

In general, particle sizes of a highly concentrated aerosol vary remarkably by Brownian coagulation, as shown in Fig. 4. It may be roughly calculated, for instance, that an aerosol of 10^{12} particles/cm³ in number concentration and $0.1\mu\text{m}$ in diameter will change to that of 10^9 particles/cm³ and $1\mu\text{m}$ in one second. Therefore it must be careful in not only sedimentational size analysis but other size analyses when particle number concentration is high.

2. 2 Deposition by Brownian diffusion

Fig. 5 shows a calculated result of monodisperse particles where the third and the fourth term of the right hand side in Eq. (1) are negligible or the effect of coagulation is unnecessary to be taken into account. This figure suggests how the dimensionless number concentration \bar{n} ($\bar{n} = n/n_0$, n_0 is initial number concentration) will depend on the lapse of time

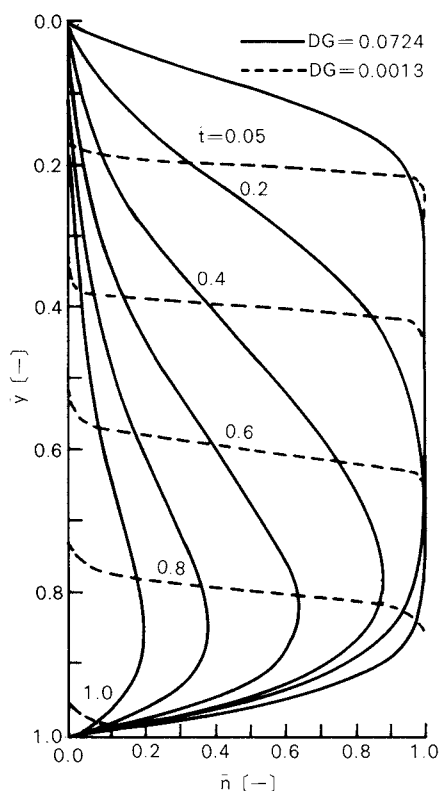


Fig. 5 Change in number concentration of particles undergoing sedimentation and diffusion

$\bar{t}(\bar{t} = u_t(r_{g0})t/H)$ at the dimensionless depth $\bar{y}(\bar{y} = y/H)$ in the sedimentation cell. Weak diffusion (DG is small) causes a sharp boundary in the concentration toward the sedimentational direction or y direction, whereas strong one (DG is large) extends a broad concentration distribution toward y direction. Accordingly monodisperse particles would be pretendedly observed as polydisperse when DG is large.

Fig. 6 shows a result experimentally obtained using the above stated analyzer to identify how such a diffusion could have effects on size measurement. The broken line represents a true particle size distribution, when the sedimentation cell is set in the centrifugal field with large Z or DG is small in Eq. (4). The solid circles in the right side, on the other hand, which were experimentally obtained, show approximate agreement with the solid line resulted from the solution of Eq. (1)

Since the diffusion coefficient D in Eq. (4) increases with the decrease in particle size, an average particle displacement in one second would become comparable to the gravitational settling velocity. A simple calculation will provide the approximate accordance between these two values under the condition of 3g/cm^3 in particle density and about $0.4\mu\text{m}$ in radius in water (1g/cm^3 and $0.25\mu\text{m}$ in air). Therefore the gravitational sedimentation in water might cause large errors in size measurement when particles are smaller than $0.4\mu\text{m}$ in radius. The

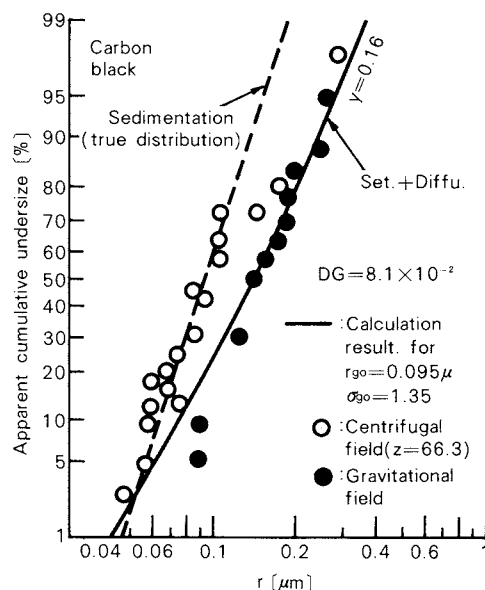


Fig. 6 Effect of diffusional deposition on size analysis (in water)

settling velocity of the above stated particles is to be estimated as $0.7\mu\text{m}/\text{sec}$, hence such a small convective flow arising in the sedimentation cell would provide a distrustful result in size measurement. Since diffusional deposition on the vertical wall is not taken into account in the analysis of this paper, an increase in H will not necessarily provide a successful conclusion in the analyzer where such an effect should be taken into account.

2. 3 Simultaneous effect of Brownian coagulation and deposition

It is possible to prevent Brownian coagulation in water by adding an appropriate dispersion agent which permits particles to repulse electrically each other. However both Brownian coagulation and deposition may have effects on particle size measurement simultaneously if a dispersion agent is inappropriate or measurement is to be conducted in air. Fig. 7 shows the particle size distributions of needlelike iron oxide particles (length-to-diameter ratio is about 6) measured in water containing no dispersion agent. The open circles illustrated in the left side represent experimental results obtained by a centrifugal sedimentation. Solid circles illustrated in the right side, on the other hand, offer those by the gravitational sedimentation method under the influence of coagulation and

deposition, and the solid line shows the corresponding result calculated by Eq. (1)

3. Evaporation and condensation

Behavior of aerosols is discussed in this section. When liquid droplets suspended in a gas is small, evaporation causes their size reduction or extinction even if a vapor pressure of the liquid is rather low. When supersaturation of a vapor is formed in a gas due to a temperature drop, the vapor condenses around the particles in the gas to increase their sizes. Such a size change will become remarkable when particles are small.

Evaporation and Condensation discussed here are based on the following equations.

$$\frac{P_0}{P_s} = \exp\left(\frac{2\bar{v}\sigma}{r\kappa T}\right) \quad (5)$$

$$\frac{dr}{dt} = \frac{D(r)M}{r\rho_d R} \left(S \frac{P_s(T_B)}{T_B} - \frac{P_0(T_0)}{T_0} \right) \left(1 + \frac{P_0(T_0) + SP_s(T_B)}{2P_t} \right) \left(\frac{K_n + 1}{1.333 K_n^2 + 1.7 K_n + 1} \right) \times \left(1 - \frac{r}{r_B} \right)^{-1} \quad (6)$$

$$T_0 = \frac{\lambda D(r)M}{KR} \left(S \frac{P_s(T_B)}{T_B} - \frac{P_0(T_0)}{T_0} \right) \times \left(1 + \frac{P_0(T_0) + SP_s(T_B)}{2P_t} \right) + T_B \quad (7)$$

Eq. (5) shows a vapor pressure rise at the particle surface by the Kelvin effect. P_0 and P_s are vapor pressures at the particle surface and at the flat surface respectively. \bar{v} is a molar volume, σ a surface tension, K the Boltzmann's constant, and T a temperature.

Eq. (6) indicates either the evaporation rate of liquid droplets, or the growth rate of particles by condensation when a vapor reaches supersaturation. M is a molecular weight, ρ_d a density of condensed liquid, R the gas constant, S a degree of saturation, T_B a temperature at the radius r_B distant from the particle center, P_t a total vapor pressure, K_n the Knudsen number, and T_0 a particle surface temperature which can be obtained from Eq. (7). In Eq. (7), λ and K are a latent heat and a thermal conductivity of a gas respectively. The radius r_B in Eq. (6), which is based on the cellular model, corresponds to that of a sphere having an average amount of gas distributed to each particle.

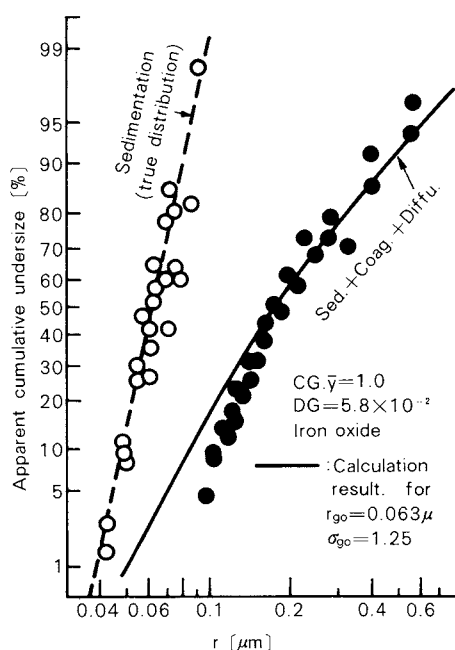


Fig. 7 Simultaneous effect of coagulation and deposition on size analysis (in water)

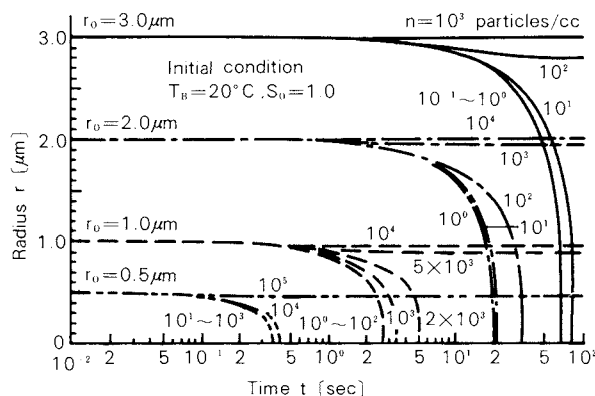


Fig. 8 Evaporation of fine water droplet clouds in saturated air

3. 1 Evaporation

The stability of water droplets suspending in air is discussed here as the most familiar instance. Fig. 8 shows a calculated result of the time-dependent change in water droplet radii obtained from Eq. (5), Eq. (6), and Eq. (7).³⁾ This figure, where r_0 denotes the initial water droplet radius, n the droplet number concentration, and S_0 the degree of initial saturation, suggests that water droplets would evaporate and vanish in a short time when r_0 and n are small. When the concentration n is high, droplets are comparably stable, because the evaporated vapor contributes to the increase in the degree of saturation. Although the droplet clouds were assumed to exist in an infinite space in Fig. 8, the droplet size will decrease in a small cell faster than in the case of Fig. 8 due to vapor condensation on the wall. It was assumed in this figure that $S_0 = 1$ (initial relative humidity = 100%); but when S is smaller than a unity, for instance $S = 0.5$ (relative humidity = 50%), water droplets of $r_0 = 1\mu\text{m}$ and $n = 10^4$ droplets/cm³ will vanish in 5×10^{-3} seconds.

Liquid droplets with lower vapor pressure than that of water such as DOP or DBP have been often applied to experiments because these droplets of more than $r_0 = 0.5\mu\text{m}$ are relatively stable. Even such droplets, which are regarded as stable in general, however, might be subject to the influence of evaporation since the Kelvin effect increases with the decrease in particle size. This is recognized in Fig. 9 which shows droplet size distributions of DOP and silicone oil obtained by a size analyzer based on the Kelvin effect.⁴⁾ These droplets were generated by an aerosol generator of an evapo-

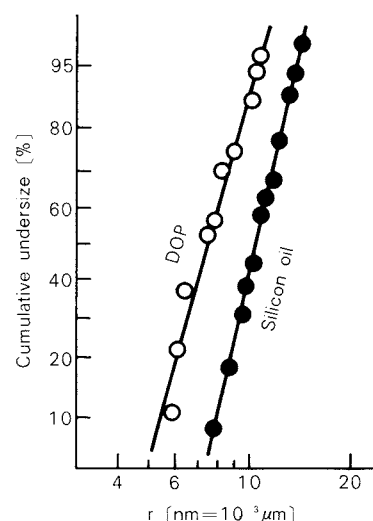


Fig. 9 Size change of ultrafine DOP droplets due to evaporation

ration-condensation type and then classified by a differential mobility analyzer (DMA). Since DOP and silicone oil droplets classified by DMA are possibly estimated to be of the same size, the difference of the distributions in Fig. 9 will depend on the evaporation which takes place in approximately 10 seconds after the DMA to the size analyzer. In other words, DOP droplets evaporates faster than silicone oil droplets. The author has been practically unable to generate ultrafine droplets with a radius of less than $0.005\mu\text{m}$, because such particles might vanish by the time when the measurement begins even if they could be generated. Therefore measurement of submicron liquid droplets should require sufficient care.

3. 2 Condensation

When adiabatic expansion or heat removal from the outside cools an aerosol containing the vapor such as water vapor under the nearly saturated condition, size enlargement will take place which results from condensation of the supersaturated vapor on the particle surface. Although this size enlargement is relatively slight in general if the particle size is large, it becomes remarkable when particle sizes are smaller than $0.1\mu\text{m}$. The size enlargement of hygroscopic particles due to condensation resulted from temperature drop could take place in unsaturated conditions, hence much care must be required in measurement of such particles. The size enlargement of NaCl particles experimentally obtained under the increased humid conditions is shown in Fig. 10 as an example.⁵⁾

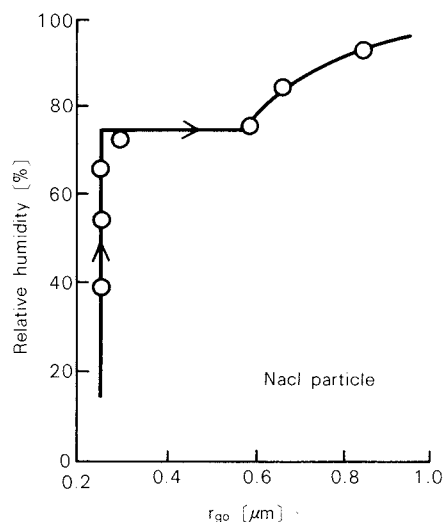


Fig. 10 Size change of NaCl particle by humidity

4. Deaggregation

Size measurement is often conducted in water to determine size distributions of primary particles. In such a case, preliminary treatments are practically performed preceding the size measurement; at first the disintegration of aggregates by a mechanical force (deaggregation), then the addition of dispersion agent to prevent reaggregation of once deaggregated particles. When particles suspended in air are to be measured, on the other hand, differently conditioned particle sizes are desired; the size of aggregated particles and that of deaggregated or primary ones.

Fig. 11 shows an experimental result obtained from the size analysis of aggregates deaggregated in air and in water by the microscopic sedimentation analyzer as previously stated. The deaggregation was achieved in water suspension containing 0.2% (weight basis) NaHMP with a repetition of strong suction and discharge using a syringe. The measured values have a good concord with Feret diameters determined by an electron microscope. The iron oxide particles used in the experiment were shaped like spheres derived from rounded cubes. The agreement of these two results suggests that particles could be completely deaggregated into primary particles in water. The solid circles in this figure, on the other hand, represent the particle size distribution of iron oxide powders which were deaggregated in air by a high speed rotating blade disperser. This result shows how difficult it is to deaggregate fine

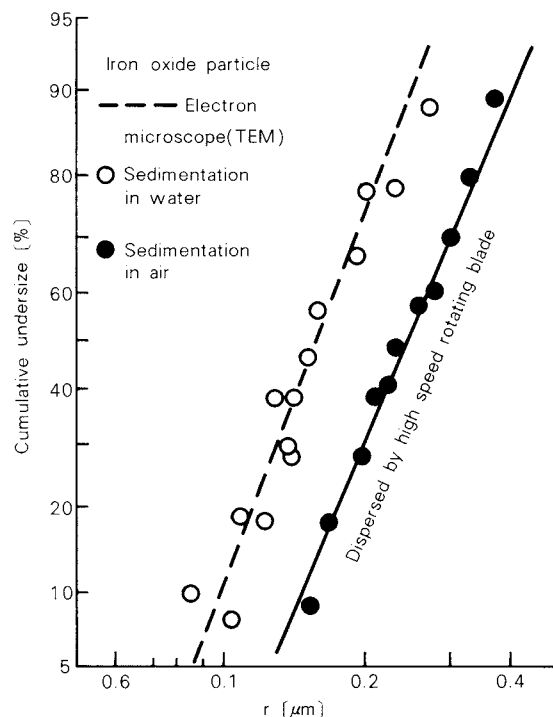


Fig. 11 Difference between deaggregation in air and water

aggregates in air.

In general aggregated particles may be effectively deaggregated by;

- velocity gradient of a fluid
- acceleration or retardation of particles in a fluid
- particle collision with obstacles in a flow field

The formers might be effective in a liquid, whereas the latter has been experimentally verified to be the most effective in air.⁶⁾ In each case, stronger mechanical forces would be required with the decrease in particle size.

The method to prevent reaggregation of once aggregated particles depends on the condition around them; the low concentration of less than 10^7 particles/cm³ is effective in air, while an addition of an appropriate dispersion agent is so in water. Fig. 12 shows the ζ -potential measured for the determination of the most suitable amount of a dispersion agent that can provide a successfully deaggregated or reaggregation-free condition. ζ -potentials in this figure were determined by observing horizontal velocity of particles using a cell with platinum electrodes instead of the cell of the analyzer previously stated. They could suggest the most suitable concentration, having a good accord-

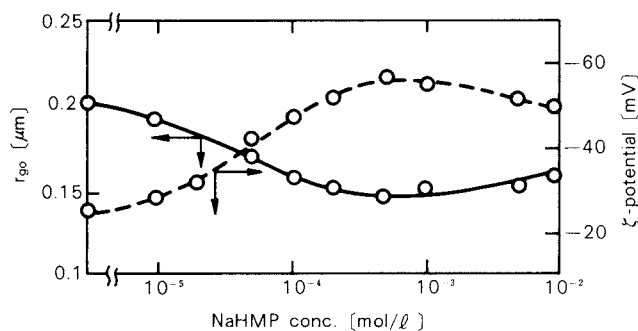


Fig. 12 Relation among NaHMP concentration, geometric particle radius and ζ -potential

ance with geometric particle radius r_{g0} , as shown in this figure.

5. Particle shape, charging and thermal convective flow

The effects of particle shape on size measurement are also important, not limited solely to submicron particles. It should be natural that a size distribution of non-spherical particles depend on the principle of the sizing method used. Fig. 13 shows Stokes diameters, Feret diameters (2-dimensional), and major axis lengths of needlelike particles with an aspect ratio (length-to-diameter ratio) of approximately 12 as an extreme example.

With respect to aggregated particles, sizing would become more difficult because of the difficulty in the estimation of the density taken porosity into account as well as the shape.⁷⁾

Fig. 14 shows the electrical charge of aggregated CaCO_3 dispersed in air which is represent-

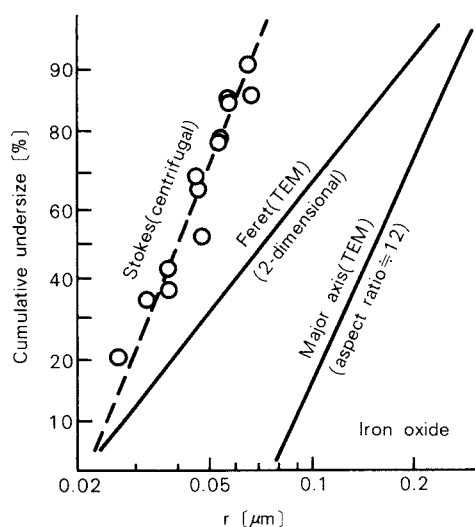


Fig. 13 Comparison among variously defined particle sizes

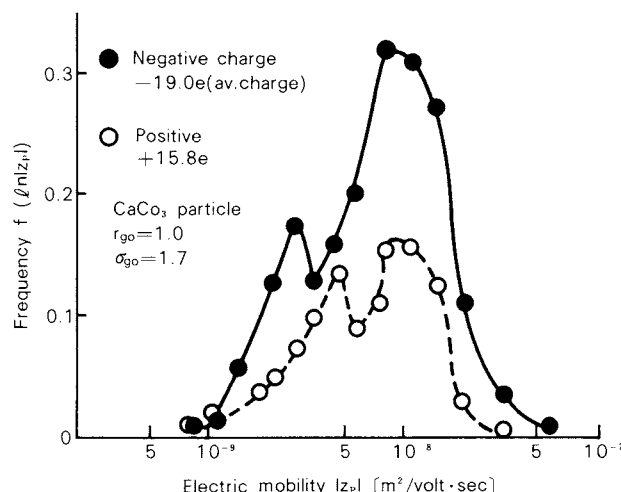


Fig. 14 Electrical mobility distribution of aggregate particles dispersed in air

ed in terms of electrical mobility.⁸⁾ This figure suggests that aggregated particles are highly charged positive or negative. Size measurement of highly charged particles in air sometimes leads to a wrong result because of the electrical precipitation of particles in a sizing instrument.

Furthermore in a sedimentation method, thermal convective flow of a fluid in the cell would cause a problem. Since a particle of $0.4\mu\text{m}$ in radius and 3g/cm^3 in density sedimentates in water at approximately $0.7\mu\text{m/sec}$ as stated in 2.2, such a velocity induced by a convective flow in the cell could be unavoidable unless the severe temperature control throughout the cell. G_r (Grashof) number will provide an approximate criteria to estimate the degree of the convective flow, but can scarcely offer a general quantitative criteria to evaluate as to various shapes of cells. Accordingly size measurement which is subject to an influence of slight convection as above stated should be avoided.

6. Conclusion

Several problems in size measurement of submicron particles were discussed through our experiences and observations. The obtained results are as follows:

- (1) The effect of Brownian diffusion of particles on sedimentational size measurement becomes important, when particle size is smaller than about $0.8\mu\text{m}$ ($0.5\mu\text{m}$ in air).
- (2) Addition of an appropriate dispersion agent in water or reduced particle number con-

centration less than 10^7 particles/cm³ in air is effective to prevent aggregation in size measurement.

- (3) Centrifugal sedimentation can minimize the effects of a convective flow in the cell as well as two above-mentioned phenomena.
- (4) Small liquid droplets are likely to vanish due to evaporation even if vapor pressure of a liquid is low.
- (5) Deaggregation of aggregated particles requires stronger mechanical forces with the decrease in particle size. Great difficulty would be encountered especially in deaggregation of particles in air.

References

- 1) Okuyama, K., Y. Kousaka, T. Miyazaki and T. Yoshida: *J. Chem. Eng. Japan*, **10**, 46 (1977).
- 2) Yoshida, T., Y. Kousaka and K. Okuyama: *I & EC Fundam.*, **14**, 47 (1975).
- 3) Kousaka, Y., K. Okuyama, K. Sumi and T. Yoshida: *J. Aerosol Sci.*, **9**, 489 (1978).
- 4) Kousaka, Y., T. Niida, K. Okuyama and T. Kuwamura: Extended Abstract of 1st Annual Conf. of AAAR p.37-1, Santa Monica, California (1982).
- 5) Kousaka, Y., K. Okuyama and C. S. Wang: *J. Chem. Eng. Japan*, **15**, 75 (1982).
- 6) Kousaka, Y., K. Okuyama, A. Shimizu and T. Yoshida: *J. Chem. Eng. Japan*, **12**, 152 (1979).
- 7) Kousaka, Y., K. Okuyama and A. C. Payatakes: *J. Coll. Interface Sci.*, **84**, 91 (1981).
- 8) Kousaka, Y., K. Okuyama, M. Adachi and K. Ebie: *J. Chem. Eng. Japan*, **14**, 54 (1981).

Direct Shear Test of Powder Beds

Kei Miyanami* and Keijiro Terashita*

*Department of Chemical Engineering
University of Osaka Prefecture*

Takeo Yano*

*Professor emeritus
University of Osaka Prefecture*

Abstract

Interrelations among shearing stress, applied vertical stress (by external load), actual vertical stress at shearing plane, vertical displacement (powder bed expansion or contraction) and shearing displacement have been extensively investigated for a number of powders under various test conditions such as the method of preconsolidation, the shearing cell diameter, the initial void fraction of powder beds and so on, by utilizing a simple shear tester capable of testing under both constant-load and constant-volume conditions and of measuring the actual vertical stresses (6 points) in the vicinity of shearing plane, the shearing stress and the vertical displacement of a powder bed simultaneously.

It has been concluded that; if the internal friction factor having a universal validity and fairly independent of the test conditions is to be obtained, it is essential to measure the mean actual vertical stress in the vicinity of shearing plane, or it is indispensable otherwise to measure at least the vertical displacement of powder beds along with the shearing displacement and to make sure that the vertical displacement is being kept as small as possible during a course of shearing.

1. Introduction

Mechanical characteristics of powder beds have been evaluated by a direct shear tester and/or uni- and tri-axial compression testers. In the field of powder technology, the direct shear tester has gained a popularity because of: simplicity in its device structure, handling and operations, reproducibility for practical powder behaviors of non uniform strains and two dimensional deformation, and giving useful and fundamental information.

A direct shear test is conducted by; first applying a vertical load onto a sample powder bed confined in a cell and second measuring the shear stress generated upon horizontal shearing movement of the bed. Finally by plotting the

shear stresses against various corresponding vertical stresses, we obtain a yield locus of the powder bed. The yield locus may represent the shearing-failure characteristics of the powder and the internal friction factor of the powder bed may be calculated from the slope of the locus. These characteristics have been widely utilized to evaluate the flowability of powders in various bulk handling processes such as transportation, storage, feeding and mixing and to establish rational criteria for design and analysis of such processes.

Although many studies on the direct shear test have been reported, the measured values of the internal friction factor, for example, are found to depend on experimental conditions, even if the same sample is tested by the same device. This is probably because the results of direct shear tests are likely to be affected by particle sizes, their distributions and packing structures of powder beds, since a powder bed consists of a great number of solid particles and

* 4-804 Mozu-Umemachi, Sakai, Osaka, 591
TEL. 0722 (52) 1161

Received May 6, 1983

a certain interaction exists among them. Unfortunately, there are few reports which investigate what effect is dominant or whether a universal internal friction factor independent of testing methods and/or experimental conditions can be obtained.

The present paper summarizes the significant results of previous studies on direct shear tests for discussions and presents our recent experimental results obtained by the direct shear tester we have developed.

2. Background

A direct shear test simultaneously measures the vertical stress applied to a powder bed and the shear stress generated when the bed is forced to slip, as illustrated in Fig. 1. The shearing cell consists of two parts stacked, the upper and lower parts, the cross section of which may be circular or square with the same cross sectional shape and area. One of the cells is movable horizontally and the other is fixed.

Taneya *et al.*¹⁾ pointed out that a direct shear test would give larger internal friction factors with decreasing the cell diameter and/or the upper powder bed height. To clarify this reason, they observed the flow patterns of colored defatted milk powder in the shearing cell by taking cross sectional pictures, and recognized that the end effect near the side wall of the cell becomes appreciable as the cell diameter and/or the upper bed height decrease. They proposed that a shear test should be conducted under the conditions of a large bed height and a constant cell diameter to reduce such end effect. Yamafuji *et al.*²⁾ summarized existing literatures to obtain the relationship between the internal friction factor and the initial void fraction of the powder bed and

found that the internal friction factor increased as the initial void fraction decreased or the powder bed was packed denser. Recently, Tsunakawa *et al.*^{3,4)} and Takagi *et al.*⁵⁾ also reported similar results.

Ohtsubo⁶⁾ suggested that a shear and vertical stresses relation, or a yield locus (YL), would not necessarily follow Coulomb's law of friction; a decrease or an increase in the void fraction of a powder bed, respectively, cause the YL to be concave or convex. Umeya *et al.*^{7,8)} verified experimentally this phenomena. Shinohara *et al.*⁹⁾ proposed a model of monodispersed powder bed made by ordered packing to investigate the effects of the void fraction on the internal friction factor. By taking surface friction at contact points between particles, mechanical gearing of particles and adhesion/cohesion of particles into considerations of the friction and cohesion mechanisms in the powder bed, they theoretically concluded that the dependency of the internal friction factor on the void fraction would be due to a nonuniformity of the powder bed structure.

Aoki *et al.*¹⁰⁾ used a constant volume direct shear tester, which allowed the tests under constant void fraction conditions, to carry out a series of direct shear tests by changing the powder bed height in the shearing cell, and found that the slope of the YL (that could be obtained by a single trial with their tester), or the internal friction factor, increased as the bed height increased. Umeya *et al.*¹¹⁾ obtained a similar results by using a constant load direct shear tester. Aoki *et al.* claimed that a direct shear test cannot give a true internal friction factor but an apparent one, and proposed that the true internal friction factor can be obtained by extrapolating the relation between the bed height-to-cell diameter ratio and the corresponding internal friction factor to zero bed height according to Janssen's formula. This finding is completely contrary to the result of Taneya¹⁾ and implied that a direct shear test should be made by keeping the powder bed height as low as possible. Furthermore, Tsunakawa *et al.*³⁾ have pointed out that the yield loci obtained by the constant volume shear tester have a tendency of being larger than those obtained by a constant load direct shear tester and this tendency becomes appreciable as the cohesiveness and compressibility of the

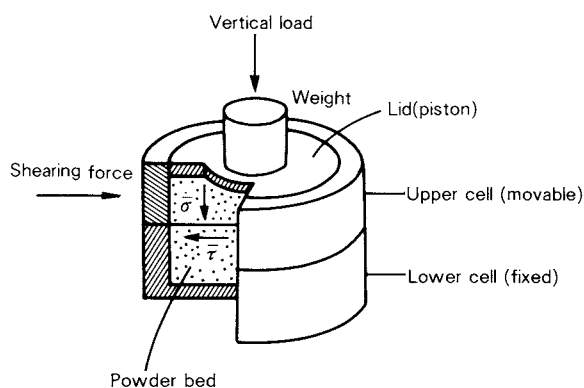


Fig. 1 Direct shearing of powder bed

powder bed tested increase.

Ashton *et al.*¹²⁾ conducted a series of shear tests for various cohesive powders by using Jenike cell^{13,14)} (a kind of constant load direct shear testers). They changed the initial void fraction (or the bulk density) of the powder bed in the cell by adjusting the preconsolidation pressure to obtain a group of convex yield loci. They also derived Eq. (1) which is a modification of Coulomb's equation ($\tau = \mu \cdot \sigma + C$; τ = shear stress, σ = vertical stress, μ = internal friction factor, C = cohesive force on shearing):

$$(\tau/C)^n = \sigma/\sigma_{\max} + 1 \quad (1)$$

where σ_{\max} = tensile strength of powder bed [Pa]
 n = shear index [—]

This expression is sometimes called Farley-Valentin equation or Warren-Spring equation. Ashton *et al.* have found that the shear index is a representative factor of the flowability of a powder and takes the value of between 1 (for very flowable powders) and 2 (for highly cohesive powders). Eelkmanrooda¹⁷⁾, Nedderman¹⁸⁾, Kocova¹⁹⁾ and Williams *et al.*²⁰⁾ have also paid their attention to the shear index. Farley *et al.*¹⁵⁾ reported that the shear index decreased as the surface area of powder particles increased. Rumpf *et al.*²¹⁾, Farley *et al.*¹⁵⁾, Aoki *et al.*²²⁾ and Jimbo *et al.*²³⁾ measured the maximum tensile strength of powder beds to determine the shear index. Steinforth *et al.*³⁴⁾ tried to estimate the shear index only by fitting numerically an equation to the YL obtained. Recently, Tsunakawa *et al.*⁴⁾ pointed out that the shear index cannot be an estimate of the flowability of powders because the different samples give almost the same value of the index within the experimental error of $\pm 10\%$.

Umeya *et al.*⁷⁾ conducted a series of direct shear tests by changing the applied vertical stress over a wide range and obtained a convex yield locus similar to the one obtained by Jenike¹⁴⁾. They expressed the locus by Eq. (2):

$$\tau = K(\sigma + \sigma_0)^m \quad (2)$$

where m = deformation index, [—]
 K = deformation coefficient, [(Pa)^{1-m} or (Kg/cm²)^{1-m}]

and found that the parameters, m and K , depend on the properties and the packed state of

the powders tested. Eq. (2) is equivalent to Eq. (1). They also have shown that the yield locus can be divided into three parts represented by $m < 1$, $m > 1$ and $m = 1$ and that a convex deviation of the locus from Coulomb's law may be due to mutual concessions of the powder particles under shearing.

Jenike *et al.*^{13,14)} developed a flow factor tester (a kind of the constant load simple shear testers) which was designed to keep an initial packed state or an initial void fraction of the powder bed in the shearing cell, $\bar{\epsilon}_0$, as constant as possible. They claimed that the tester can provide yield loci under constant void fraction conditions if the shear test is done at the vertical stress less than the preconsolidation pressure. A series of the tests under various preconsolidation pressures can also give a set of the yield loci, the end point of which is at the respective preconsolidation pressure. The envelop of Mohr circles which are in contact with the yield loci at each end point, becomes the straight line passing through the origin as shown in Fig. 2. This fact has also been confirmed by Ashton *et al.*¹²⁾. This straight line is called an effective yield locus (E.Y.L.) and its slope an effective friction angle. It is reasoned that the convex nature of the yield locus is due to the energy consumed at the slip plane for dilatation of the powder bed under shearing, which is added to the friction force between solid particles.

It can be noted from the survey of the literatures reported so far, that the vertical stress and its distribution in the vicinity of shearing plane have not yet been measured directly. All the yield loci reported so far are based on an apparent vertical stress calculated from the externally applied vertical load on the shearing cell, divided by the shearing area. It is also

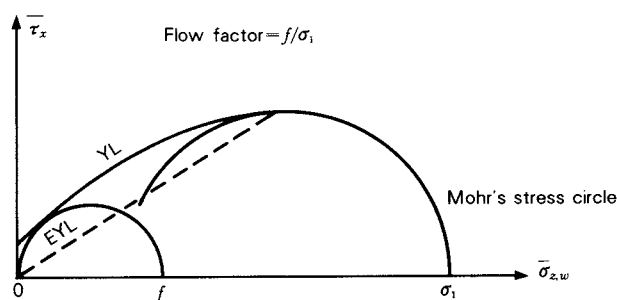


Fig. 2 Yield locus, effective yield locus and Jenike's flow factor

noteworthy that little attempt has been made to measure the shear force and the dilatation and/or contraction of the powder bed in the shearing cell simultaneously, though the volume change in the bed has been long considered to take place as a result of shearing^{1,11,25,26,35}).

Consider a “differential” area, dS , on the shearing plane (area S) in a powder bed under shearing (“differential” in this case means very small but still as large as sufficient numbers of solid particles can be contained so that the identity as a powder is not lost) as shown in Fig. 3. The vertical stress applied on dS , σ_z , and the shearing stress, τ_x , can be related by Eq. (3), if Coulomb’s law without cohesive force is assumed to hold:

$$\tau_x \cdot dS = \mu \cdot \sigma_z \cdot dS \quad (3)$$

where μ represents an internal friction factor.

Integration of Eq. (3) over the whole shearing plane gives Eq. (4) if μ is assumed to be a constant:

$$T_x = \mu \cdot \Sigma_z \quad (4)$$

where

$$T_x = \int_S \tau_x \cdot dS \quad \Sigma_z = \int_S \sigma_z \cdot dS$$

Eq. (4) may be rewritten by introducing the mean values as follows:

$$\bar{\tau}_x = \mu \cdot \bar{\sigma}_z \quad (5)$$

where

$$\bar{\tau}_x = T_x/S, \quad \bar{\sigma}_z = \Sigma_z/S$$

It should be noticed that the results of con-

ventional shear tests have not been expressed in terms of τ_x and σ_z but in terms of $\bar{\tau}_x$ and $\bar{\sigma}_z$. Although shearing does not take place on a single plane but in multiple layers^{8,27,28,29}, it may be allowed that the mean value, $\bar{\tau}_x$, of the measured shear force, T_x , divided by the shearing area, S , is regarded as τ_x . It is still controversial, however, whether the whole vertical load externally applied, Σ_w (the weight put on the powder bed in the shearing cell), can be assumed to be equal to Σ_z (the vertical load in the vicinity of the shearing plane). As is well known, the pressure force applied on the top of a powder bed never propagates isotropically throughout the bed and there is no universal and quantitative law on the propagation of pressure force through a powder bed. Whether Σ_z equals to Σ_w is dependent on materials, methods of measurements and experimental conditions. It is worthy to note that Aoki *et al.*¹⁰ have used Janssen’s formula to correct the difference between Σ_z and Σ_w . It has also been found, however, that the formula cannot be applied to the powder bed under shearing but to stationary powder beds^{30,31}).

If the $\tau_x - \sigma_z$ relation is linear, it may be possible to calculate a universal internal friction factor μ from Eq. (5) by measuring the actual vertical stresses at several points in the vicinity of the shearing plane and regarding their arithmetic mean as σ_z . With this in mind, we have developed an improved direct shear tester to test a variety of powders under various experimental conditions.

3. Experimental

The direct shear tester developed is shown in Fig. 4, which can test powders under both a constant load and a constant volume conditions. The tester has a pair of cylindrical shearing cells with the inner diameters of 40, 80, 100 and 120 mm; the upper part ⑤ is fixed and the lower one ⑥ movable. The shear rate can be varied over the range of 0.25 to 15 mm/min.

In case of constant load shear tests, both the weight ⑨ and the length of lever on the beam ③ were adjusted to change the vertical load on the powder bed in the shearing cell from 0.78 to 147 kPa. In case of constant volume shear tests, on the other hand, the beam ③ was fixed tightly at the horizontal position by the clamp ⑫ installed on the

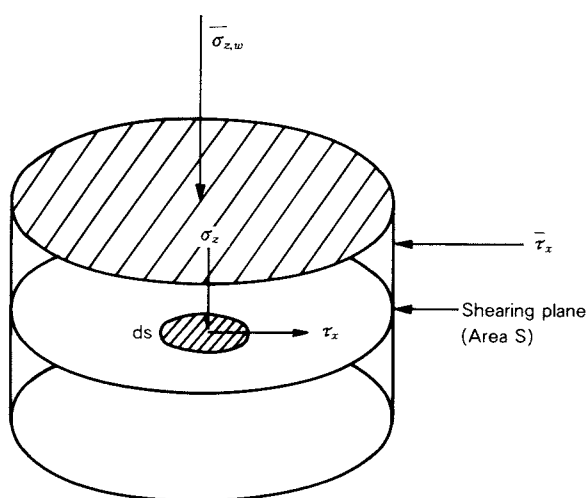


Fig. 3 Stress on shearing plane

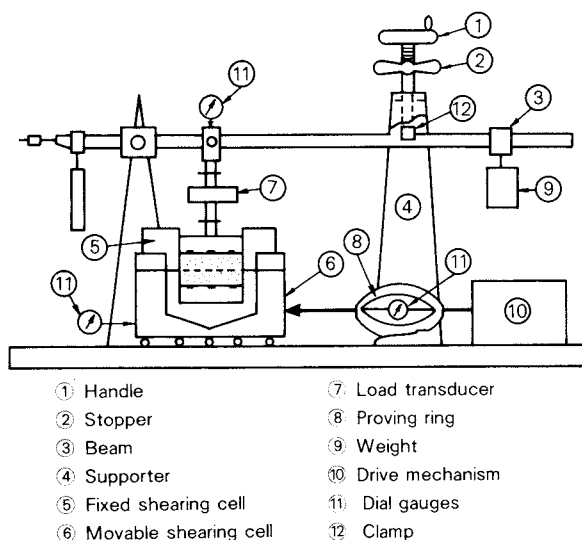


Fig. 4 Direct shear tester

supporter ④ and the stopper ② to keep the powder bed volume in the shearing cell constant during a course of shearing. The compressive load transducer ⑦ connected to the lid of the shearing cell measures the vertical force Σ_w which is a part of the expanding force of the powder bed under shearing.

The proving ring ⑧ and the electric dial

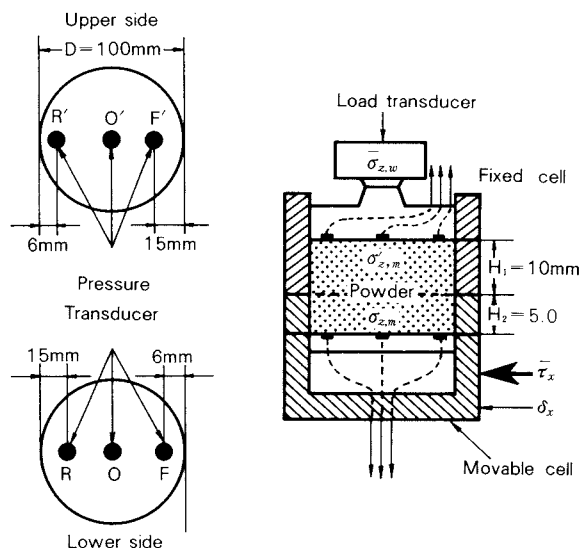


Fig. 5 Layout of pressure transducers in the vicinity of shearing plane

gauge ⑪ were used to determine the shear force T_x . The horizontal or shearing displacement δ_x was measured by using the electrical dial gauge ⑪ attached to the side wall of the movable cell ⑥. To observe dilatation and/or contraction of the powder bed in the shearing cell during a course of constant load shear tests, the dial gauge ⑪ was put on the part of the

Table 1 Properties of powders tested

Powder		Mean diameter [μm]	Density [kg/m^3]	Bulk density [kg/m^3]
Coarse powders	Zircon sand	130	4,660	2,910
	Toyoura sand	200	2,730	1,610
	Glass powder	220	2,620	1,240
	White alundum	190	3,800	2,010
	Sodium carbonate	180	2,550	1,030
	Potassium bicarbonate	152	2,240	1,240
	P.V.C. powder	160	1,560	570
	Glass spheres I	140	2,560	1,580
	Glass spheres II	960	2,690	1,570
	Carborandum	670	3,270	1,690
	Iron powders	80	7,860	2,220
Fine powders	Calcium carbonate (P-30)	1.75	2,700	530
	Talc	1.50	2,830	590
	Sugar powder	1.15	1,510	410
	Carbon black	1.44	1,800	170
	Magnesium stearate	1.75	1,040	200
	Zinc oxide	0.73	2,070	530
	Kanto loam (JIS #11)	0.82	3,000	460
	Corn starch	0.97	1,510	340
	Flyash	2.42	2,140	530
	Titanium oxide	0.2 ~ 0.4	3,930	350
	Alumina	0.5 ~ 3	3,980	780
	Soft flour	1 ~ 10	1,460	320
	Kaolin	1 ~ 10	2,850	390

beam ③ just above the center of the shearing cell.

In order to measure the actual vertical stresses in the vicinity of shearing plane, each three pressure transducers of a strain gauge type of 6 mm diameter were installed in both the upper and lower shearing cells, as shown in Fig. 5.

All the electric signals from these transducers were recorded on a multi-pen recorder and/or an X-Y recorder, or on a data-acquisition system with a micro computer, simultaneously from the beginning to the end of a shear test.

Since the shearing process in a direct shear test exhibits a variety of characteristics depending on the initial void fraction \bar{e}_0 of the powder bed in the shearing cell and hence it is indispensable to vary the void fraction positively over a wide range, it is essential to pack the sample powder into the cell as uniformly as possible. In case of the experiments under dense packing, the sample powder was charged into the cell little by little to a specified bed height and the surface of the powder bed was leveled by a flat plate at every moment of powder charge. Then, a preconsolidation pressure, $\bar{\sigma}_{z,p}$, is applied to the bed until the bed height stops changing. After $\bar{\sigma}_{z,p}$ was removed, the bed was sheared under various vertical stresses of less than $\bar{\sigma}_{z,p}$.

In case of the experiments under loose pack-

ing, on the other hand, the sample powder was charged gently into the cell at a stretch, then the surface of the bed was leveled by a wiper and even no preconsolidation pressure was applied in some cases. The sample powders used in our experiments and their properties are summarized in Table 1.

4. Results and discussion

4. 1 Constant load direct shear tests

The horizontal (shearing) displacement δ_x — shearing stress $\bar{\tau}_x$ and δ_x — vertical displacement δ_z curves (will be called the shearing process characteristics in what follows) for all the sample powders under various initial void fractions could be classified into the three typical patterns as shown in Fig. 6: Pattern I (dense packing), Pattern II (optimal packing) and Pattern III (loose packing). The table below Fig. 6 shows the effects of the shearing cell diameter D and the height of the powder bed in the upper fixed cell H_1 on the interrelations between the external vertical stress applied, $\bar{\sigma}_{z,w}$ and the actual mean vertical stress, $\bar{\sigma}_{z,m}$ (the arithmetic mean of the vertical stresses measured at the points R , O and F in Fig. 5) in the vicinity of the shearing plane. The height of the bed in the lower movable cell has been kept constant at 5 mm, which has been deter-

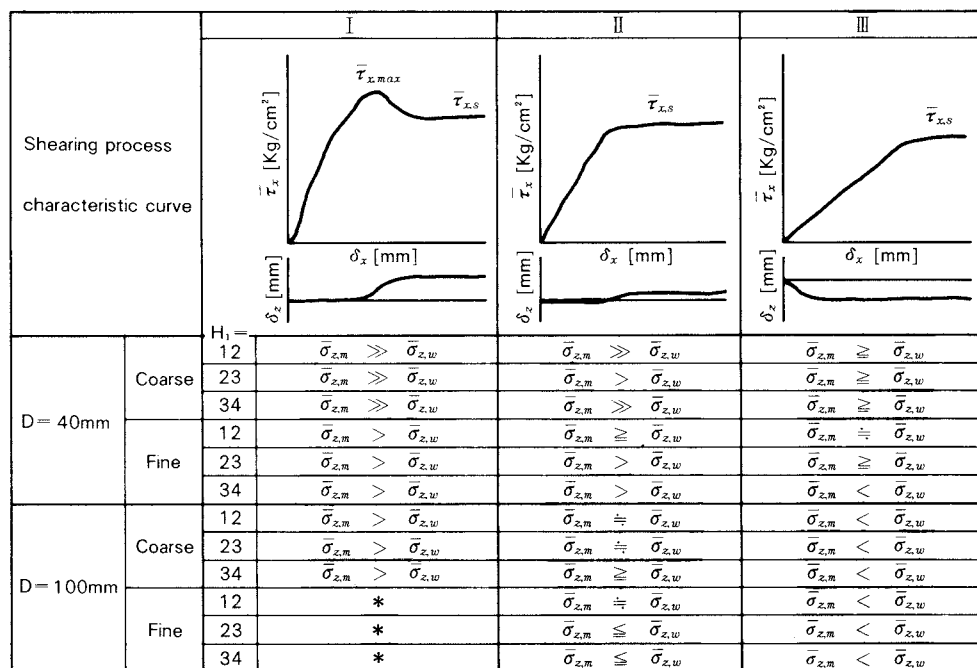


Fig. 6 Shearing process characteristics

mined by another series of experiments. The interrelations between $\bar{\sigma}_{z,w}$ and the mean actual vertical stress at the points R' , O' and F' in Fig. 5, $\bar{\sigma}_{z,m}$ have been very similar to those between $\bar{\sigma}_{z,w}$ and $\bar{\sigma}_{z,m}$. As can be seen from Fig. 6, in the case of the Pattern I shearing process characteristics, the shear stress $\bar{\tau}_x$ increases steeply, and reaches a steady state value $\bar{\tau}_{x,s}$ after showing a clear maximum value $\bar{\tau}_{x,max}$. The vertical displacement δ_z is rather large in the positive direction and this means an expansion of the powder bed in the cell from a state of small initial void fraction (dense packing). In this case, the distribution of the vertical stress in the vicinity of shearing plane is not uniform and generally $\bar{\sigma}_{z,m}$ is larger than $\bar{\sigma}_{z,w}$ in the majority of cases. In the case of the Pattern III, on the other hand, $\bar{\tau}_x$ increases slowly and monotonically to reach a steady state value $\bar{\tau}_{x,s}$ at a large value of δ_x without showing a maximum. The vertical displacement δ_z is rather large in the negative direction, and this implies the contraction of the powder bed with a loose initial packing upon shearing. In this case, $\bar{\sigma}_{z,m}$ is generally smaller than $\bar{\sigma}_{z,w}$.

On the contrary, in the case of the Pattern II, where $\bar{\tau}_x$ reaches a steady state value $\bar{\tau}_{x,s}$ at a rather small value of δ_x without showing a maximum, and the vertical displacement δ_z is almost constant around nearly zero, $\bar{\sigma}_{z,m}$ is very close to $\bar{\sigma}_{z,w}$ in many cases.

These findings suggest that the internal friction factor can be correctly estimated by using $\bar{\sigma}_{z,w}$ only in the limited cases when the shearing process characteristics show the Pattern II. It is highly desirable, however, to measure the actual vertical stresses in the vicinity of shearing plane, or otherwise the vertical displacement of the powder bed in the shearing cell, δ_z , should be measured at least.

(1) Effect of powder bed height H_1 on $\bar{\tau}_x - \bar{\sigma}_z$ relation

Figs. 7, 8 and 9 show the effects of the upper powder bed height H_1 on the yield loci in terms of $\bar{\tau}_x - \bar{\sigma}_{z,w}$ and $\bar{\tau}_x - \bar{\sigma}_{z,m}$ relations. In Fig. 8, $\mu_{m,max}$ stands for the internal friction factor calculated from the $\bar{\tau}_{x,max} - \bar{\sigma}_{z,m}$ relation and $\mu_{m,s}$ from $\bar{\tau}_{x,s} - \bar{\sigma}_{z,m}$ relation, respectively. It is clear from Fig. 9 and a comparison of Fig. 8 with Fig. 7, that all the $\bar{\tau}_{x,max} - \bar{\sigma}_{z,m}$ and $\bar{\tau}_{x,s} - \bar{\sigma}_{z,m}$ relations with different values of H_1 fall into the respective single lines to give

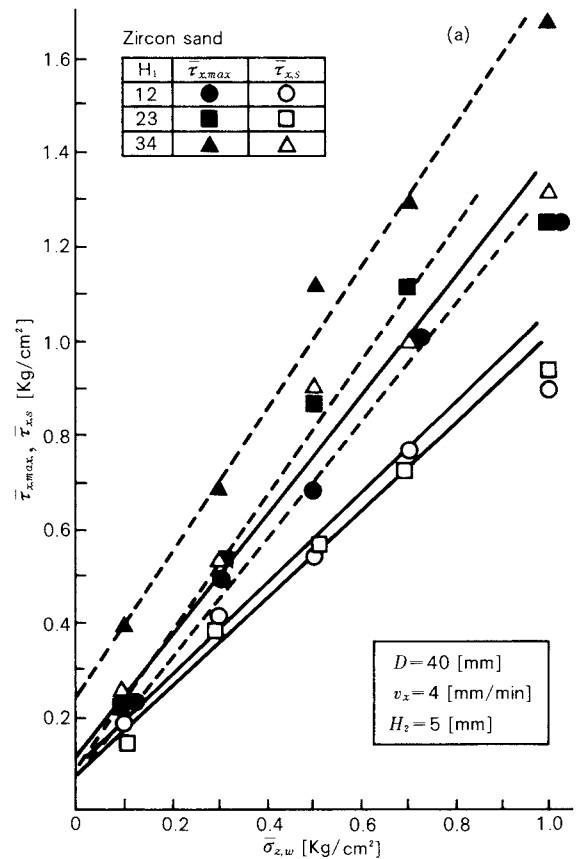


Fig. 7 Effect of upper powder bed height H_1 on the yield locus of a coarse powder in terms of $\bar{\tau}_x$ and $\bar{\sigma}_{z,w}$

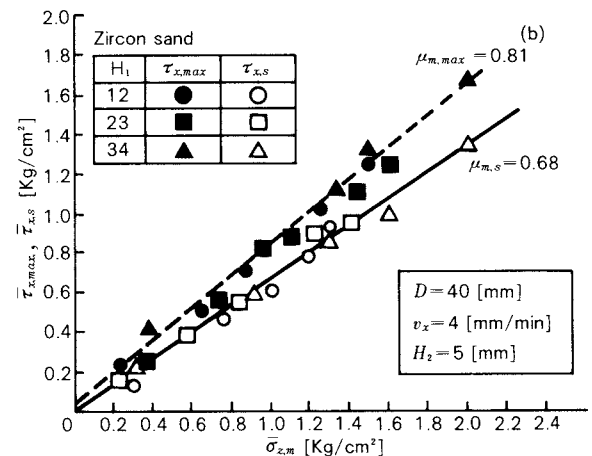


Fig. 8 Effect of upper powder bed height H_1 on the yield locus of a coarse powder in terms of $\bar{\tau}_x$ and $\bar{\sigma}_{z,m}$

the internal friction factors independent fairly of H_1 , though the internal friction factors evaluated from the $\bar{\tau}_x - \bar{\sigma}_{z,w}$ relations have been influenced by H_1 . This finding has also been observed in the shear tests of the other powders.

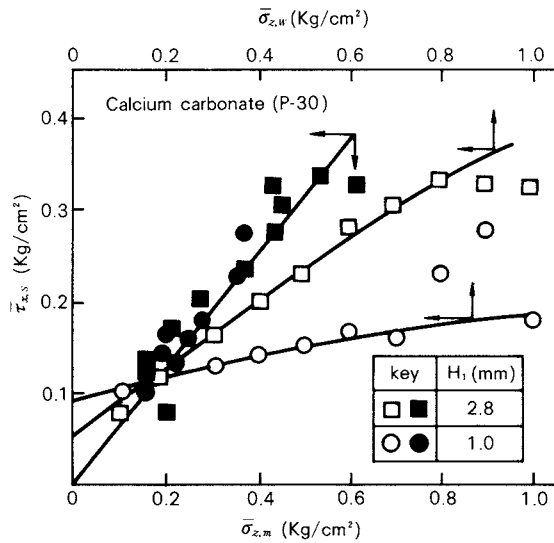


Fig. 9 Effect of upper powder bed height H_1 on the yield locus of a fine powder in terms of $\bar{\tau}_{x,s} - \bar{\sigma}_{z,w}$ and $\bar{\tau}_{x,s} - \bar{\sigma}_{z,m}$ relations

(2) Effect of shearing cell diameter D on $\bar{\tau}_x - \bar{\sigma}_z$ relation

As shown in Fig. 10, the diameter of the shearing cell D does not affect the $\bar{\tau}_{x,s} - \bar{\sigma}_{z,m}$ relations, and thus the internal friction factors independent of D can be obtained.

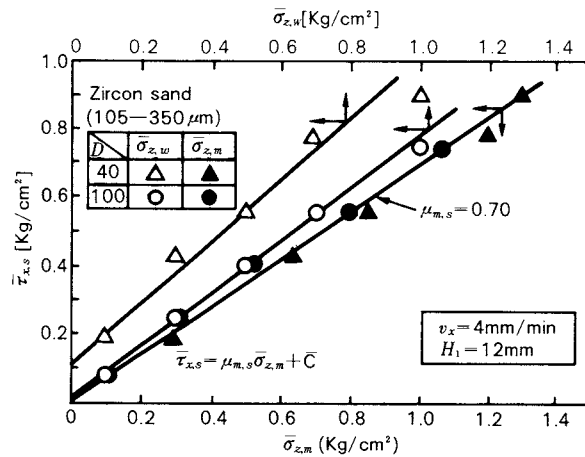


Fig. 10 Effect of shearing cell diameter D on the yield locus of a coarse powder in terms of $\bar{\tau}_{x,s} - \bar{\sigma}_{z,w}$ and $\bar{\tau}_{x,s} - \bar{\sigma}_{z,m}$ relations

(3) Effect of initial void fraction $\bar{\epsilon}_0$ on $\tau_x - \bar{\sigma}_z$ relation

The initial void fraction $\bar{\epsilon}_0$ has been calculated by Eq. (6):

$$\bar{\epsilon}_0 = 1 - M/\rho V \quad (6)$$

where M = mass of powder charged in shearing cell, [kg]

V = initial volume of powder in shearing cell, [m^3]

ρ = density of powder particle, [kg/m^3]

The effects of $\bar{\epsilon}_0$ on the $\bar{\tau}_x - \bar{\sigma}_z$ relations are shown in Fig. 11 for a coarse powder and in Figs. 12 and 13 for fine powders. It can be seen from these figures, that the $\bar{\tau}_{x,s} - \bar{\sigma}_{z,m}$ relations are fairly independent of $\bar{\epsilon}_0$, thus giving the unique or universal internal friction factor. The relations shown in Fig. 12 should be paid a special attention; although the $\bar{\tau}_{x,s} - \bar{\sigma}_{z,m}$ relations are convex for respective $\bar{\epsilon}_0$'s as is often the case for fine powders, the $\bar{\tau}_{x,s} - \bar{\sigma}_{z,m}$ relation gives a single straight line and is independent of $\bar{\epsilon}_0$. Since it is conventional to calculate the shear index n according to Warren-Spring equation, Eq. (1), in the case of convex $\bar{\tau}_{x,s} - \bar{\sigma}_{z,w}$ relations, we have also done such calculations. The results, however, have been pessimistic and strongly influenced by the experimental conditions, and so scattered that the shear index n cannot be any representative

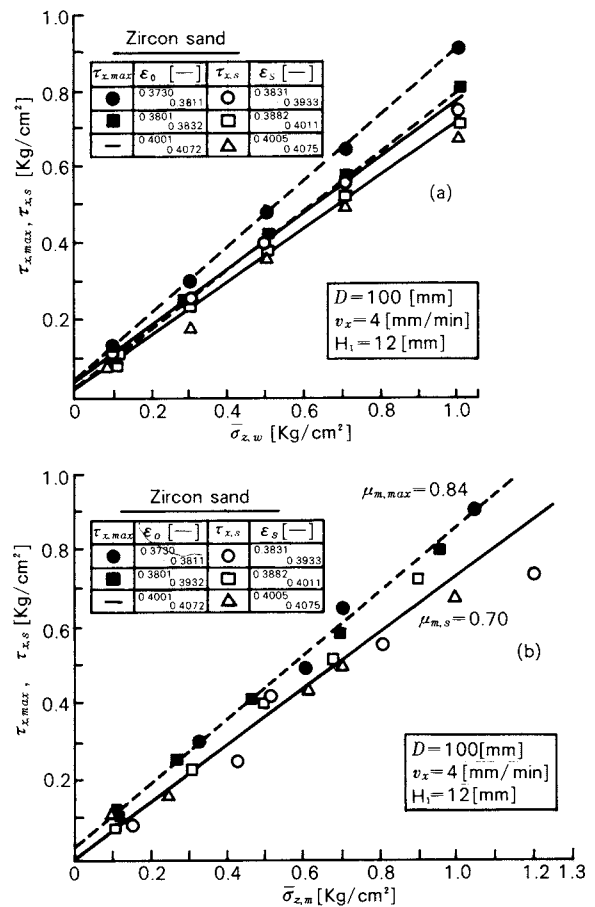


Fig. 11 Effect of initial void fraction $\bar{\epsilon}_0$ on the yield locus of a coarse powder in terms of $\bar{\tau}_x - \bar{\sigma}_{z,w}$ and $\bar{\tau}_x - \bar{\sigma}_{z,m}$ relations

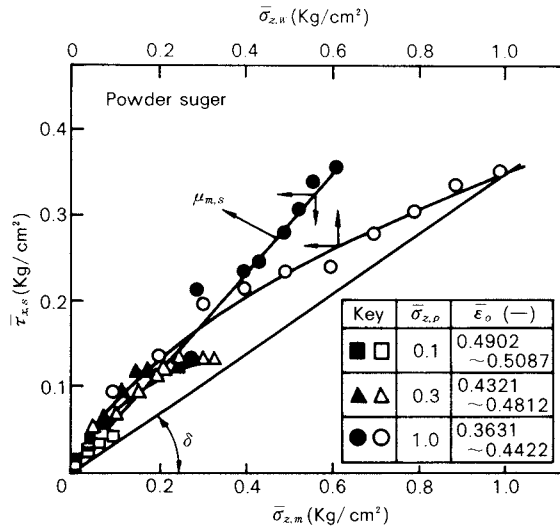


Fig. 12 Effect of initial void fraction $\bar{\epsilon}_0$ on the yield locus of a fine powder in terms of $\bar{\tau}_{x,s} - \bar{\sigma}_{z,w}$ and $\bar{\tau}_{x,s} - \bar{\sigma}_{z,m}$ relations

of the friction characteristics of powders. This has also been the case in calculating Jenike's flow factor.

(4) $\bar{\tau}_x - \bar{\sigma}_z$ relation under low vertical stresses

As a typical example of showing an appreciable difference between the $\bar{\tau}_{x,s} - \bar{\sigma}_{z,w}$ relation and the $\bar{\tau}_{x,s} - \bar{\sigma}_{z,m}$ relation, the results of the

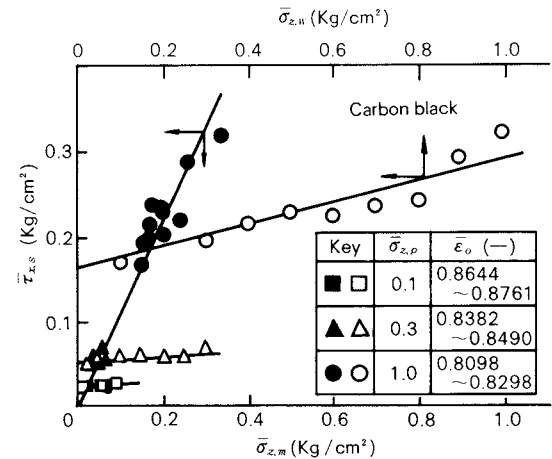


Fig. 13 Effect of initial void fraction $\bar{\epsilon}_0$ on the yield locus of a fine powder in terms of $\bar{\tau}_{x,s} - \bar{\sigma}_{z,w}$ and $\bar{\tau}_{x,s} - \bar{\sigma}_{z,m}$ relations

simple shear tests under low vertical stresses are shown in Fig. 14. In spite of convex nature in the $\bar{\tau}_{x,s} - \bar{\sigma}_{z,w}$ relation, the relation between $\bar{\tau}_{x,s}$ and $\bar{\sigma}_{z,m}$ has become a straight line as well. Besides, it has been verified that even some of fine powders give the shearing process characteristics of the Pattern I in Fig. 6 under low vertical stresses (one order of magnitude lower than the case of coarse powders). Unfortunately-

Table 2 Internal friction factors of powders tested

Powder		$\mu_{m,s}$	$\mu_{m,max}$
Coarse powders	Zircon sand	0.68 ~ 0.70	0.81 ~ 0.84
	Toyoura sand	0.62	0.84
	Glass powder	0.87	0.92
	White alundum	0.75	0.80
	Sodium carbonate	0.75	0.83
	Potassium bicarbonate	0.83	0.86
	P.V.C. powder	0.70	0.80
	Glass spheres-I	0.30	0.35
	Glass spheres-II	0.31	0.39
	Carborandum	0.73	0.80
	Iron powder	0.85	0.91
Fine powders	Calcium carbonate (P-30)	0.67	—
	Talc	0.42	—
	Sugar powder	0.55	—
	Carbon black	1.10	—
	Magnesium stearate	0.64	—
	Zinc oxide	1.02	—
	Kanto loam (JIS #11)	0.78	—
	Corn starch	0.81	—
	Flyash	0.46	—
	Titanium oxide	1.23	—
	Alumina	0.65	—
	Soft flour	0.78	—
	Kaolin	0.80	—

Table 3 Internal friction factors by constant-volume and constant-load shear testers

Powder (Mean diameter, μm)	μ by const. volume shear test	$\mu_{m,s}$ or $\mu_{m,\max}$ by const. load shear test
Toyouura sand (200)	0.88	0.84
Glass powder (180)	0.64	0.57
White alundum (150)	0.50	0.45
Glass sphere-II (140)	0.40	0.39
Magnesium stearate (1.75)	0.63	0.64
Sugar powder (1.15)	0.62	0.55

The results of the constant load and volume shear tests for a glass powder ($210 \sim 350\mu\text{m}$) are compared with each other in Fig. 15. Since $\bar{\tau}_{x,\max}$ is considered to be observed as the shear stress in case of the constant volume direct shear test, the $\bar{\tau}_{x,\max} - \bar{\sigma}_{z,w}$ and $\bar{\sigma}_{z,m}$ relations are shown in Fig. 15. The $\bar{\tau}_{x,\max} - \bar{\sigma}_{z,m}$ relations in the both tests are almost identical with each other. The $\bar{\tau}_{x,\max} - \bar{\sigma}_{z,m}$ relations in the both cases are also similar to each other and they have a less steep slope.

Figs. 16 and 17, respectively, compare the result of constant volume shear test with those of constant load test for sugar powder ($1.15\mu\text{m}$) and for Magnesium Stearate ($1.75\mu\text{m}$). In these figures, the yield loci in terms of $\bar{\tau}_{x,s}$ and $\bar{\sigma}_{z,m}$ are shown by broken lines. Since $\bar{\tau}_{x,s}$ is considered to be observed as the shear stress in case of the constant volume shear test of fine powders, the $\bar{\tau}_{x,s} - \bar{\sigma}_{z,w}$ and $\bar{\sigma}_{z,m}$ relations are plotted. It can be seen from Figs. 16 and 17, that the $\bar{\tau}_{x,s} - \bar{\sigma}_{z,w}$ relations obtained by the constant volume test are convex as if they deviate from Coulomb's law, the $\bar{\tau}_{x,s} - \bar{\sigma}_{z,m}$ relations, however, can be regarded to be almost linear with some data scattered. An agreement between the results of the constant load and volume shear tests is fairly well.

The internal friction factors obtained by the both shear tests are summarized in Table 3 for a couple of the powders. The internal friction factors of the coarse powders in this table are based on the $\bar{\tau}_{x,\max} - \bar{\sigma}_{z,m}$ relations and those of the fine powders on the $\bar{\tau}_{x,s} - \bar{\sigma}_{z,m}$ relations. They may be considered to be in a good agreement with each other.

5. Conclusion

It has been made clear by illustrating some examples, that the measurements of the actual vertical stress and its distribution in the vicinity

of shearing plane are indispensable for evaluating a universal internal friction factor of a powder bed, which is fairly independent of experimental methods and conditions, by simple direct shear tests. If the actual vertical stresses cannot be measured in case of the constant load shear test, the initial void fraction of the powder bed in the shearing cell should be varied over a certain range to find the experimental condition where almost no dilatation and/or contraction of the powder bed takes place. Therefore, it is at least necessary to measure the vertical displacement of the powder bed during a course of shearing.

If the vertical stresses in the vicinity of shearing plane cannot be measured in case of the constant volume shear test, on the other hand, there is no way to evaluate a universal internal friction factor but to know the effect of the upper powder bed height on the yield loci. Even after the effect is known, however, there still remains a problem unsolved in how the yield loci are to be extrapolated to zero bed height.

In either case, the flowability or similar characteristics of a powder can be assessed by the internal friction factor only if the factor is correctly evaluated and is fairly independent of the experimental methods and conditions.

Nomenclature

- C : shearing cohesive force [Pa or Kg/cm^2]
- D : inside diameter of shearing cell [m]
- H_1 : height of powder bed in upper shearing cell [m]
- H_2 : height of powder bed in lower shearing cell [m]
- K : deformation coefficient, defined in Eq. (2) $[(\text{Pa})^{1-m} \text{ or } (\text{Kg}/\text{cm}^2)^{1-m}]$
- m : deformation index, defined in Eq. (2) [—]
- M : mass of powder in shearing cell [kg]
- n : shear index, defined in Eq. (1) [—]

- S : cross sectional area of shearing cell [m²]
 T_x : total shear force [N or Kg]
 v_x : shearing rate [m/s]
 V : initial volume of powder in shearing cell [m³]
 δ_x : shearing or horizontal displacement [m]
 δ_z : vertical displacement of powder bed in shearing cell [m]
 $\bar{\epsilon}_0$: initial void fraction of powder bed in shearing cell [—]
 μ : internal friction factor [—]
 $\mu_{m, \max}$: internal friction factor derived from $\bar{\tau}_{x, \max}$ — $\bar{\sigma}_{z, m}$ relation [—]
 $\mu_{m, s}$: internal friction factor derived from $\bar{\tau}_{x, s}$ — $\bar{\sigma}_{z, m}$ relation [—]
 ρ : density of powder particle [Kg/m³]
 σ_z : vertical stress in powder bed [Pa or Kg/cm²]
 $\bar{\sigma}_{z, m}$: actual mean vertical stress in the vicinity of shearing plane [Pa or Kg/cm²]
 $\bar{\sigma}_{z, p}$: preconsolidation pressure [Pa or Kg/cm²]
 $\bar{\sigma}_{z, w}$: apparent vertical stress calculated from external load applied, $\Sigma_{z, w}$ [Pa or Kg/cm²]
 $\Sigma_{z, w}$: external vertical load [N or Kg]
 τ_x : shearing force [N or Kg]
 $\bar{\tau}_x$: shearing stress calculated from T_x [Pa or Kg/cm²]
 $\bar{\tau}_{x, \max}$: maximum value of $\bar{\tau}_x$ during a course of shearing [Pa or Kg/cm²]
 $\bar{\tau}_{x, s}$: steady state value of $\bar{\tau}_x$ during a course of shearing [Pa or Kg/cm²]

References

- 1) Taneya, S. and T. Sone: *Oyo Butsuri (A monthly publication of the Japanese Society of Applied Physics)*, **31**, 286 (1962).
- 2) Yamafuji, K. and R. Aoki: *Kagaku Kogaku (A monthly publication of the Society of Chemical Engineers, Japan)*, **28**, 691 (1964).
- 3) Tsunakawa, H. and R. Aoki: *Journal of the Research Association of Powder Technology, Japan*, **11**, 263 (1974).
- 4) Tsunakawa, H. and T. Saegusa: *Journal of the Society of Powder Technology, Japan*, **15**, 342 (1978).
- 5) Takagi, F. and M. Sugita: *ibid.*, **16**, 277 (1979).
- 6) Ohtsubo, K.: *Funtai Kogaku*, **1**, 27 (1964).
- 7) Umeya, K., N. Kitamori, M. Araki and H. Mima: *Journal of the Society of Material Science, Japan*, **15**, 166 (1966).
- 8) Umeya, K., N. Kitamori, R. Hara and T. Yoshida: *ibid.*, **18**, 489 (1969).
- 9) Shinohara, K. and T. Tanaka: *Kagaku Kogaku*, **32**, 88 (1968).
- 10) Aoki, R. and H. Tsunakawa: *J. Chem. Eng., Japan*, **6**, 462 (1973).
- 11) Umeya, K., R. Hara, T. Yoshida and S. Naruhiro: *Journal of the Society of Material Science, Japan*, **19**, 521 (1970).
- 12) Ashton, M. D., D. C. H. Cheng, R. Farley and F. H. H. Valentin: *Rheol. Acta*, **4**, 206 (1965).
- 13) Andrew, W. and A. W. Jenike: *Trans. Instn. Chem. Engrs.*, **40**, 264 (1962).
- 14) Jenike, A. W.: *Bull. of Univ. of Utah*, No. 108 (1961), No. 123 (1964).
- 15) Farley, R. and F. H. H. Valentin: *Trans. Instn. Chem. Engrs.*, **43**, 1973 (1965).
- 16) idem: *Powder Technology*, **1**, 344 (1967/68).
- 17) Eelkmanrooda, J.: *ibid.*, **12**, 97 (1975).
- 18) Nedderman, R. M.: *ibid.*, **19**, 287 (1978).
- 19) Kocova, S. N. and N. Pilpel: *ibid.*, **5**, 329 (1971/72).
- 20) Williams, J. C. and A. H. Birks: *ibid.*, **1**, 199 (1967).
- 21) Rumpf, H. and H. Schubert: *J. Chem. Eng., Japan*, **7**, 294 (1974).
- 22) Aoki, R. and H. Tsunakawa: *Journal of the Society of Material Science, Japan*, **18**, 497 (1969).
- 23) Jimbo, G., S. Asakawa and H. Soga: *ibid.*, **17**, 540 (1968).
- 24) Umeya, K., T. Isoda, R. Hara and Y. Kato: *ibid.*, **22**, 637 (1973).
- 25) Yamaguchi, H.: "Tsuchi no Rikigaku" (Soil Mechanics), p.26, Kyoritsu Pub. Co. (1976).
- 26) Terashita, K., K. Miyanami, M. Yoshida and T. Yano: *Journal of the Society of Powder Technology, Japan*, **15**, 515 (1978).
- 27) Morgenstern, N. R. and J. S. Tchalenko: *Geotechnique*, **17**, 309 (1967).
- 28) Schwedes, J.: *Powder Technology*, **11**, 59 (1975).
- 29) Miyanami, K., K. Terashita, T. Ozaki and T. Yano: *Journal of the Society of Powder Technology, Japan*, **16**, 173 (1979).
- 30) Terashita, K., K. Miyanami, T. Yano and S. Uno: *ibid.*, **16**, 394 (1979).
- 31) Terashita, K., K. Miyanami and T. Yano: *ibid.*, **16**, 406 (1979).
- 32) Terashita, K., K. Miyanami, T. Yamamoto and T. Yano: *ibid.*, **15**, 526 (1978).
- 33) Terashita, K., K. Miyanami, T. Yano and Y. Yamamoto: *ibid.*, **15**, 583 (1978).
- 34) Steinforth, P. T. and R. E. R. Berry: *Powder Technology*, **8**, 243 (1973).
- 35) Stutz, P: Comportement elasto-plastique des milieux granulaires, A. Sawczuk, ed. "Mechanics of Plastic Solids", p.37-p.49, Noordhoff International Publishing, Netherland (1973).

The Development and Evaluation of New Measuring Methods of the Adhesion Force of Single Particles

Genji Jimbo* and Ryohei Yamazaki*

Department of Chemical Engineering,
Nagoya University

Abstract

To make clear the problems in the measurement of the adhesion force of powder, new measuring principles and methods were developed, in which emphasis was laid on extending measuring ranges especially to high temperature condition.

As measuring methods for the adhesion force of single particles, vibration and impaction separation methods were developed, and it was found that in separating a particle, the rolling motion by tangential force was very important, for which a fundamental equation was derived. The application of this tangential force to the adhesion measurement was proposed. Some additional measurements were carried out at high temperature to investigate the effect of temperature on the adhesion force of single particles.

1. Introduction

A large number of phenomena concerning particulate materials are still unexplained and the reason for the present great dependence on the experiences in making use of the phenomena or in solving the problems caused by them is the poor knowledge about the fundamental dynamic properties of the particulate materials. In spite of the active researches and developments of the measuring methods for the adhesion, agglomeration, friction property, flowability etc, of the powder for these 20 years, especially these 5 years, it is still difficult to say that they provide enough accuracy, reproducibility and exchangeability of the data among them. Above all, with regard to the adhesion force of powder, the measured values are extremely different depending upon the measuring method, as the authors have reported previously.¹⁾ Some examples gave the difference of the adhesion force of a single particle in the range of the seventh power of ten.

On the other hand, the necessity for the

measurement of the adhesion force shows increasing variety including that at high temperature in the atmosphere of various gases or under the condition with mass transfer and chemical reactions, especially owing to the recent rapid development of new energy.

An improved measuring method has been developed to obtain the adhesion force which is regarded as an important fundamental physical property of powder. In this report, it was attempted to investigate the reasons for the variance of the measured data obtained by the various conventional methods and to extend the conditions for the measurement and the measuring range to a great extent by using the newly developed method.

2. Principles of measuring methods for adhesion force of single particles

The simplest method for the measurement of the adhesion force of single particles is performed separating the particles from solid surface in the normal direction to the contacting surface by some force. The features of the practical separation methods where the gravity, centrifugal and inertia forces working on the particles are mainly made use of for the separation, are summarized in **Table 1**.

* Furo-cho, Chigusa-ku, Nagoya, Aichi, 464
TEL. 052 (781) 5111

Received April 25, 1983

Table 1. The characteristics of various kinds of fundamental measuring methods of adhesion force of single particles

Principle	Characteristics and problems
Centrifugal separation method ²⁾ *	Almost established. Accurate but expensive. Difficult in high temperature condition.
Vibration separation method ^{3),4)} **	Simple but less accurate. Only in the range of small force.
Impaction separation method ⁵⁾ **	Difficult in the measurement of separation force. Less expensive. Easy to apply to high temperature case.

* denotes the methods investigated by the authors

** denotes the methods newly developed by the authors

Although the centrifugal separation method developed earliest among them is well known as a standardized one, it is disadvantageous as a general routine method because of the equipment's cost and its operational procedure and besides it is not suitable for the measurement at high temperature and under other special conditions. For these reasons, a vibration and an impaction separation method were tried to develop in order to increase the reliability of the measured adhesion force of a single particle by comparison of data and to make possible the measurement under special conditions including high temperature.

3. Measurement of adhesion force by impaction separation method

3. 1 Measuring method and experimental apparatus

As shown in Fig. 1, particles are dispersed and adhere to a plate (usually glass plate) which is fixed onto a base. By giving the base one-

dimensional vibration, some of the particles will be separated from the plate by separation force caused by the vibration. The proceeding of the separation is analysed by micrographs which are taken before and after the separation. The adhesion force is supposed to be equal to the separation force $m\alpha\omega^2$ where the weight of a particle m is calculated from the particle size. In this case, the vibration base should be inclined with a little angle so that the once separated particles may leave the plate swiftly.

The authors have found that the adhesion forces obtained by the vibration method with a simple modified vibration feeder were less than the data measured by the centrifugal method and that the fact was related to the inclination of the plate and the shape of vibration. Therefore, in the present experiments, a magnetic vibrator (Node made, Model VT-25) was used to produce strictly one-dimensional vibration and the inclination φ was exactly set.

3. 2 Measured results

Some examples of the adhesion force measured by the vibration separation method are shown in Figs. 2 and 3. The glass beads adopted here were Toshiba glass beads GB703K, from which only the beads blocking 145 mesh screen were used for the measurement. The glass plate applied was micro slide glass (Matsunami Glass Industries, Ltd.) with the 1st grade after JIS R3703.

In Figs. 2 and 3, the separation force F_s is taken on the abscissa and the residual percentage of particles on the ordinate. As reported previously²⁾, the relation described by the following logarithmic-normal distribution function has been found between the separation force and the residual percentage of particles.

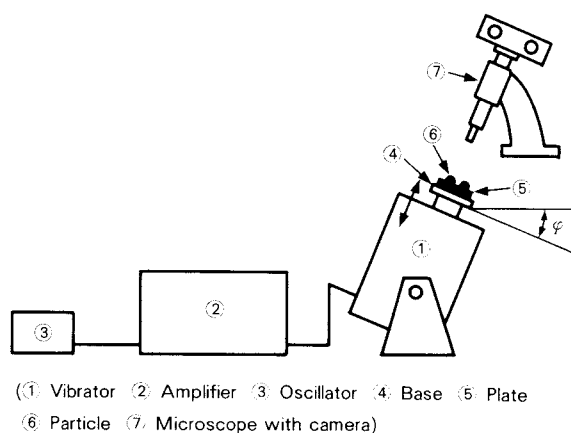


Fig. 1 The experimental apparatus of vibration separation method

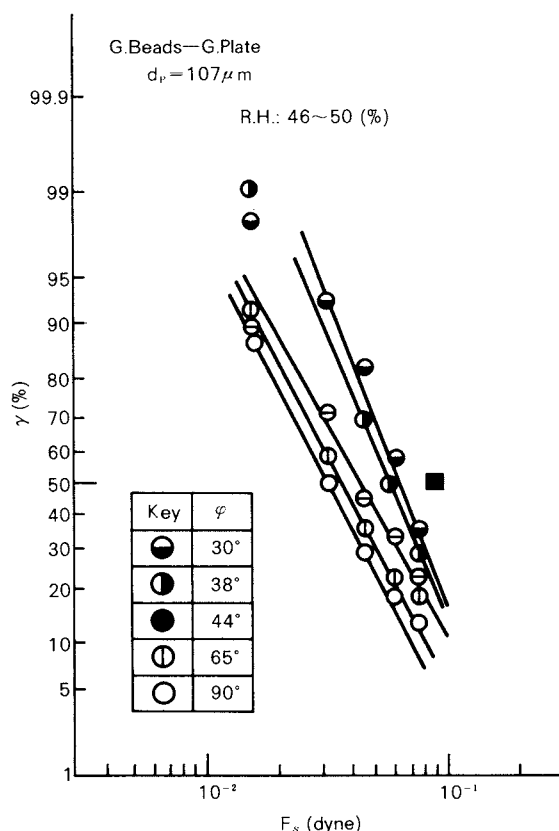


Fig. 2 The results of measurement of glass beads by vibration separation method (normal separation)

$$\gamma = \frac{100}{\sqrt{2\pi} \log \sigma} \int \exp \left[\frac{(\log F_s - \log \bar{F}_s)^2}{2 \log^2 \sigma} \right] \times d(\log F_s) \quad (1)$$

The effect of the inclination of the adhesion plate shown in Fig. 2 and the temperature effect in Fig. 3 will be discussed in the following section and in chapter 5, respectively.

3. 3 Discussion on the results

From the results obtained by the vibration method, some problems can be noticed with regard to the measurement of adhesion force by this method. First, it is generally difficult to give particles a large separation force with exactly one-dimensional vibration as seen in Fig. 3. Especially, when a heating device is attached to the vibrator, the intensity of the vibration is further reduced. Therefore in case large separation force is required, this vibration method is not suitable. Secondly, the adhesion force measured by this method was much smaller than that obtained by the centrifugal method as seen in Fig. 2, where the point with

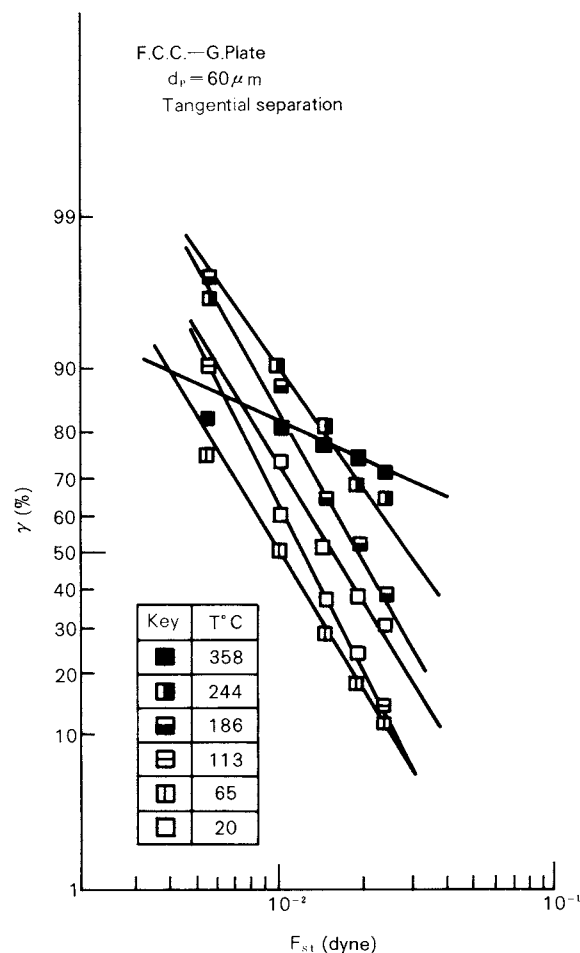


Fig. 3 The results of measurement of F.C.C. Particles by vibration separation method (tangential separation)

a symbol ■ is the value by the centrifugal method. It was also found that the difference was affected by the inclination φ .

3. 4 Analysis of measured adhesion force using a rolling model

The reduction of the adhesion force measured by the vibration method was tried to explain using a following rolling model.

A particle is supposed to adhere to a material with some contacting plane which can be approximated as a flat circle, as shown in Fig. 4. When a separation force is given on the particle by vibration, the normal component of the separation force F_{sn} acts to separate the particle from the contacting plane and at the same time the tangential component F_{st} acts to separate the particle by rotation around the bottom edge of the contacting plane H in general cases, because it is difficult to give the vibration in

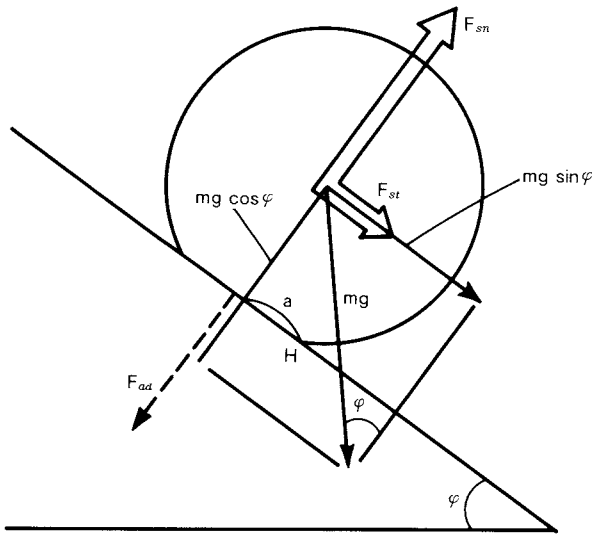


Fig. 4 The model of separation of a single particle from a plane surface.

the exactly vertical direction.

The momental balance around the point H is expressed by the following equation taking all these forces into consideration, where the adhesion force per unit area f_{ad} is supposed to work uniformly over the contacting plane.

$$aF_{sn} + 1/2(\sqrt{d_p^2 - 4a^2}) mg \sin \varphi + 1/2(\sqrt{d_p^2 - 4a^2}) F_{st} = \pi a^3 f_{ad} + amg \cos \varphi \quad (2)$$

From the above equation, the separation force F_{sn} is obtained as follows.

$$\begin{aligned} F_{sn} &= \pi a^2 f_{ad} + mg[\cos \varphi - (\sqrt{(d_p/2a)^2 - 1}) \\ &\quad \times \sin \varphi] - (\sqrt{(d_p/2a)^2 - 1}) F_{st} \\ &= F_{ad} + (\pi/6)d_p^3 \rho_s g[\cos \varphi - (\sqrt{(d_p/2a)^2 - 1}) \\ &\quad \times \sin \varphi] - (\sqrt{(d_p/2a)^2 - 1}) F_{st} \end{aligned} \quad (3)$$

This equation shows that the separation force F_{sn} is the adhesion force F_{ad} added by the forces implied in the 2nd and 3rd terms of the right hand side, which are usually negative.

With the reasonable assumptions of $d_p \gg a$, therefore

$$\sqrt{(d_p/2a)^2 - 1} \doteq d_p/2a$$

and $(d_p/a) \sin \varphi \gg \cos \varphi$, the equation (3) comes to the next equation.

$$F_{sn} \doteq F_{ad} - (\pi/6)d_p^3 \rho_s g(d_p/2a) \sin \varphi - (d_p/2a) F_{st} \quad (4)$$

As seen in this equation, the tangential component of the separation force F_{st} multiplied by $d_p/2a$, which is about 30 as discussed later, has the same magnitude as the normal component F_{sn} . This is the reason for the vibration to be required strictly one-dimensional.

(1) When only the effect of inclination is considered

As the tangential component of the vibration is neglected in this case,

$$F_s = F_{ad} - (\pi/6)d_p^3 \rho_s g(d_p/2a) \sin \varphi \quad (5)$$

The data shown in Fig. 2 are plotted in Fig. 5 which confirms the relation implied by the equation (5). From the gradient of the straight line in this figure and the equation (5), the radius of the contacting surface is calculated to be about $1.4 \mu\text{m}$.

The contacting condition may be expressed in the following Hertz's equation taking the pressure caused by the self weight and the adhesion force into consideration.

$$(a/d_p)^3 = (3/4)(mg/d_p^2)(1 - \nu)/E \quad (6)$$

From the equation with the practical data for glass ($\nu = 0.2$, $E = 8,000 \text{ kg/mm}^2$), the value a of deformation by self weight comes to about 230 \AA for a particle of $d_p = 107 \mu\text{m}$. It is much smaller even added by the adhesion force than $1.4 \mu\text{m}$ obtained from the equation (5) and data.

Then the scanning microscopic photograph of the surface of a glass sphere showed the

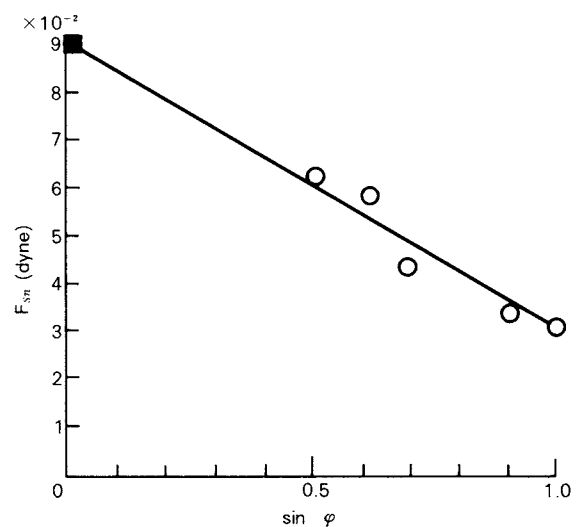


Fig. 5 Relation between separation force F_{sn} and inclination φ with a point by centrifugal method

roughness of about $5\mu\text{m}$. On the other hand, the calculation of the imaginary contacting circle for the stablest position gave the radius of $3.2\mu\text{m}$ (in case $d_p = 107\mu\text{m}$) and $2.5\mu\text{m}$ (in case $d_p = 61\mu\text{m}$) with the assumption of the roughness of $0.1\mu\text{m}$ for the surface of glass beads which was based on the roughness of glass slide surface according to the maker's information.

From these results it was made clear that the glass bead had a contact area having a diameter of a few μm with the plate by some reason and that the particle can be separated with a much smaller force to cause its rotation than the force working merely in the normal direction. Assuming the relation expressed by equation (5), the adhesion force of single particles F_{ad} can be estimated from the intercept of ordinate at $\varphi = 0$.

(2) Discussion on tangential separation method making use of tangential component of vibration

As mentioned in the previous section, the tangential component of vibration is very effective to separate the particles and so it may be possibly made use of for the measurement of adhesion force. Especially, when the separation force is not strong enough, this tangential separation method seems very useful.

In this case, where $F_{sn} = 0$ and $\varphi = 90^\circ$,

$$F_{st} = (2a/d_p)F_{ad} - (\pi/6)d_p^3\rho_s g \quad (7)$$

As this method is used in case the particles adhere to a vertical plate, namely $F_{st} \gg mg = (\pi/6)d_p^3\rho_s g$, therefore

$$F_{st} \doteq (2a/d_p)F_{ad} \quad (8)$$

This means that the vibration force required to separate a particle is only a few % of the adhesion force working on it. It would be still less, as the particle weight is subtracted as seen in equation (7).

For the centrifugal separation method to separate a particle in the tangential direction, the equation (8) is obtained by introducing the relations $F_{sn} = 0$ and $\sin\varphi = 0$ into the fundamental equation (4). This equation was derived using a different method by Polke.⁶⁾

In order to confirm this relation, the adhesion force was measured by the tangential vibration method with a newly developed ap-

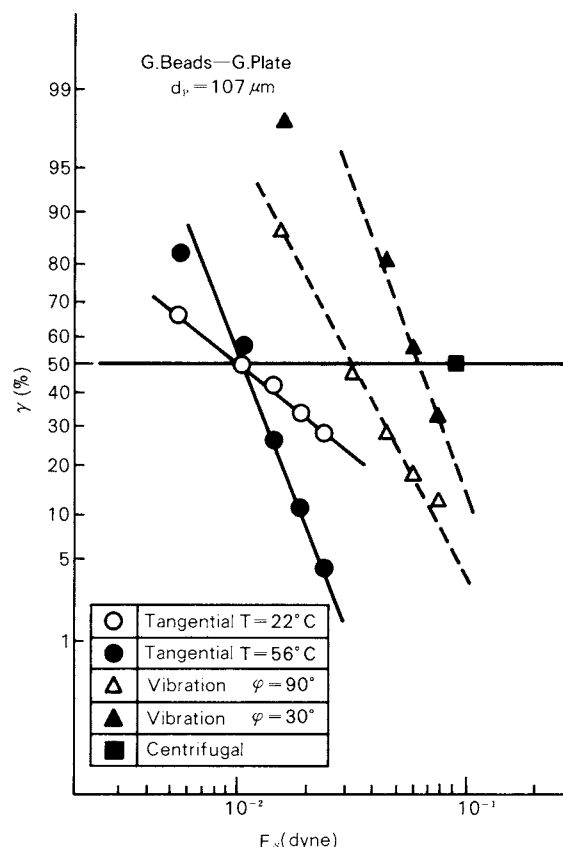


Fig. 6 The results by tangential separation method, with the results by other methods.

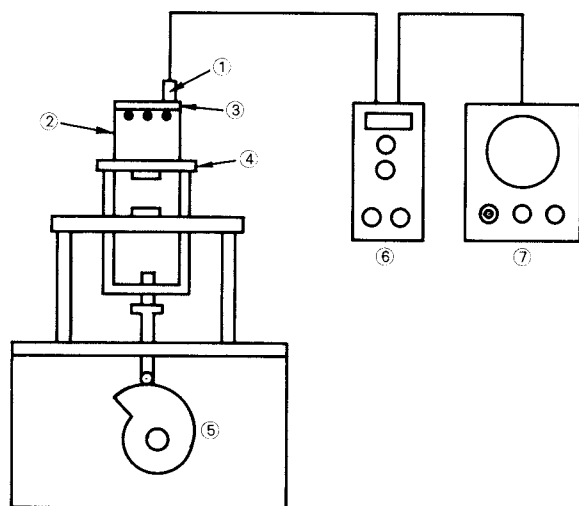
paratus. Some examples of the results depicted in Fig. 6 show that they are smaller not only than the data obtained by the centrifugal method (marked with ■) but also than that by the normal vibration method.

Regarding the separation force by the centrifugal method as F_{ad} and using the 50% - value of the one obtained by the tangential method at 22°C and 56°C in Fig. 6 for F_{st} , the calculation of a from the equation (7) gave $5.6\mu\text{m}$. It is nearly 4 times as large as $1.4\mu\text{m}$ obtained in the previous section but seems reasonable considering the accuracy of the present experiments.

Therefore the tangential vibration method has a great chance for the measurement of the adhesion force of a single particle, when the contacting conditions of the particle can be made clear quantitatively.

4. Measurement of adhesion force by impaction separation method

4. 1 Measuring method and experimental apparatus



(1) Accelerometer pick-up (2) Cell (3) Plane surface
(4) Tapping table (5) Cam (6) Amplifier (7) Synchroscope)

Fig. 7 The experimental apparatus of impaction separation method

In order to extend the measuring range of the adhesion force which was limited in case of the vibration separation method as mentioned above, an impact separation method was developed using a measuring apparatus for which so-called tapping equipment for packing was reconstructed as shown in Fig. 7.

In this case, the acceleration of the particle was measured by the accelerometer pick-up (EMIC made, 509 - CA type) fixed on the top of the measuring cell. As it changed complicatedly with time, the data was taken as the maximum value in the beginning period of the impaction, which would require further investigation. The size of the separated particles and the residual percentage of particles were obtained by the micrographs before and after impaction as above.

4 2 Results and discussions

In Fig. 8, the data obtained by the normal and the tangential impaction method are potted with those by the tangential vibration method. In case the acceleration is given in the tangential direction, the data by the impaction method agree with those by the vibration one very well, while the impaction separation method in the normal direction gives a few times as large data as those by the centrifugal method.

Using equation (7) with the above data by different separation methods, the radius of the contacting plane can be estimated to be $6.9\mu\text{m}$

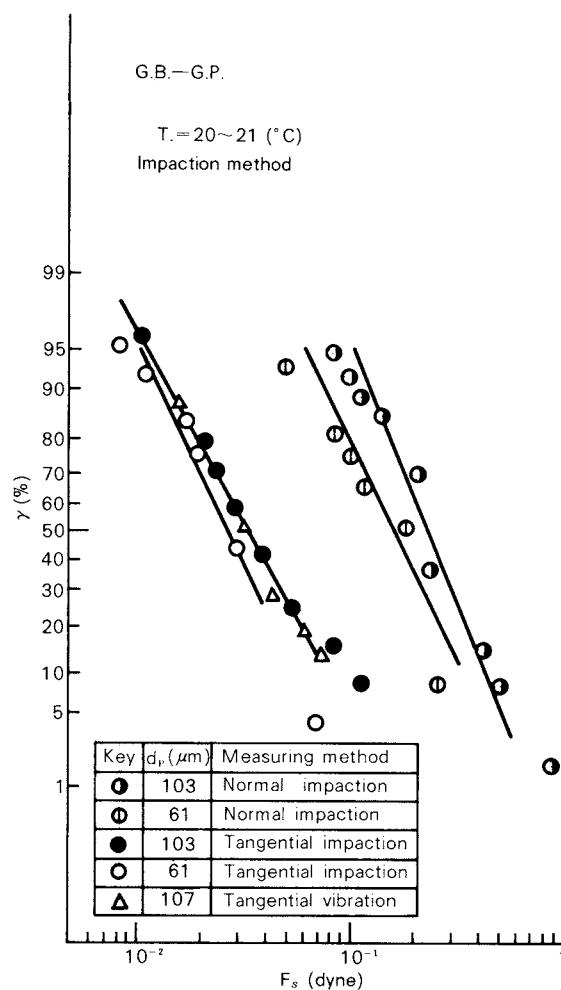


Fig. 8 The results of impaction separation method
Comparison of normal and tangential separation

and $6.1\mu\text{m}$ for the particles of $103\mu\text{m}$ and $61\mu\text{m}$ in diameter respectively. These results are much larger than those estimated from Hertz's theory mentioned in 3.4 (1) but correspond to the roughness of solid surface observed by a microscope. And it must be pointed out that the difference between these two radii of contacting plane of two particles with different diameter is much smaller than the differences of the values calculated and estimated with equation (6) and by Dahneke, who took account of the effect of adhesion force between a particle and a plane surface. At this stage of investigation, it can be supposed from these results that the contacting conditions determined by the roughness of the glass surface which does not depend upon particle size is more important than those caused by the deformation of the particle on the contacting plane depending upon the particle size.

5. Measurement of adhesion force at high temperature

5. 1 Measuring method

For the vibration method, a heater was attached to the back side of the adhesion plate. As increase of the adhesion force was expected at the higher temperature, a tangential separation method requiring small separation force was adopted in the temperature range up to about 350°C. In the impaction method, on the other hand, the tapping was conducted in a small oven covering the whole measuring cell, which performed the measurement up to about 460°C.

5. 2 Results and discussions

The effect of temperature on the separation force by the tangential vibration method and by the tangential impaction method are shown in Figs. 9 and 10 respectively.

The effect of temperature on the average value of separation force of glass beads is shown in Fig. 11, where the following tendency can be seen. The adhesion force reduces with increasing temperature to reach the minimum value around 100°C. After that it continues to in-

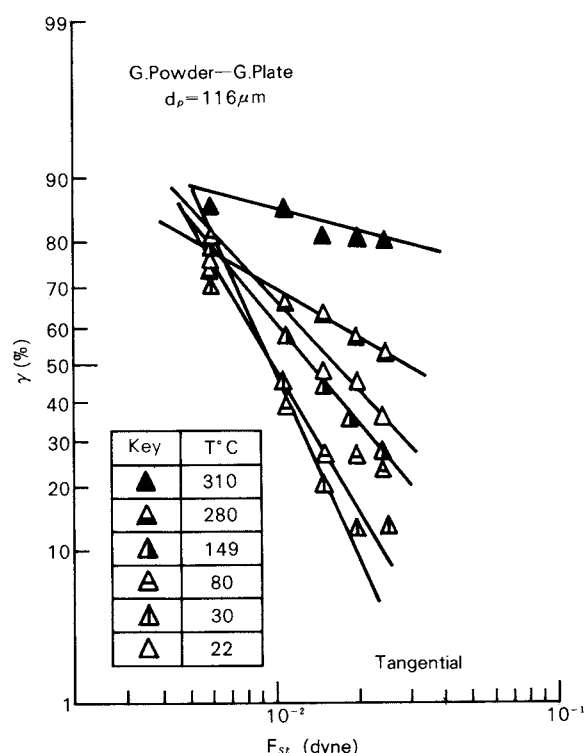


Fig. 9 The effect of temperature on the separation force by vibration tangential separation method

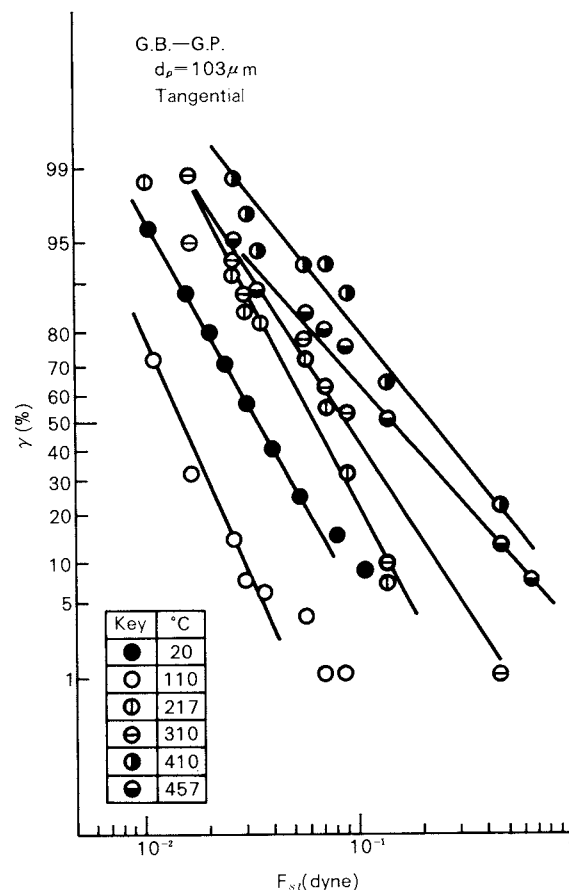


Fig. 10 The effect of temperature on separation force of glass beads by impaction tangential method

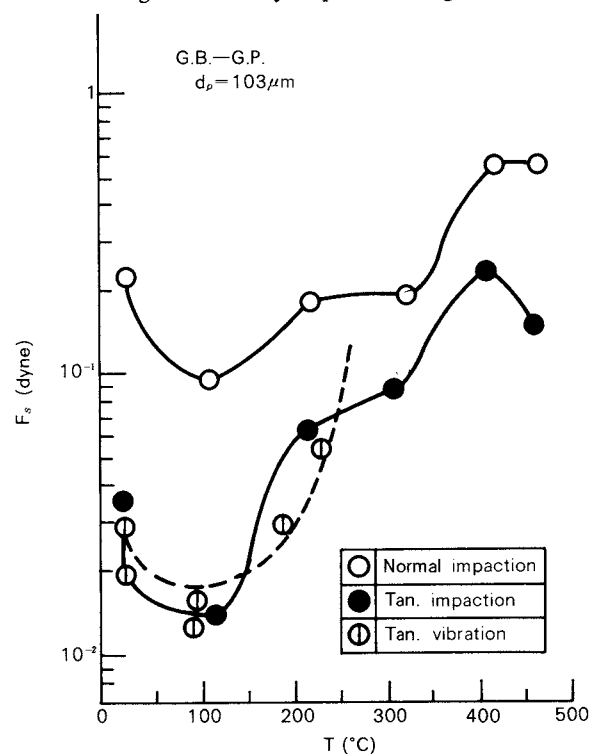


Fig. 11 The effect of temperature on the average value of separation force of glass beads.

crease with rising temperature to exceed the value of the room temperature in the range between about 200 and 300°C. At about 400°C, it shows a few times as large value as that of the room temperature and does not seem to increase at the higher temperature. The tendency of the adhesion force having the minimum value at about 100°C can be regarded as a general one, as it is seen with the material such as silica sand and FCC catalyst particles. It was also generally admitted that the adhesion force increases considerably with further rising temperature.

The detailed comparison of the data by the normal impaction method with those by the tangential one made clear that the difference between them reduced with the increasing temperature. Using equation (7), it was found that the radius of contacting plane a increased from 7.7 μ m at room temperature to 23 μ m at 310°C.

In this way, an experimental explanation has been given to realize the mechanism for the change of adhesion force by the indirect estimation of the deformation of the contacting plane from the separating mechanism of particles.

6. Conclusions

To make clear the problems in the measurement of adhesion force of single particles of powder and to extend the measurement range, new measuring equipments were developed, which also made possible the measurement under special conditions such as high temperature. From these results, the following points were made clear.

(1) For the measurement of adhesion force of single particles, a vibration separation method and an impaction separation method have been developed and proved to be useful methods.

(2) It was found that the rolling of particles gives remarkable effect on the separation in these methods. A fundamental equation was derived based on the theoretical consideration of the separating mechanism with rolling of particles.

(3) Additionally, a tangential separation method making use of the rolling action of particles has been developed and it has been shown that useful informations about the contacting condition and separating mechanism of a particle can be obtained from comparison of

the tangential and the normal separation method.

(4) The applicability of the above method to the measurement at high temperature was confirmed and it was found that the adhesion force of glass beads reduced with increasing temperature up to 100°C and then continued to increase.

Acknowledgements

This research was supported by the Asahi Glass Foundation for Industrial Technology in 1978 and 1979, and by a Grant-in-Aid for Scientific Research from the Ministry of Education, Science and Culture, Japan in 1979 and 1980 (No. 443024).

Nomenclature

a	: radius of contact circle	[μ m]
d_p	: diameter of particle	[μ m or mm]
E	: Young's modulus	[kg/mm ²]
f_{ad}	: adhesion force per unit surface	[dyne/cm ²]
F_{ad}	: separation force of a particle to normal direction	[dyne]
F_s	: separation force	[dyne]
\bar{F}_s	: F_s at $\gamma = 50\%$	[dyne]
F_{sn}	: normal component of separation force	[dyne]
F_{st}	: tangential component of separation force	[dyne]
H	: adhesion force of a single particle	[dyne]
m	: mass of a particle	[g]
α	: amplitude of vibration	[cm or mm]
γ	: residual percentage of particles	[%]
ν	: Poisson's ratio	[-]
ρ_s	: density of particle	[g/cm ³]
σ	: standard deviation	[-]
φ	: inclination of plane surface	[°]
ω	: angular velocity of vibration	[°/sec or rad/sec]

References

- 1) Jimbo, G.: *J. Soc. Material Sci., Japan*, **16**, 291 (1967).
- 2) Asakawa, S. and G. Jimbo: *ibid*, **16**, 358 (1967).
- 3) Jimbo, G., R. Yamazaki, G. Hong and H. Hirano: 11th Fall Meeting of Soc. Chem. Eng., Japan, Preprint, p.445 (Tokyo 1977).
- 4) Yamazaki, R., Y. Imai, G. Hong and G. Jimbo: 12th Fall Meeting of Soc. Chem. Eng., Japan, Preprint p.335 (Tokyo 1978).
- 5) Jimbo, G. and R. Yamazaki: European Symposium Particle Technology 1980, Preprint p.1064 (June 3-5, 1980, Amsterdam).
- 6) Polke, R.: *Chemie - Ing. - Technik*, **40**, 1057 (1968).
- 7) Dahneke, B.: *J. Colloid & Interface Sci.*, **40**, 1 (1972).

Criteria of Activation of Powdery Materials by a Preliminary Mechanical Treatment

Mamoru Senna*

Faculty of Science and Technology,
Keio University

Abstract

γ -Fe₂O₃ was vibration ball-milled with varying amplitude, α , from 8 to 24mm and grinding time. The enthalpy increase, ΔH^* , due to mechanical treatment was measured by a differential scanning calorimeter. Pretreated sample was subsequently heated at 693K for 60min, and the fractional transformation into α -phase, a_1 , was obtained. Both ΔH^* and a_1 increased monotonically with grinding time with levelling off at longer milling time. The tendency of a level off was different, however, between ΔH^* and a_1 . ΔH^* increased monotonically with increasing amplitude whereas a_1 showed a maximum at $\alpha = 10$ mm. The correlation between a_1 and the lattice disturbance, the latter being obtained from the relative intensity of X-ray diffraction peaks, was not uniquely determined, but depended on the amplitude. This suggests that the same lattice disturbance does not always lead to the same degree of acceleration of the subsequent reaction. The reason was discussed on the basis of the content of ΔH^* and the nuclei-growth mechanism of $\gamma \rightarrow \alpha$ transformation of Fe₂O₃.

1. Introduction

A number of examples were found in the field of mechanochemical activation of finely divided solids in the last two decades^{1,2)} Some of them are promising for the technological application. Until now, however, most of the industrial branches which have good possibilities to make use of mechanochemical activation techniques are reluctant to introduce them into an actual production line. One of the most serious objections for the application of such techniques is obviously the lack of quantitative data warranting the benefit of the technique.

Much effort has been made to quantify the mechanochemical effects through thermoanalytical and calorimetric studies³⁾. Stored energy, ΔH^* is most frequently used as a measure of activation. The increase in the enthalpy or the excess enthalpy is the thermodynamical definition of the measured stored energy. For the

critical discussion, the change in the free energy is more desirable. However, we have to tolerate a substitute use of the enthalpy, letting the contribution of the entropy still open to the question⁴⁾, for the time being, since a direct measurement of the free energy on powdery material is hardly possible.

The main purpose of the present study is to answer the question, if partly, whether and to what extent the stored energy can be used as a real criterion or a practical measure of mechanochemical activation. γ -Fe₂O₃ was used as a model substance, since the stored energy of mechanically treated γ -Fe₂O₃ is easily measured by DSC⁵⁾. Different kinds of mechanical treatments were used and the correlation between ΔH^* and the enhancement of the rate of transformation into α -Fe₂O₃ on subsequent heating was compared.

2. Experimental

Pure γ -Fe₂O₃ for magnetic recording (Toda Kogyo, Hiroshima, Japan) was used as a starting material without any special treatment. Primary particles are acicular with an average

* Hiyoshi, Yokohama, Kanagawa, 223
TEL. 044 (63) 1141

Received March 24, 1983

length about $0.5\mu\text{m}$. The material was mechanically treated in two ways, i.e., by grinding with a vibratory mill and by compressing in a die. Vibration ball-milling was carried out by using a laboratory-sized mill with a varying amplitude, α , from 8 to 24mm. The frequency was kept constant at 12Hz. 1.5g starting material was put into a cylindrical steel vessel of 50cm^3 , together with 100 pieces of 6mm steel balls and 30cm^3 cyclohexane. Mechanical treatment was also carried out by compressing dry $\gamma\text{-Fe}_2\text{O}_3$ powder in a die cavity (0.05 - 0.5 GPa) or between a gap of a tapered anvil (1.0 - 2.0 GPa).

Stored energy, i.e., excess enthalpy, ΔH^* was measured by using a differential scanning calorimeter (DSC, Thermoflex, High-Temperature type, Rigaku, Tokyo, Japan). The thermoanalysis was carried out at constant rate of heating, 10K min^{-1} , in air. An X-ray diffractometry was carried out in order to determine the extent of lattice disturbance and lattice distortion. The relative intensity of diffraction peaks from $\gamma\text{-Fe}_2\text{O}_3$ (220), (311) and (400) was determined by using CaF_2 as an internal standard.

$\gamma\text{-Fe}_2\text{O}_3$ with and without mechanical pretreatment were subsequently heated in air. Fractional conversion into α -phase was determined by an X-ray diffractometry. Detailed analytical method was described elsewhere⁶⁾.

3. Results and discussion

3.1 DSC profile

Typical DSC profiles of original, vibration ball-milled and compressed $\gamma\text{-Fe}_2\text{O}_3$ are shown in Fig. 1. For the original as-received material, only a single exothermic peak was observed at ca. 843K, which corresponds to the heat of

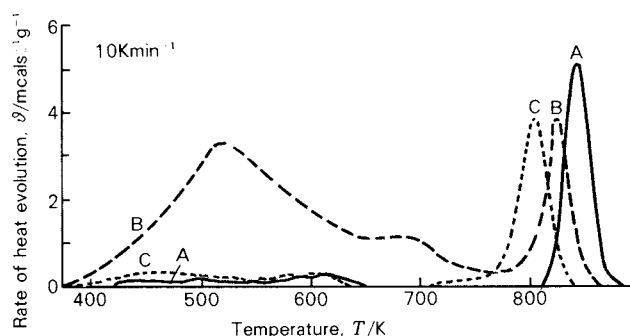


Fig. 1 DSC-profile. A: starting material; B: vibration ball-milled at $\alpha = 24\text{mm}$ for 300min; C: compressed 5 times at 0.25 GPa.

transformation into α -phase⁵⁾. A vibration ball-milled sample showed, on the other hand, an additional broad peak at lower temperatures. The latter is interpreted to be caused by the liberation of stored energy⁵⁾, from which the enthalpy excess was calculated in a manner given elsewhere⁷⁾. Compressed $\gamma\text{-Fe}_2\text{O}_3$ indicated little amount of energy storage, although the temperature of the transformation lowered significantly.

3.2 Variation of ΔH^* with grinding time and amplitude

ΔH^* increased monotonically with grinding time with a tendency of levelling off at longer grinding time, as shown in Fig. 2. Larger amplitude brought about higher excess enthalpy. These two observations are quite natural to be accepted, because the energy input or the work done increases linearly with time and parabolically with the amplitude⁸⁾.

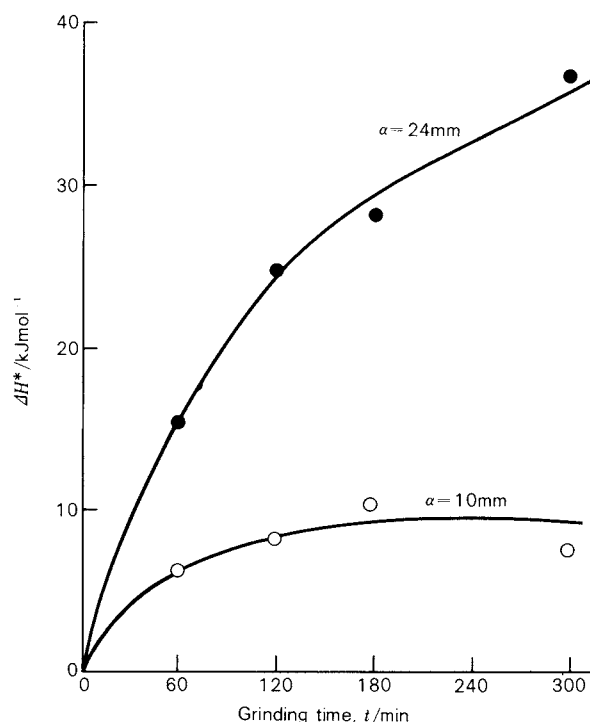


Fig. 2 Relation between ΔH^* and grinding time.

3.3 Variation of lattice disturbance with grinding time and amplitude

Relative intensity of X-ray diffraction peaks from $\gamma\text{-Fe}_2\text{O}_3$ (220), (311) and (400) were averaged. The mean value of the relative intensity was then divided by that of as-received sample to obtain the relative crystallinity, I_f . $1-I_f$ is understood as a measure of the lattice

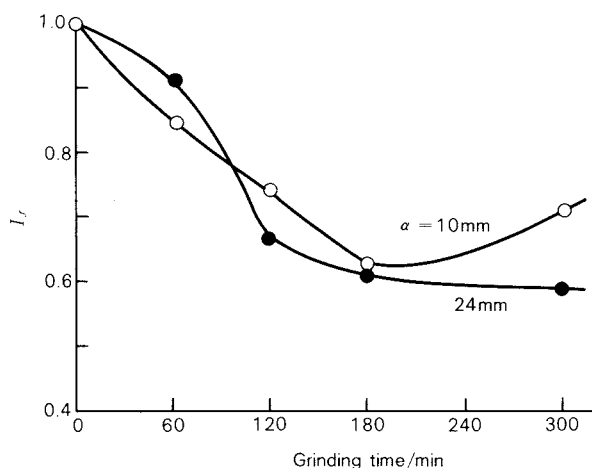


Fig. 3 Relation between I_f and grinding time.

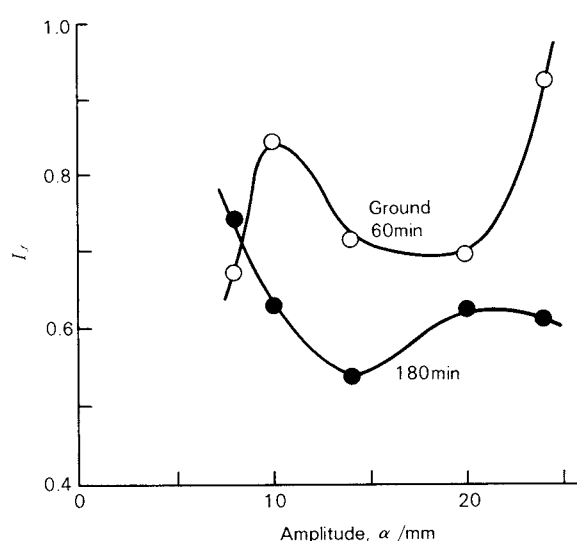


Fig. 4 Relation between I_f and amplitude.

disturbance introduced during a preliminary mechanical treatment.

When I_f is plotted against grinding time, an almost monotonic decrease with levelling off at longer grinding time was observed as shown in Fig. 3. This corresponds seemingly well to the monotonic increase in ΔH^* shown in Fig. 2. It is noteworthy, however, that, whereas the effect of increasing amplitude is profound in the case of ΔH^* , two curves of Fig. 3 for different amplitudes run almost the same track, indicating little effect of increasing amplitude on I_f . On the other hand, variation of I_f with the amplitude is somehow peculiar as shown in Fig. 4.

3.4 Reactivity increase

When mechanically pretreated $\gamma\text{-Fe}_2\text{O}_3$ is heated at 673-713K, a part of the sample trans-

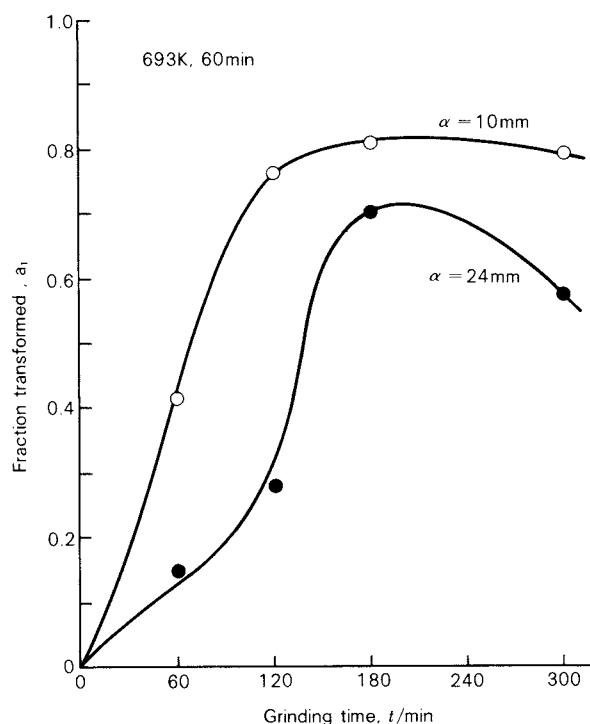


Fig. 5 Relation between a_1 and grinding time.

formed into α -phase very rapidly, followed by a much slower second step⁷⁾. As reported previously, as-received $\gamma\text{-Fe}_2\text{O}_3$ never transformed into α -phase when heated at 713K even for 9 hr. Therefore the fraction transformed, a_1 , after heating at 693K for 60 min in air was chosen as a measure of the increased reactivity.

Relation between a_1 and the grinding time is shown in Fig. 5. a_1 increased with grinding time. However, the tendency of levelling off was much more significant than in the case of ΔH^* . With $\alpha = 24\text{mm}$, a_1 even decreased when ground for 300 min. Furthermore, samples ground with smaller amplitude showed higher reactivity.

3.5 Relation between ΔH^* and a_1

As expected from Figs. 2 and 5, the correlation between ΔH^* and a_1 is by no means straightforward. Both quantities are plotted in Fig. 6 against the amplitude of the vibration mill. In the amplitude range smaller than 10mm, both ΔH^* and a_1 increased, the correlation therebetween being positive. ΔH^* further increased with increasing amplitude. Since a_1 little increased with increasing amplitude between $\alpha = 10\text{mm}$ and 14mm, the correlation between ΔH^* and a_1 is not so clear as with smaller amplitudes. With the amplitude larger

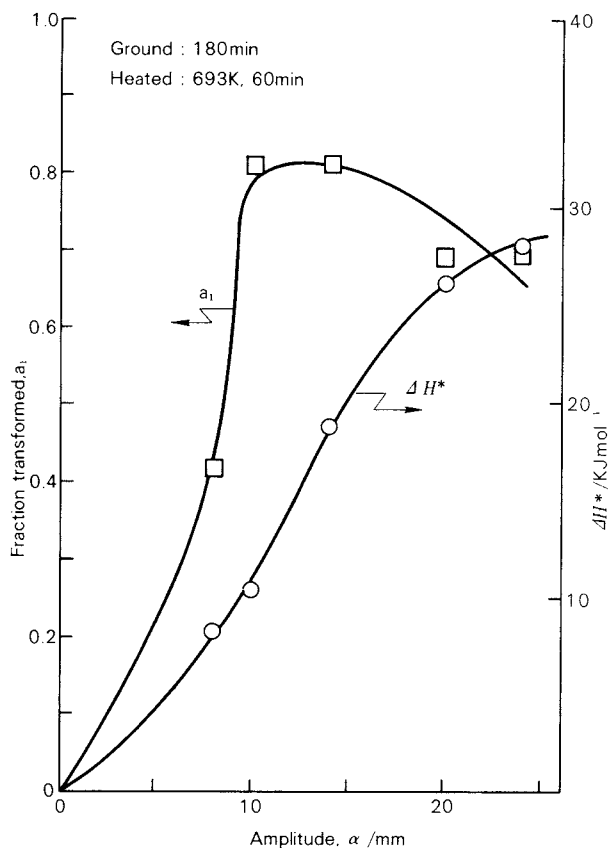


Fig. 6 Variation of a_1 and ΔH^* with amplitude.

than 14mm, the correlation between ΔH^* and a_1 is even negative.

3.6 Relation between I_f and a_1

The relation between I_f and a_1 are shown for varying grinding time in Fig. 7, and varying amplitude in Fig. 8. Figs. 7 and 8 suggest that the same lattice disturbance does not always lead to the same degree of acceleration for the subsequent reaction. Lattice imperfection introduced at early stages of grinding with larger amplitude contribute quite significantly to I_f , as shown in Fig. 7, but not very much for the acceleration of the transformation. When I_f is plotted against a_1 for serial data of varying amplitude as in Fig. 8, the curve falls on between the two curves of Fig. 7. The correlation between I_f and a_1 is rather simple and straightforward.

3.7 Contents of ΔH^*

The excess enthalpy of mechanically pretreated $\gamma\text{-Fe}_2\text{O}_3$ is attributed partly to the lattice disturbance⁵⁾. As shown just above, the same extent of lattice disturbance does not always correspond to the same increase in the

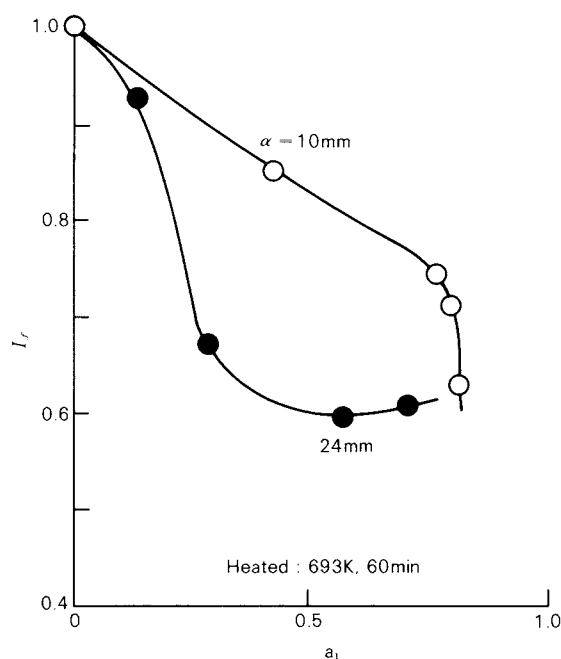


Fig. 7 Relation between I_f and a_1 for varying grinding time.

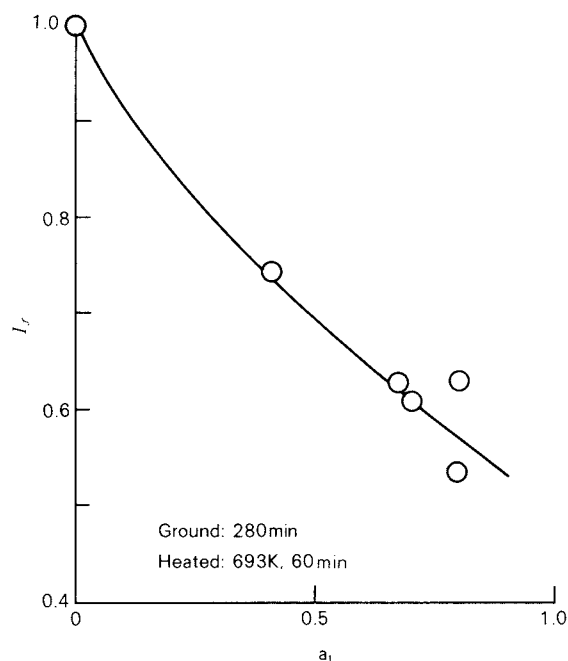


Fig. 8 Relation between I_f and a_1 for varying amplitude.

enthalpy, e.g., when the amplitude is different. The tendency is much more striking when we compare the results of vibration ball-milling and compressing experiments. Since the lattice disturbance was also observed for compressed samples where no significant energy storage was detected, the lattice disturbance solely cannot be the reason of the energy storage. Disorder

of the structural vacancy and/or the site exchange of the vacancy could also share a part of energy storage⁹⁾. The present experimental results point out that not all of the stored energy can contribute to the enhancement of the transformation.

3.8 Enhancement of phase transformation

Transformation of $\gamma\text{-Fe}_2\text{O}_3$ into $\alpha\text{-Fe}_2\text{O}_3$ is initiated by the nucleation of hematite in the matrix of the spinel structure of maghemite. In the case of mechanical pretreatment, a part of the fcc stacking of oxygen (111) plane in the spinel is supposed to be faulted, resulting in the local hexagonal stacking. This stacking fault can serve as an embryo of hematite⁵⁾. The embryo can become easily a nucleus of hematite with a slight displacement of Fe^{3+} ions¹⁰⁾.

The enhancement of the transformation is achieved mainly through the enhanced nucleation rate, as inferred from the kinetic analysis¹¹⁾. The same is true for the isomorphous transformation of $\gamma\text{-Al}_2\text{O}_3$ into $\alpha\text{-Al}_2\text{O}_3$ ¹²⁾. It is therefore to be expected, that only a part of the lattice imperfection which directly serves as an embryo, viz., the stacking fault of oxygen layers, contribute significantly to the enhancement of the transformation.

When the nature and the distribution of the crystal imperfection generated during mechanical treatment favors the nucleation, the ratio $a_1/\Delta H^*$ is larger, as in the case of vibration ball-milling with $\alpha = 10\text{mm}$. The ratio $a_1/\Delta H^*$ may be even much larger in the case of compressed material, since ΔH^* is much smaller or even null for the compressed material. Details of press experiments will be reported elsewhere.

4. Concluding remarks

The present experiment suggests that the nature and the distribution of the crystal imperfection is largely different, depending on the method of mechanical pretreatment and accordingly on the distribution of the applied external stress. The overall relationships among the crystallographical, thermal and chemical properties are therefore often ambiguous. Topological studies with regard to the mechanical activation are of urgent importance for the further elucidation of the usefulness of the mechanochemical activation. Enlightening in-

vestigations are now in the course of their development in some institutions^{13, 14)}.

Acknowledgement

A part of the present work was financially supported by The Kurata Research Grant. The author expresses his sincere appreciation to The Kurata Foundation. He is also grateful to Mr. T. Iwamoto for his experimental cooperation, and Toda Kogyo Ltd. for the donation of $\gamma\text{-Fe}_2\text{O}_3$.

References

- 1) Heinicke, G.: "Moderne Probleme der chemischen Technologie" Akademie-Verlag, Berlin, p.297 (1980).
- 2) Boldyrev, V. V.: Ann. Chim. Fr., **6**, 359 (1981).
- 3) Heegn, H.: "Untersuchungsmethoden zur Charakterisierung mechanisch aktivierter Festkörper", Juhász, Z. (Ed.) Közdot, Budapest, p.139 (1978). Huhn, H.-J., *ibid.*, p.149.
- 4) Torkar, K.: Proc. 4th Int. Symp. Reactivity Solids, Amsterdam, 1960, deBoer, J.H. (Ed.) Elsevier, Amsterdam, p.400 (1961).
- 5) Imai, H. and M. Senna: *J. Appl. Phys.*, **49**, 4433 (1978).
- 6) Senna, M., S. Tojo and H. Kuno: Keio Eng. Rep., **24**, 111 (1971).
- 7) Shinozaki, M. and M. Senna: *Ind. Eng. Chem. Fundam.*, **20**, 159 (1981).
- 8) Raasch, J.: *Chem.-Ing.-Techn.*, **36**, 125 (1964).
- 9) Kimura, T.: private communication.
- 10) Kachi, S.; K. Momiyama and J. Shimizu: *J. Phys. Soc. Jpn.*, **18**, 106 (1963).
- 11) Senna, M.: *J. Appl. Phys.*, **49**, 4580 (1978).
- 12) Dynys, F.W. and J.W. Halloran: *J. Am. Ceram. Soc.*, **65**, 442 (1982).
- 13) Kretzschmar, U., I. Ebert, U. Steinicke and H. P. Hennig: *Cryst. Res. Technol.*, **16**, 949 (1981); *ibid.*, **17**, 257 (1982).
- 14) Chupakhin, A. P. and V. V. Boldyrev: *Izv. Sib. Otd. Akad. Nauk SSSR, Ser. Khim.*, (4), 3 (1982).

Ultra-Fine Grinding and Consequent Changes of Powder Characteristics

Tohei Yokoyama*, Kiyoshi Urayama*
and Toyokazu Yokoyama*
Hosokawa Micromeritics Laboratory

Abstract

Some characteristic changes of ultra-fine powders obtained by a recently developed dry grinding system called UMF were introduced together with the performance of the grinding system. UMF has made it possible to grind not only the general minerals but also some hard substances like zirconium oxide, silicon nitride etc. down to sub-micron powder in dry condition. In addition, the grinding capacity was greater than that expected from conventional mills taking into account product fineness.

The differences of some powder characteristics between the ground product and the raw material were confirmed, using an electron microscope, thermogravimetry, differential thermal analysis and X-ray diffraction analysis for several materials including calcium carbonate, mica, barium titanate and so on.

1. Introduction

The recent advances in the frontier technologies are remarkable especially in the electronic and mechanical industries, new energy development, biochemistry and so forth, where a great number of materials are handled in the particulate or powdery form, e.g. ultra-fine metal powder, new ceramics, catalysts, fine chemicals etc. The new technologies have been requiring severer specifications regarding several powder characteristics including particle shape, activity, homogeneity as well as particle size and specific area.

Ultra-fine powder is produced by either a chemical synthetic method or mechanical grinding, and the latter is divided broadly into wet and dry methods. Dry grinding is an important conventional unit operation that has various advantages in numerous processes. Taking account of the industrial productive capacity, however, it seemed that general materials had a lower limit of average size of about 2 to 3 μ m by conventional dry grinding, though it depended

upon the powder characteristics.

The new grinding system (abbreviated as "UMF" hereafter) developed recently in our laboratory realized the ultra-fine dry grinding to produce submicron powder having an average size from 0.3 to 1.6 μ m with not only general minerals such as natural calcium carbonate, talc and mica but also some hard materials such as magnesia, zirconium oxide, silicon nitride, glass etc. The mechanical grinding of the latter materials used to be generally regarded as extremely difficult owing to the high hardness of the materials.

In this report, we first compare the power consumption of UMF with that of conventional grinding mills and then introduce the powder characteristics of the ultra-fine powders obtained by UMF comparing them with those of the raw materials.

2. Fineness of ground product and power consumption for grinding

With regard to energy consumption for grinding, a number of reports have been published, including the well-known Rittinger's, Kick's and Bond's law, but it would be difficult to give a general expression for energy consumption in each case of grinding, as it depends much upon

* 9, Shodai-tajika 1-chome, Hirakata, Osaka, 573
TEL. 0720 (57) 3721

Received June 28, 1983

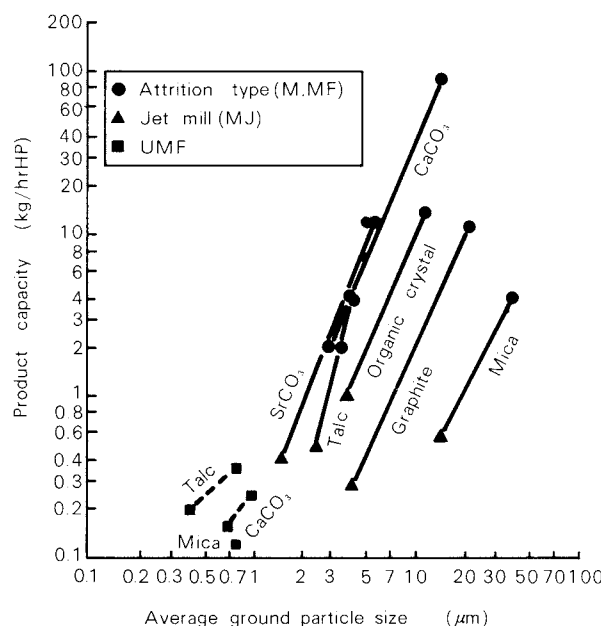


Fig. 1 Relationship between average particle size of ground product and grinding capacity

the physical properties of the material to be ground, the grinding mechanisms, the concerned particle size range etc. In addition, the overall energy consumed by mills in the actual grinding operations includes a great deal of heat loss by friction, the kinetic energy of powder, parts of mills and circulating air, and so on, besides the energy for only the physical size reduction of the materials.

Fig. 1 shows some examples of relationship between grinding capacity and achievable minimum average particle size of ground products in the practical operational range of a few kinds of fine grinding mills. As seen from this figure, the grinding capacity per unit power consumption is proportional to the average particle size of the product approximately in the 2.5 to 4th power of 10 on the logarithmic scale in case of conventional mills, depending upon the kinds of material and the grinding mechanisms. Thus the grinding capacity decreases extremely with reducing particle size of ground products, and there seems to be a lower limit of average size of ground powder around 2 to 3 μm by conventional grinding methods.

On the other hand, UMF has exceeded the limit and made possible the size reduction down to submicron range as far as 0.4 μm with the grinding capacity which is not smaller than that to be expected from the conventional mills. It is noticeable from the data obtained

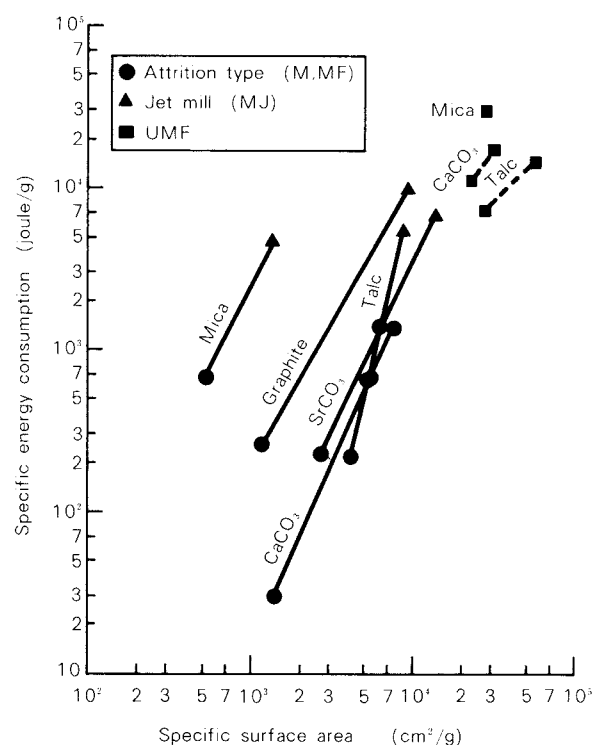


Fig. 2 Relationship between specific surface area and energy consumption for grinding

so far that the grinding effectiveness of UMF is especially remarkable with flake-shaped particles like mica and talc, the fine grinding of which used to be difficult by conventional mills of impact-attrition type and even jet mills.

Fig. 2 displays the relationship between the energy consumption for grinding and the specific surface area of ground products, which were calculated using the data in Fig. 1 with a simple assumption of spherical particles.

3. Particle size reduction and incidental change of physical characteristics

3. 1 Natural calcium carbonate

Raw material having an average size of 30 μm was ground by UMF to a fineness of 0.7 μm . For the measurement of particle size, we adopted a gravitational sedimentation method which has a clearly defined physical meaning.

Photos. 1a and 1b are electron micrographs of the ground material.

According to thermogravimetry of the raw material and the ground product, they both decomposed and changed to calcium oxide releasing carbon dioxide gas around 750°C as seen in Fig. 3 and showed the terminal weight loss of about 44%, which corresponded to the

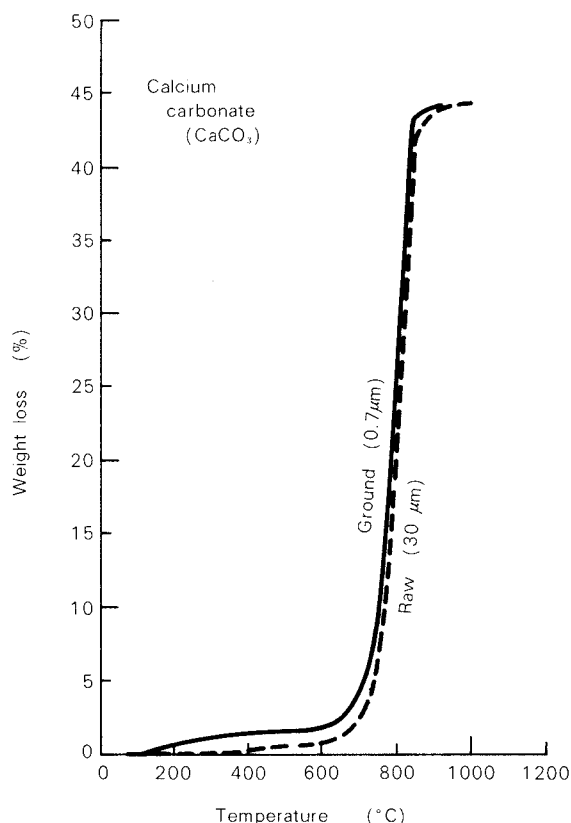


Fig. 3 Thermogravimetry of calcium carbonate

theoretical weight of carbon dioxide included in the material. Though there was no considerable difference in changes of weight loss between them, decomposition of the ground product started already around 200°C and was slightly more active than the raw material up to the temperature where rapid decomposition occurred.

The X-ray diffraction analysis gave the result that the peak of the relative intensity of the ground product was lower and its half-value width is broader than that of the raw material, suggesting occurrence of lattice distortion in the crystal structure of the particle (Fig. 4).

3. 2 Talc

UMF ground the raw material having an average size of 50μm down to 0.5μm (Photos 2a and 2b). The thermogravimetry of the ground product and the raw material showed a difference of about 1% in weight loss between the two even as high as around 1000°C, which might be caused by adsorption of some materials like moisture on the ground product sample owing to its high activity (Fig. 5). It is apparent that the ground fine particles began to decom-

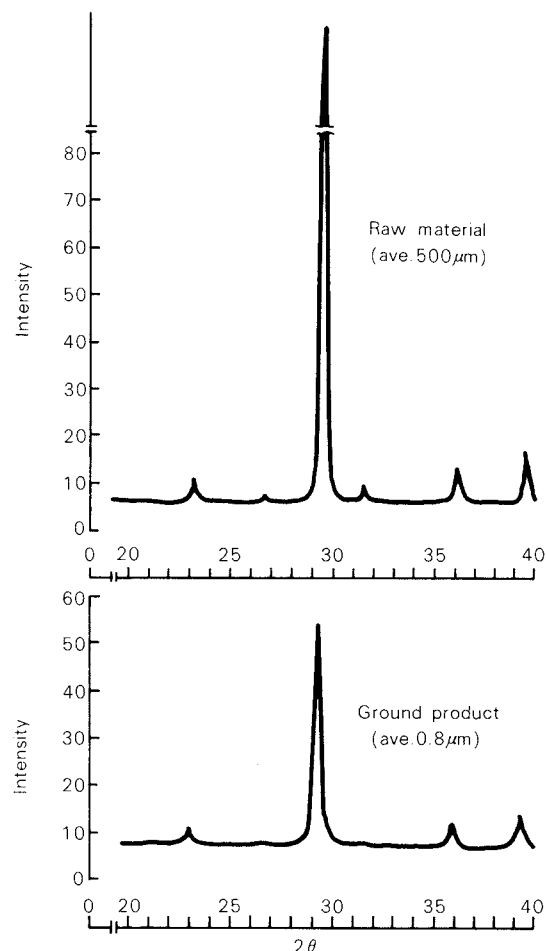


Fig. 4 X-ray diffraction (Cu-Kα) of calcium carbonate

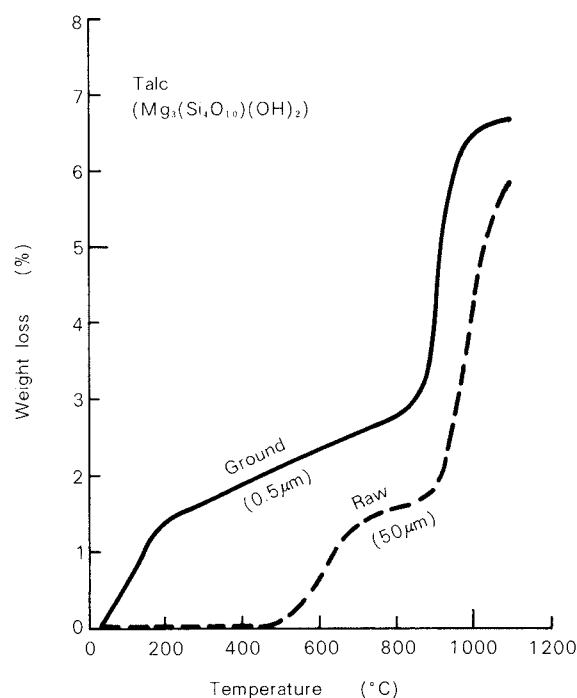


Fig. 5 Thermogravimetry of talc

pose releasing hydroxyl group at lower temperature, and its weight loss percentage was higher than the raw material.

3. 3 Mica

Mica is generally more difficult to grind to fine size by dry method than the above-mentioned two materials, and the finest average size of various kinds of available mica lies around $10\mu\text{m}$. By UMF, on the other hand, the raw material having an average size of $200\mu\text{m}$ could be ground to the product of $0.7\mu\text{m}$, which besides had narrow size distribution (**Photos 3a, 3b**). An enlarged picture of a part of **Photo 3b** is shown in **Photo 3c**, where the moiré fringes caused by lattice distortion is observed.

The ground product of mica started to decompose at lower temperature than the raw material, and X-ray diffraction analysis of the former showed lower and broader peaks than the latter in the similar way to calcium carbonate and talc (**Fig. 6**).

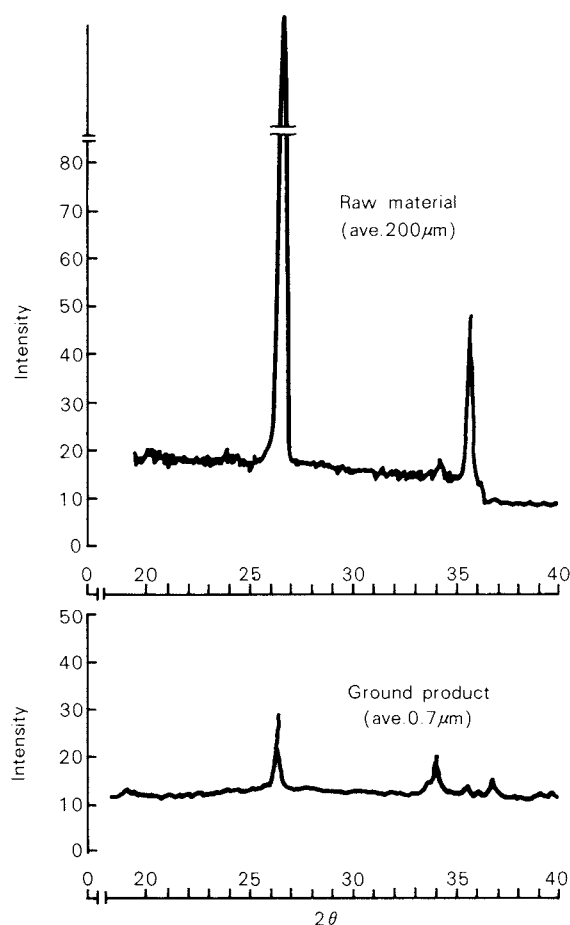


Fig. 6 X-ray diffraction (Cu-K α) of mica

3. 4 Barium titanate

Barium titanate has been increasing its demand very rapidly in recent years for condensers used in video tape recorders, piezoelectric pieces etc. The raw material processed by UMF had an average size of $1.6\mu\text{m}$ and was ground down to $0.8\mu\text{m}$ with a narrow size distribution. As seen in the micrographs (**Photos 4a, 4b**), the ground particles were spherulized to some extent having similar size.

Weight loss of the ground and the raw material could hardly be noticed when this substance was heated from ambient temperature up to 1000°C . It is known that barium titanate usually changes its crystal structure from tetragonal to cubic system at 120°C and to hexagonal system at 1460°C . According to differential thermal analysis, the raw material indicated no peak up to 1000°C except for a very small one around 120°C , while the ground showed a sharp exothermic peak just below 1000°C as seen in **Fig. 7**, which might have resulted from the change of crystal structure of the material by grinding.

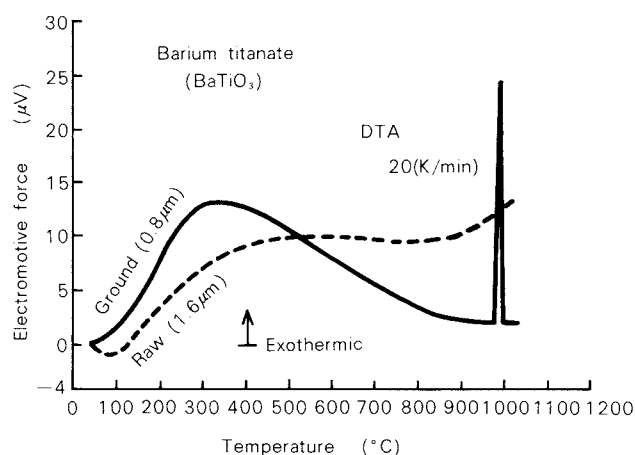


Fig. 7 Differential thermal analysis of barium titanate (Thermocouple Pt-PtRh 13%)

3. 5 Zinc oxide

The raw material adopted here had an average size of $1.5\mu\text{m}$ and included many fine particles under $1\mu\text{m}$ and coarse hard agglomerates of about 6 to $7\mu\text{m}$ (**Photo 5a**). After grinding by UMF, the product had an average size of $0.7\mu\text{m}$ and scarcely contained too fine or coarse particles (**Photo 5b**).

3. 6 Flint glass

This has a hardness of nearly 6 after Mohs's scale and is very difficult to grind because of its high abrasiveness.

UMF succeeded in grinding the material having an average size over $40\mu\text{m}$ (**Photo 6a**) down to $1.6\mu\text{m}$ (**Photo 6b**). The ground particles had a rounded shape with a narrower size distribution than the raw material as in the case of barium titanate.

4. Conclusions

Some characteristic changes in ultra-fine powders obtained by a newly developed dry grinding system UMF were introduced together with the relationship between power consumption for grinding and product fineness. They are summarized in the following.

- 1) It succeeded in size reduction down to as fine as submicron by dry method, which could hardly be achieved by conventional grinding method.
- 2) Power consumption is relatively low compared with that expected from the data by conventional mills, taking account of product fineness.
- 3) Grinding efficiency was especially high with flake-shaped materials like mica and talc which are difficult to grind to fine powder by dry method.
- 4) The ground particles had a rounded shape and relatively narrow size distribution. (barium titanate, flint glass, zinc oxide etc.)
- 5) According to thermogravimetry, the ground products began to decompose at lower temperature than the raw materials (calcium carbonate, talc, mica, etc.)
- 6) According to differential thermal analysis, the ground product seemed to transit at lower temperature than the raw material in one case. (barium titanate)
- 7) In X-ray diffraction analysis, the ground particles showed lower and broader peaks of intensity than the raw material, suggesting increased lattice distortion in the crystal structure of the particle. (talc, calcium carbonate, mica etc.)

Though there are no sufficient data available yet concerning UMF and ultra-fine powders obtained with it, it seems to have a great possibility

for wide applications. Therefore, it will be necessary to grasp the characteristics of ultra-fine powder such as the structure inside the particles, activity, and so on, as well as fineness and shape of particles, and to investigate further the mechanochemical phenomena related with those characteristics.

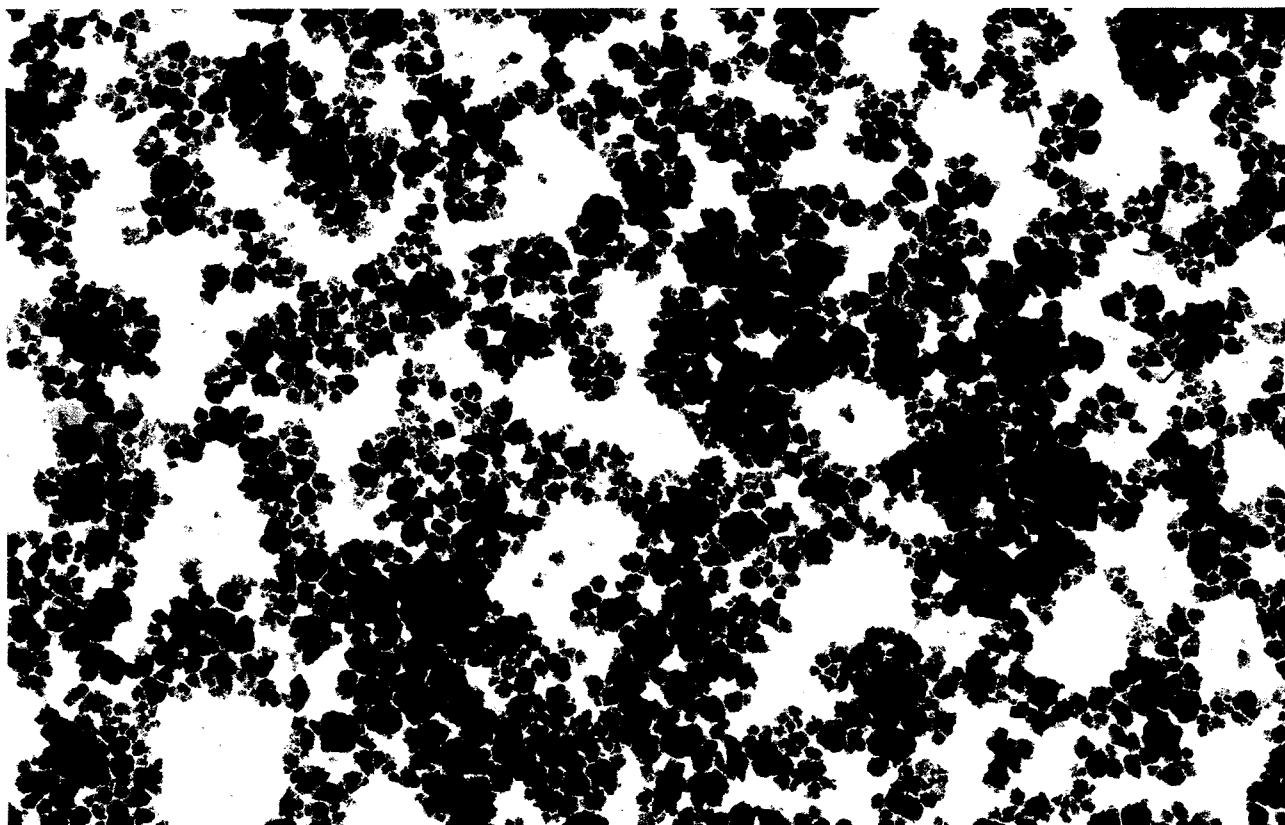


Photo 1a

1 μm

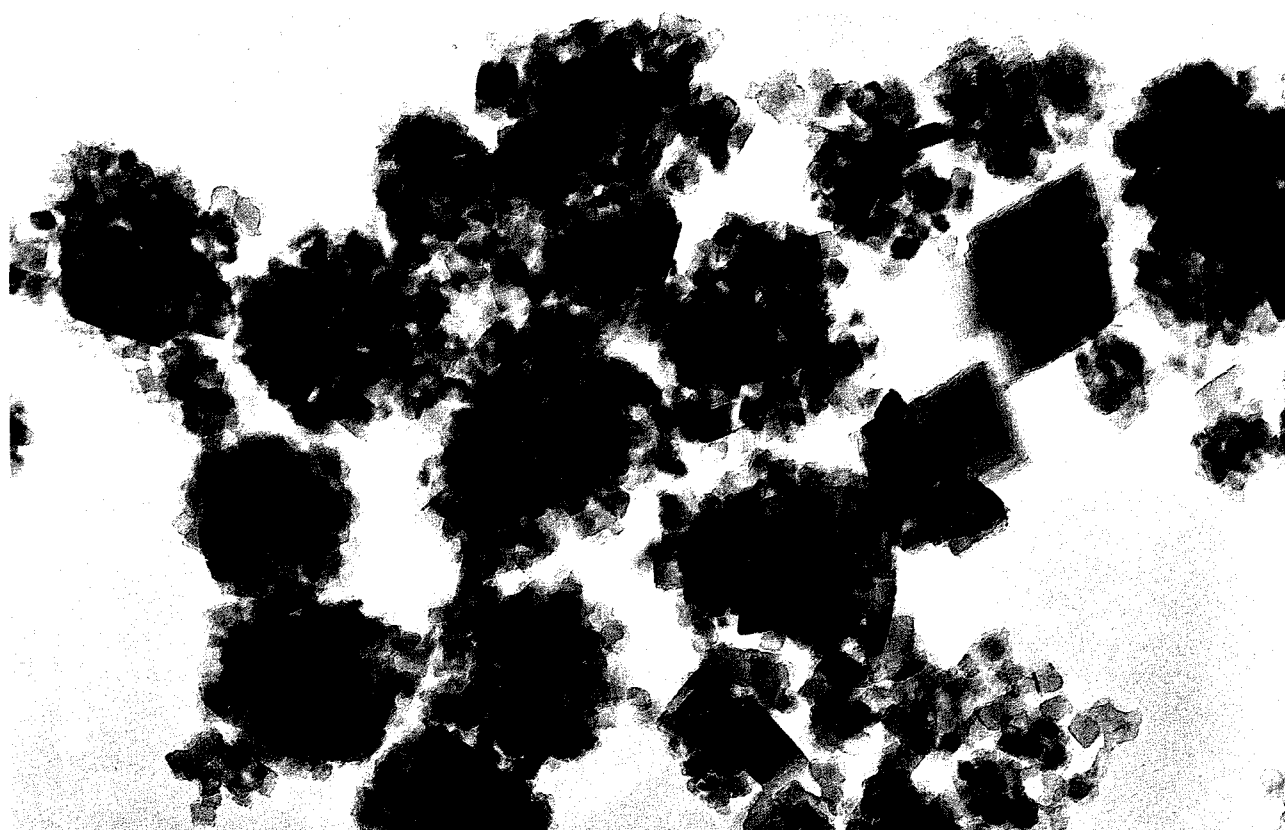


Photo 1b

0.1 μm

Electron micrographs of **calcium carbonate** ground by UMF.

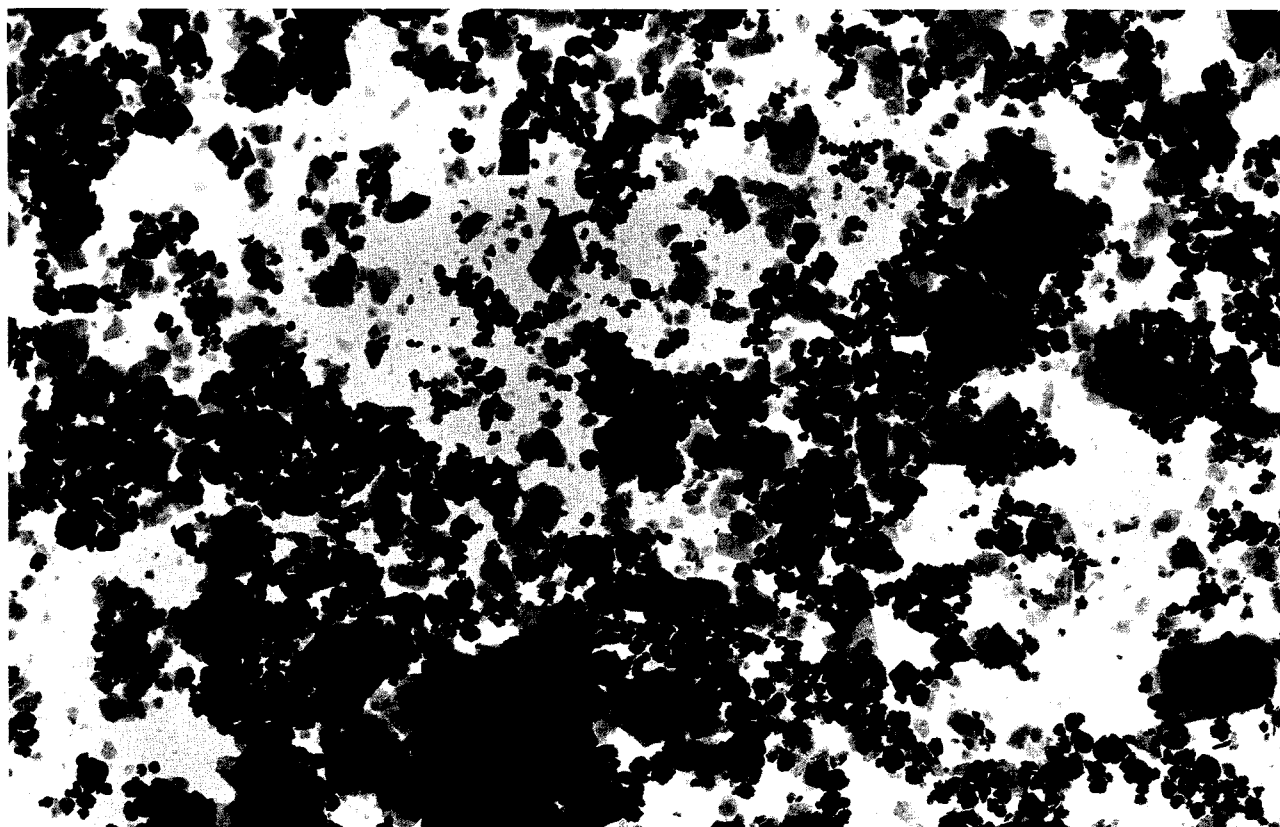


Photo 2a

1 μm



Photo 2b

0.1 μm

Electron micrographs of **talc** ground by UMF.

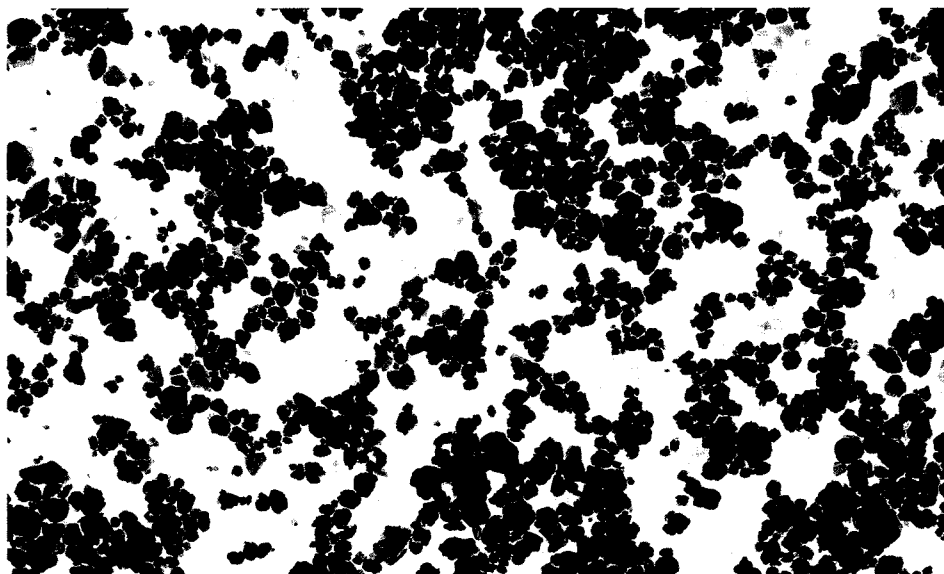


Photo 3a



Photo 3b



Photo 3c

Electron micrographs of **mica** ground by UMF.



Photo 4a

Raw material

1 μ m

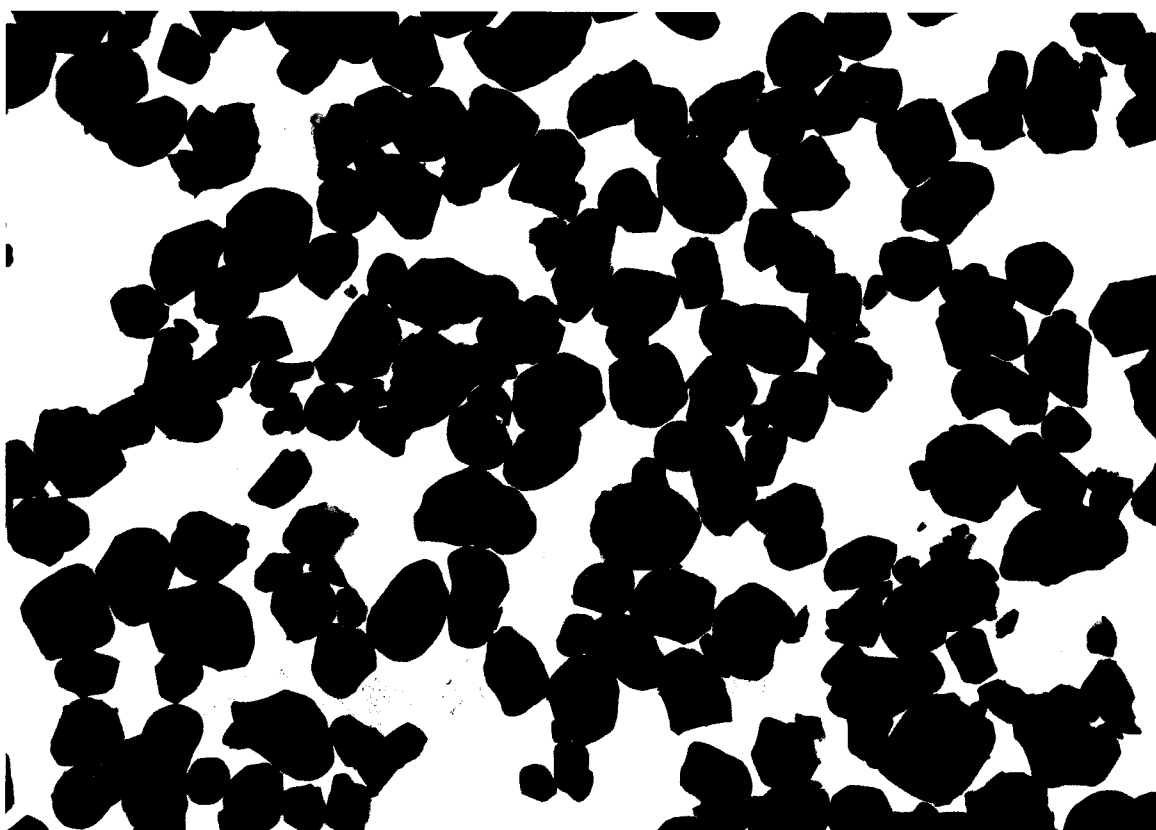


Photo 4b

Ground product by UMF

1 μ m

Electron micrographs of **barium titanate**.

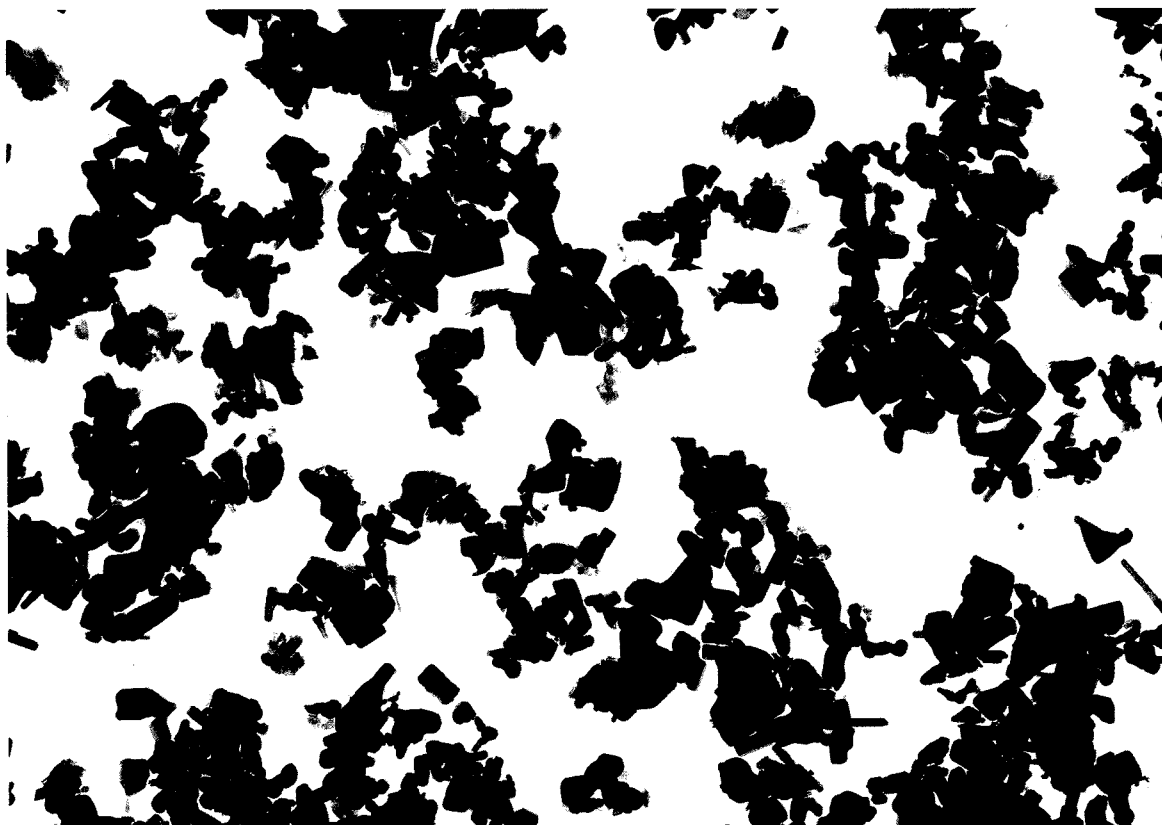


Photo 5a

Raw material

1 μ m

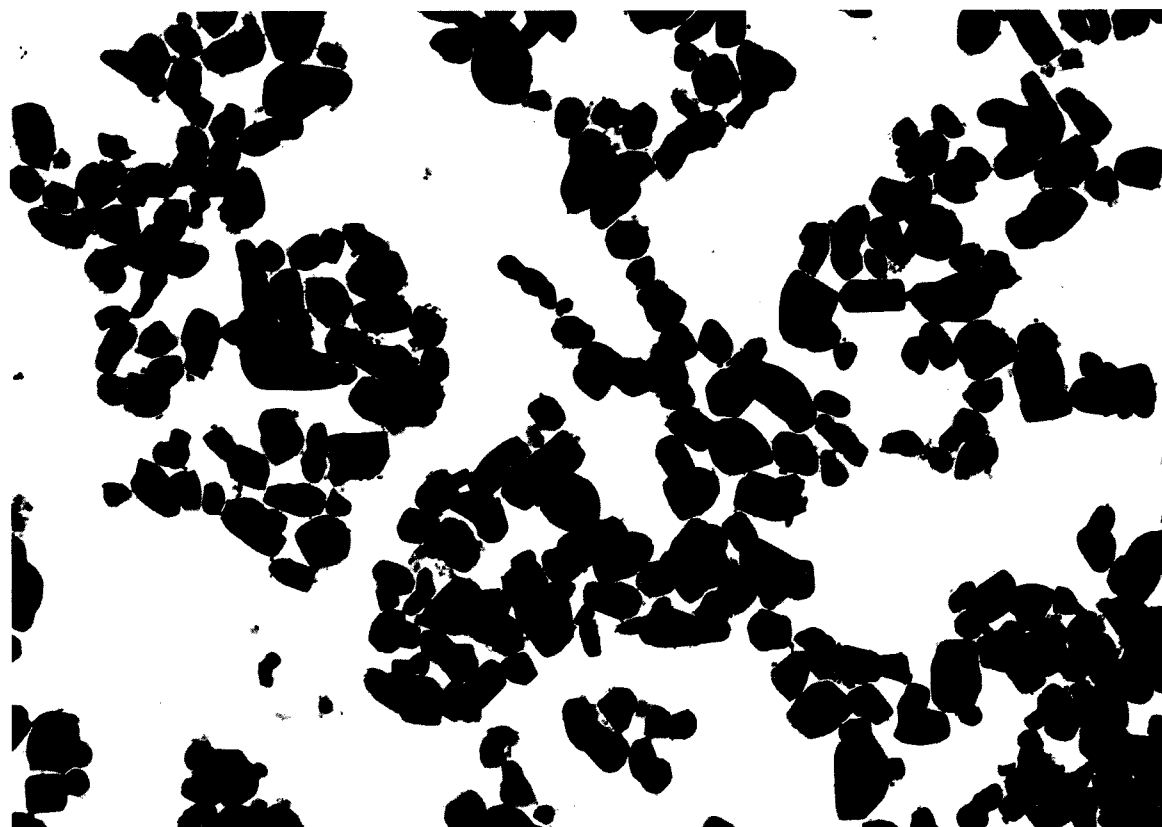


Photo 5b

Ground product by UMF

1 μ m

Electron micrographs of **zinc oxide**.



Photo 6a

Raw material

40µm



Photo 6b

Grout product by UMF

1µm

Micrographs of **flint glass**.

Musical Sand

Shigeo Miwa*, Jusuke Hidaka*
and Atsuko Shimosaka*

Department of Chemical Engineering
Doshisha University

Abstract

Since last century, a number of investigations were reported on the peculiar sound producing beach or desert sands. The so-called musical sand, which emits a musical sound when walked on, can be found in several parts of the world.

A long time ago, many Japanese beaches were known as musical one. However, recently almost all the beaches have lost the peculiar properties with pollution attributed to various human activities. Various fine dusts and oily materials adhered to the surface of the sand grains. If additional influx of polluted materials had been stopped for a very long period of time, they would have been cleaned up by the mechanical washing action of sea wave, so-called beach action, in natural environment.

Laboratory experiments were conducted in an attempt to simulate the natural process. For this purpose, gyratory motion washer was used, because the movement speed and pattern of water and sand were nearly similar to beach action. The washed sand had excellent sound producing properties and pronounced not only in the air but also in the water.

The perfectly cleaned up sand was characterized by very high friction coefficient of the sand layer, so the penetration test of the sand layer showed clear stepwise characteristics, resulting from significant difference of static and dynamic friction coefficient.

Moreover, from the correspondence of the wave form of sound pressure and stress in sand layer, an explanation of sound producing mechanism was described.

1. Introduction

There are some beach sands which emit loud and distinct, often music-like sounds, when you walk on them. It is called singing sand, squeaky sand, sonorous sand, whistling sand or musical sand. The beach sand shows the sonorous property in the rare cases where the sand deposited on the beach undergoes the abrasion and sorting by the strong wave action for a long time. There is as a result sometimes well-sorted, well-polished and well-rounded quartz grains accumulated on the seashore. The condition of the natural environment for the occurrence of the

musical sand is that the beach should be so-called high-energy one where the wave action is very powerful and with a stationary shoreline. It is also required that the considerable amount of the fluvial sand or mud does not flow from the neighboring rivers onto the beach and that the seawater is less polluted.

In the foreign countries, some musical sands in the lake environment are well-known with some examples of Lake Michigan and Lake Baikal. It is also reported that a large-scale sound-producing dune (booming sand) lies in the aeolian sand deposit to be found in the desert environment.

The existence of the sands with the sonorous property has been confirmed in more than ten beaches in Japan. But recently these beach sands have been gradually losing the sonorous

* Karasuma-Imadegawa, Kamigyo-ku, Kyoto, 602
TEL. 075 (251) 3849

Received March 10, 1983

property because of the heavy adhesion of the dust or oily materials onto the sand surface, which has been caused by the destruction of the land surface adjacent to the beach, the artificial deformation of the shoreline, the pollution of river and seawater and so forth. Some beaches have disappeared completely owing to the artificial construction such as nuclear power plants. Therefore, the elimination of the effect of the pollution is required first of all in order to investigate the sonorous property of the beach sand.

This study is related with the washing method for the beach sand having such sonorous property (called "musical sand" hereafter) and with the resulting sonorous property as well as the dynamic property of the sand.

2. Occurrence of musical sand

Since the beginning of the previous century, scores of reports including some letters and books of travels have been published with regard to the musical sands all over the world. The details of those reports are omitted here, as they have been mentioned in our recent work.¹⁾

The survey of the world-wide occurrence of the musical sands and its detailed distribution in Japan are displayed in Figs. 1 and 2 respectively. As you can find some places called singing beach or squeaky beach in the foreign countries, there are several beaches in Japan which are named after the sound. Some of them are Kukunaki Beach (Miyagi Pref.) which has the meaning of the beach emitting ku-ku like sound and Kugunari Beach (Miyagi Pref.) which is related with the number 18 equal to a double of 9 which is pronounced as "ku" in Japanese. Kotobiki Beach and Kotoga Beach are named after the sound produced with a Japanese stringed instrument called "koto". Another example is Gomeki Beach (Ishikawa Pref.) whose name originates from "gomeku" that is a dialectal word meaning to weep. Moreover, Osodani (Yamagata Pref.) which is located in the inland area is a beach placer originating in the Pliocene epoch.

3. Washing of beach sand

The incoming waves at beach start becoming steeper after they touch the ground. Ultimate-

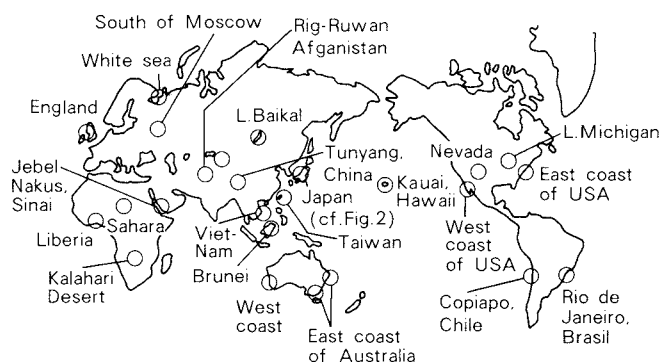


Fig. 1 Map showing the location of musical sands in the world

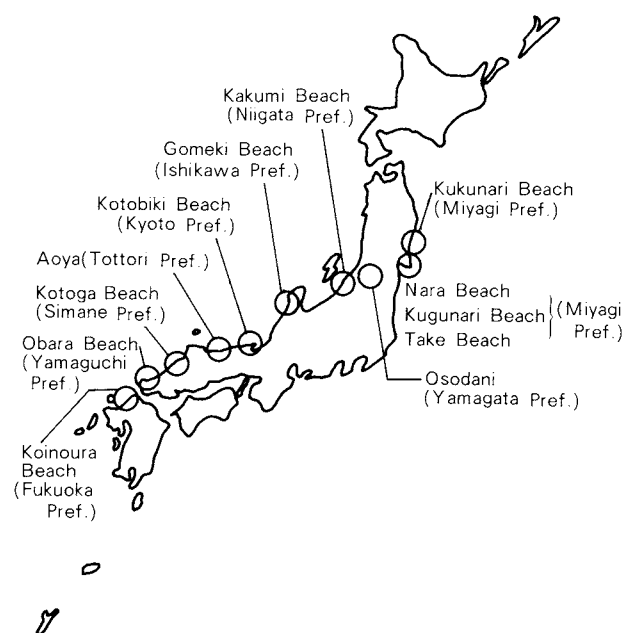


Fig. 2 Map showing the location of musical sands in Japan

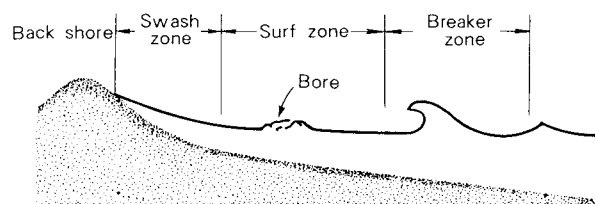


Fig. 3 Profile of the near-shore current system.
(On moderately sloping beaches surf zone is commonly lacking during high tide conditions.)

ly, they are oversteepened and break up in the breaker zone (Fig. 3). The breaker zone is followed by the surf zone, which at the shoreline is followed by the swash zone.

In both of the surf and the breaker zones, the beach sand is violently stirred up periodically and the most powerful mechanical washing of the sand takes place. Then we studied the

methods of simulating this washing effect on the laboratory scale.

In order to avoid the destruction of the sand grains and the scarring of their surface, we have not adopted stirring with the rapidly rotating blades to produce the water vortex for washing the sand. First, we tried the shaking of a cylindrical vessel made of polyethylene with a capacity of 1 liter containing the sand for washing. But it was difficult to process more than 1 kg of sand because of its unstable motion and the operation was too noisy. Also the washing of the sand was not so effective, as the sand grains mainly collide with one another and the shearing force hardly worked within the body of the sand. We next attempted another way to inject water tangentially into a cylindrical vessel containing the sand from its bottom section. But it was not appropriate because the local abrasion of the sand grains and the wear of vessel was considerable owing to the high moving velocity of the sand grains. In the rotating cylindrical vessel such as a ball mill the moving velocity was too low, though some shearing force worked within the body of the sand. The vibration ball mill which gives the vertical gyratory motion in a cylindrical vessel with a horizontal axis was also not suitable because of its little shearing effect, although the impact effect was noticeable between the sand grains suspended in the water. As a result from the above-mentioned trial and error, the most efficient and reasonable method of washing we have reached was performed with the device shown in Fig. 4, in which a cylindrical polyethylene vessel with a capacity of 10 liter containing the sand and water is fixed vertically onto a base giving the horizontal gyratory motion. This device is called Gyratory Washer in the following sections. In this case, about 5 kgs of mixture of the sand and water comes into rigorous rotating motion in the vessel and the rotation speed of the water in the upper layer becomes the same as that of the gyratory motion producer. Since the sand deposited at the bottom rotates more slowly in the deeper under layer, it receives the strong shearing effect under the gravitational force. It resembles the mechanical action taking place in both the surf zone and the breaker zone of the sea coast. The settings of the rotation radius of the gyratory motion at 30mm and the rotation

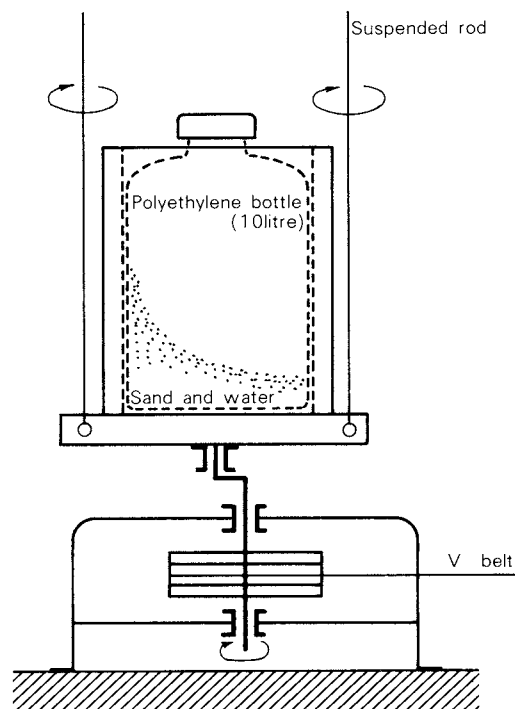


Fig. 4 Gyratory washer

speed at 220 rpm and with the diameter of the cylindrical vessel of 210mm give 2.4m/s as the maximum tangential speed of water in the upper layer, which is similar to the moving velocity of the sea waves. It also corresponds to 864 kms of travel when the device is operated for 100 hours and to about twice of the velocity used for the study of the experimental abrasion by the fluvial action on sand conducted by Kuenen²⁾.

4. Washing characteristics of Gyratory Washer

If the surface of the sand grains is scarred or the abrasion of the particles takes place when they are washed in the device for a long time, it is not suitable as it changes the surface texture of the beach sand produced in the natural environment. In order to investigate Gyratory Washer from this point of view, the following experiments were carried out. The sand grains of the Gairome silica sand (produced in Mizunami City, Gifu Pref.) which is supposed to have been deposited with clay in the lake originating in the Tertiary period are very angular, because they have not gone through the sea wave action and the resultant abrasion. Observing the sand grains with electron microscope (SEM) after washing 1 kg of the sand by Gyratory Washer for 500 hrs, no trace of abrasion of the



Fig. 5 SEM photograph of Gairome silica sand

sand grains was found, even if they were as coarse as 1 mm (Fig 5). It is known that the medium or fine sand grains are not abraded so much, even when the coarse ones are. From this fact we concluded that the surface of the sand grains should not be artificially deformed by this washing method.

Next, we washed in the same way 1 kg of the sand from Kotobiki Beach (Kyoto Pref.), where there have been the least deformation of the natural environment and the smallest effect by the inflow of the fluvial sand or mud. The sample of the sand was taken from the back shore where the sand had the good sonorous property. Water of the same volume as the bulk one of the sand was poured into a polyethylene vessel with a capacity of 10 liter which contained the sand. When it was shaken by hands scores of times, the water became turbid to a little extent but it got clear by sedimentation soon after keeping it quiet. Washing this with Gyrotory Washer for about 100 hours produced reddish-turbid water containing the colloidal particles which would not settle down even kept quiet for a few days. Then we threw away the turbid water and repeated the decantation of the sand with fresh water scores of times. Swinging the vessel after that, the sand emitted

the loud sound like “boo” even in the water. When dried and poked lightly with a stick, it produced the sound like “po-po”. Compared with the previous condition before washing when the sand had hardly emitted any sound without moving it pretty hard, it was admitted that the sonorous property of the sand had been improved considerably and that they had changed from the squeaky sand to the musical one according to the definition to be mentioned later.

There is an ancient dune formed in the Pleistocene epoch on the land side of Kotobiki Beach. As this dune contains the volcanic ash soil and is covered with the vegetation now, the sand has naturally no sonorous property as it is. We, however, found the sand grains of the dune had the same appearance as the beach sand from Kotobiki Beach with a microscope. And so we washed them in the same way as above for about 100 hours. Consequently they showed the same sonorous property as the beach sand. In this case, we found the reddish brown turbid water at the first stage of washing, which got clear when kept quiet. By throwing it away and repeating the decantation as mentioned above, the water became to contain only the gray muddy colloidal particles which would not settle down even if kept quiet for a long time. The change of the condition of the turbid water can be a measure to judge the degree of washing effect.

In the same way, we have succeeded in the recovery of the sonorous property of the beach sand from Gomeki Beach (Ishikawa Pref.) and Kakumi Beach (Niigata Pref.) and so on. On these beaches the sonorous property has been lost because of public works and the inflow of polluted water, while the inhabitants remember that the beach sand squeaked when they walked on it a few decades ago. Additionally we had the similar result with the sand from Osodani. The musical sand in the following experiments was processed by this washing method to remove the contamination completely.

5. Properties of musical sand

5. 1 Particle size distribution of musical sands

The size distributions of the musical sands used for the present experiment and those of the foreign musical sands introduced in the

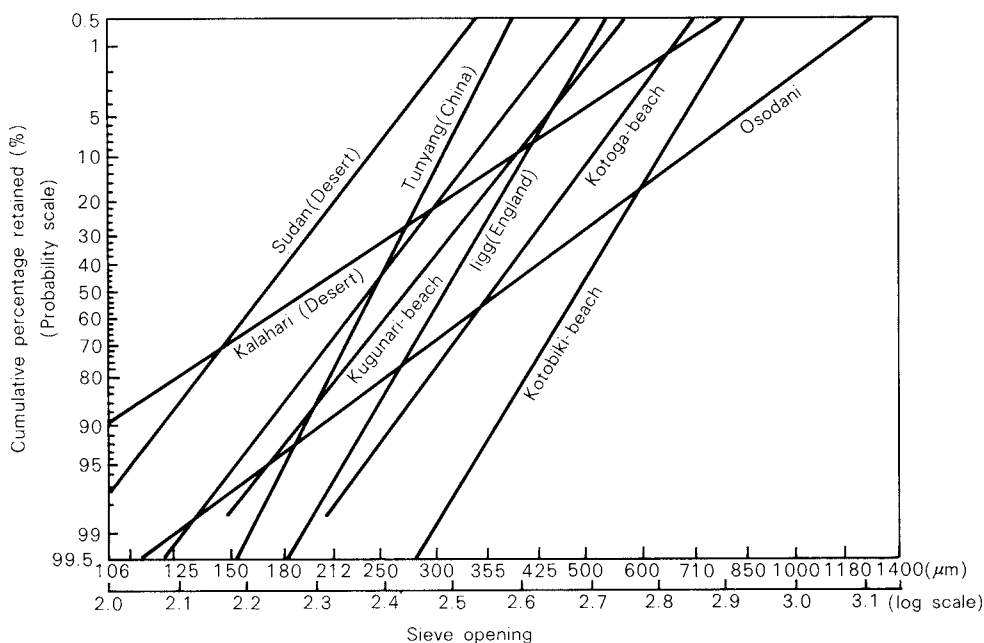


Fig. 6 Particle size distribution of musical sands

literatures are displayed in Fig. 6. According to the geological classification of sands, they belong to the coarse sand, medium sand and fine sand, most of which have the size between $100\mu\text{m}$ and 1mm . The silt and clay are removed almost completely from them owing to the wave or wind action.

5. 2 Shape and surface texture of musical sand grains

The musical sands differ not only in the size distribution but also in the shape and surface texture to a great extent depending on the area of deposition. Most of the beach sands are well rounded but it is not an essential condition for the musical sands, some of which are very angular. The scanning electron microscope (SEM) photographs of some typical examples of the musical sands are shown in Fig. 7. The common characteristic feature of the surface

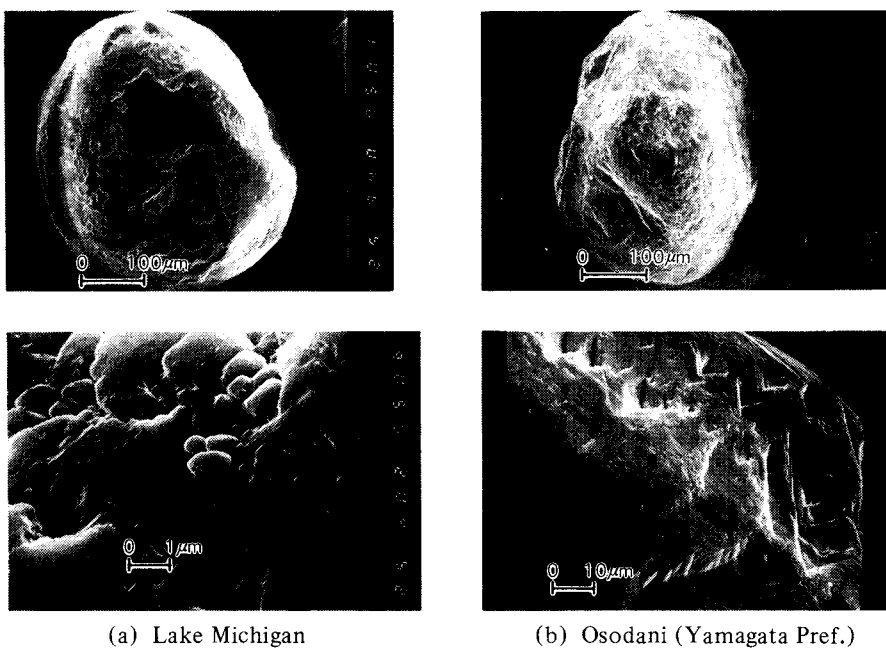


Fig. 7 Scanning electron microscope photographs of musical sand grains.

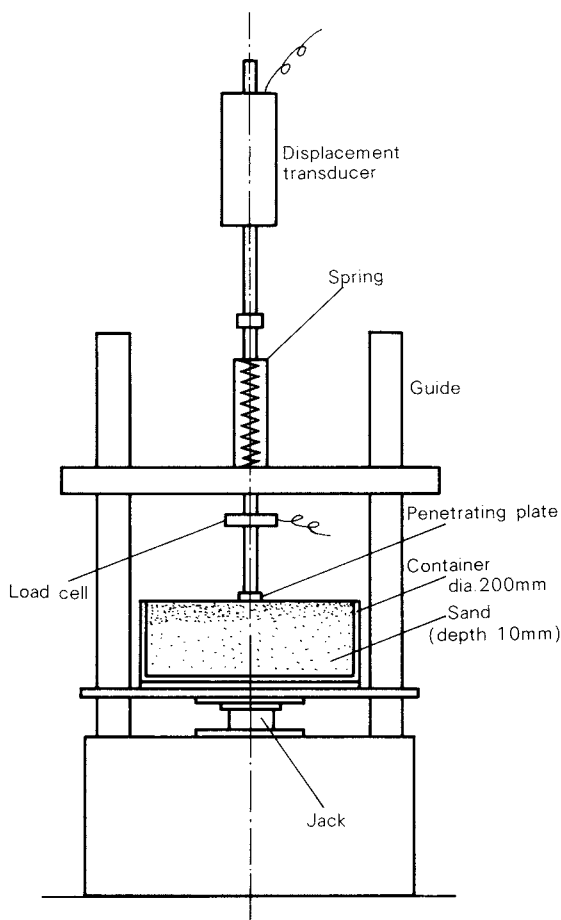


Fig. 8 Penetrometer

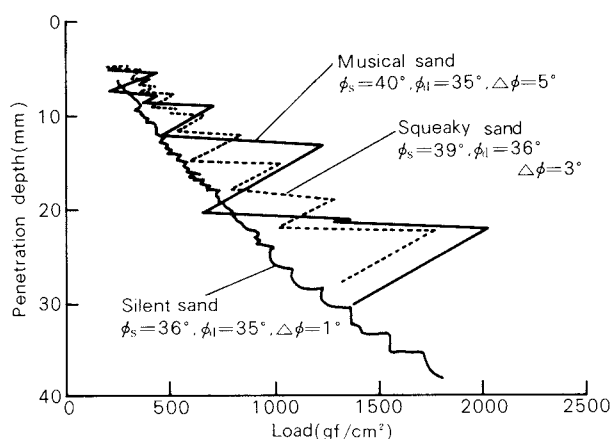


Fig. 9 Penetration characteristic curve for musical, squeaky and silent sands

texture of these musical sands is the well-polished surface.

5. 3 Stepwise penetration characteristics

The following example of the experiment applies as a sample so-called Ottawa sand which was produced from the sand dune near Lake Michigan in the U.S.A. The produced sand does not show the sonorous property as it is, though they have undergone some simple industrial washing. This is called silent sand from now on. As this is washed by Gyratory Washer for a long time, it becomes to show the sonorous property gradually.

Using the penetrometer shown in Fig. 8 in which a disk penetrates into the sand layer from the surface, we have investigated the relationship between the load required for the penetration and the penetration depth. The container used for the measurement was large enough to avoid the wall effect from it. The acquired penetration characteristic curve is depicted in Fig. 9. In case of the silent sand the disk penetrates continuously and the stepwise change is hardly found in the curve. But the stepwise curve is obtained after about 60 hrs of washing. The sand in this stage is called squeaky sand, because it has the poor sonorous property as described later. After the further washing over 100 hrs, the sand shows a remarkable sonorous property and the stepwise characteristics of the curve becomes significant. It is called musical sand. Though the musical sand and the squeaky one have had no exact definition so far, we have given a clear definition for them based on the penetration characteristic curve and the sonorous property in this report.

Generally speaking, when a cylindrical plunger with a certain sectional area penetrates into the particulate material quasi-statically, the resistant force working on the cylinder depends on the angle of internal friction of the particulate material and the penetration depth.²⁾ We

Table 1 Coefficients of internal friction

	Shear test	Tilting box Static	Penetrometer		
			Static (tan φ _s)	Dynamic (tan φ _d)	Difference
Musical sand	0.988	0.906	0.839	0.700	0.139
Squeaky sand	0.947	—	0.809	0.726	0.083
Silent sand	0.908	0.810	0.726	0.700	0.026

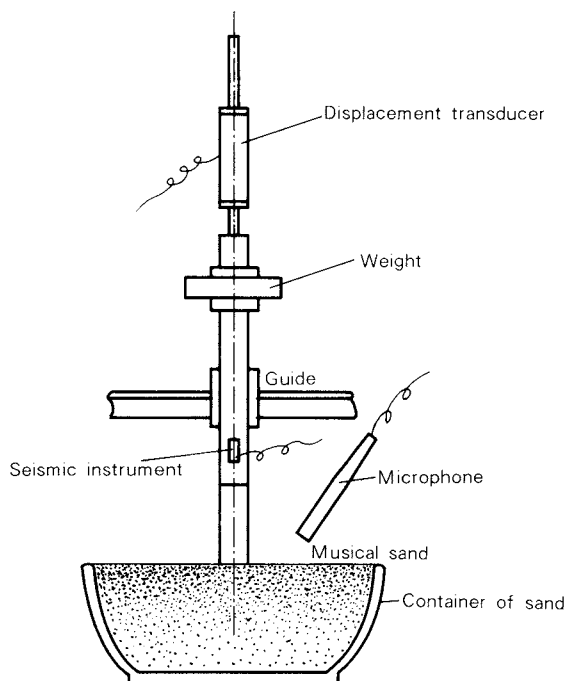


Fig. 10 Apparatus used for the testing of sonorous property of musical sand

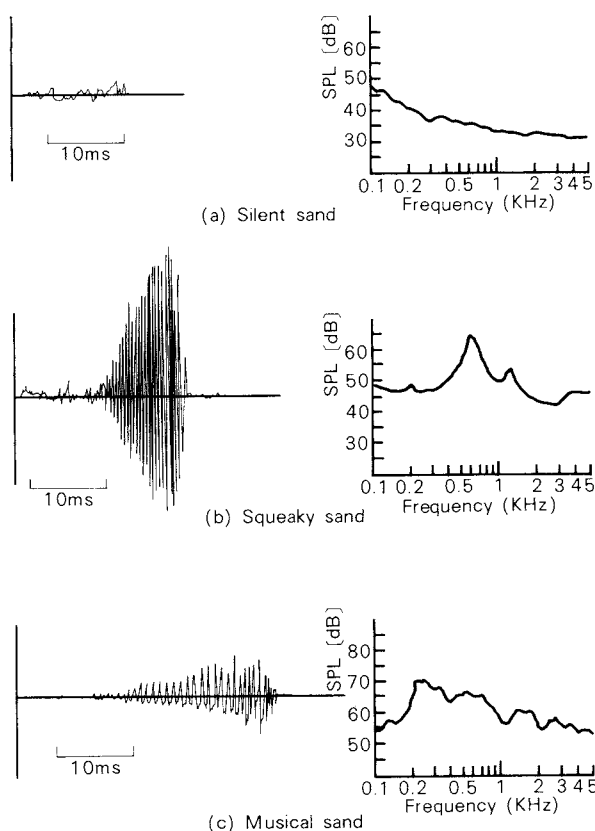


Fig. 11 Comparison of sonorous properties of silent, squeaky and musical sands

have already reported^{3~5)} that the static and dynamic coefficient of internal friction of the

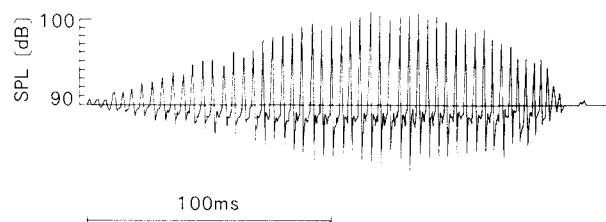
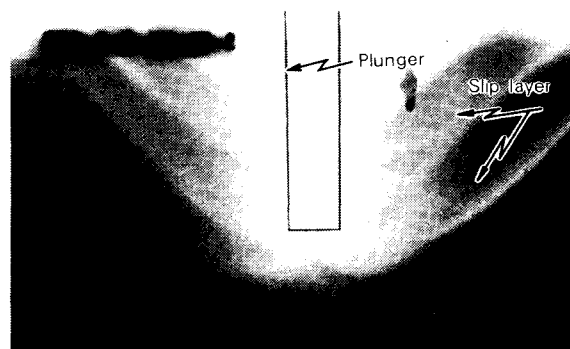
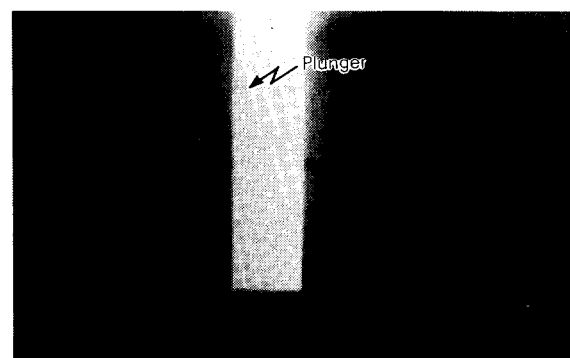


Fig. 12 Typical sound pressure wave form of musical sand



a) Musical sand
(number of distinct and periodical occurrence of slip layers correspond to Hz of sound)



b) Silent sand no slip layer

Fig. 13 X-ray radiographs of the slip layers

particulate materials can be obtained from this curve. As seen in Fig. 9 which shows the angle of internal friction of the silent, squeaky and musical sands, the difference $\Delta\phi$ between the static and the dynamic angle of internal friction (ϕ_s , ϕ_d) increases with the improvement of the sonorous property.

The coefficients of internal friction obtained from the tilting box and shear test are compared with the above-mentioned values in Table 1, which shows good agreement of the tendency of each value.

5. 4 Sonorous property

In the apparatus shown in Fig. 10, a plunger

penetrated into the silent, squeaky and musical sand on the same conditions. The sound pressure wave form and its frequency spectrum of the sound produced in the apparatus are displayed in Fig. 11. The container was large enough to avoid the wall effect in this case, too. The sound pressure emitted from the silent sand was so low that it hardly produced audible sounds. The squeaky sand produced the sound with relatively high frequency only at the last short period of penetration when the velocity was high and the larger force worked on the sand. The musical sand emitted the audible sound with high sound pressure and relatively low-frequency which lasted for a long time. The characteristics of the produced sound depended on the conditions for the penetration of the plunger. When the plunger penetrated into the musical sand relatively slowly (about 30 cm/s) and even lightly, it produced the sound which resembled the pure sound and had the sound pressure wave form similar to the sine curve as seen in Fig. 12. It seems to be the reason for the musical sand to have its name.

6. Mechanism of sound production

As the penetration characteristic curve shows, the musical sand displays a discontinuous destruction behavior by the external force. Figs. 13 (a) and (b) are the radiographs of the musical sand and the silent one with the penetrating plunger respectively.⁴⁾ When the plunger penetrates into the musical sand, the sand layer collapses with the periodical occurrence of the slip layer in it. The periodical change of load on the penetration characteristic curve corresponds to the formation of this slip layer. Its periodical formation with the expanding movement of the sand layer is the main source of the sound production.

In the silent sand the slip layer is not formed and only the local expansion occurs around the plunger and then it emits no sound.

In Fig. 14, the experimental results assure that the periodical occurrence of the slip layer is the reason for the sound production. The time trace of the penetration load and the sound pressure wave form of the produced sound as well as the frequency spectrum of the both show fair correspondence, which was confirmed also by the radiographs.

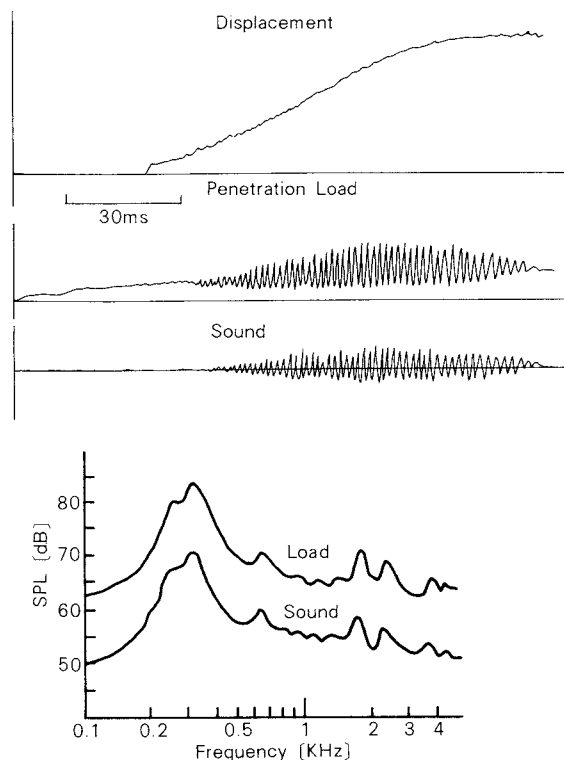


Fig. 14 Correspondence of load and sound

7. Conclusions

Although a number of reports have been published with regard to the musical sand so far, sufficient considerations have not been taken in any report concerning the complete elimination of the contaminations taking place in the natural environment.

The authors have investigated the method to eliminate the contamination from the musical sand using Gyratory Washer, whose washing mechanism is similar to that of the beach sand by the wave action in the sea coast. As a result, the musical sand could be studied in the more sensitive conditions. Besides, it became possible to revive the musical sand from the silent sand which had lost the sonorous property by the contamination in the natural environment. In this way some lost singing beaches have been found out.

It was also made possible to find the ancient musical sand in the ancient dunes or in the ancient coasts which form the lands now as a result of the repeated transgressions and regressions of seas in the geologic time. The Osodani-sand is one of those examples. This method seems to be able to offer a new point of view to investigate the depositional environ-

ment in the study of the geological environment.

In addition, the singularity of the penetration characteristic curve was investigated as the dynamic property of the musical sand in the ideal conditions obtained by the above-mentioned method. Besides, from its correspondence with the sound pressure wave form of the produced sound and their frequency spectrum, the sound producing mechanism of the musical sand could be explained.

Additional remarks

Though it was not mentioned in this report, a very interesting fact was observed recently. When the musical sand is oscillated quietly in the water after several hundreds hours washing by Gyrotory Washer, it produces a sound as if many steel ball would roll over. If this sand would be deposited on a beach, it could produce the audible sound with even small ripples on the shore line. In a Japanese ancient document, the sound produced by the sand of Koto-biki Beach is described as “There is a silvery (琅然) and subtle sound”. The adjective “silvery” was used by Soshoku (蘇軾), a prominent chinese poet about 1000 years ago to modify the rolling sound-producing gems. Here may be some clue to recall the natural romance of the ancient time when the natural environment was not contaminated considerably. This is another aspect of this study.

References

- 1) Miwa, S.: “Fantasy of Musical Sand,, , Diamond Pub. Co. [Book] 1982.
- 2) Kuenen, Ph.H.: *Am. J. of Sci.*, **257**, 172-190 (1959).
- 3) Meyerhof. G.G.: *Geotechnique*, **2**, 301-332 (1951).
- 4) Hidaka, J. and S. Miwa: *Kagaku Kogaku Ronbunshu*, **7**, 184-190 (1981).
- 5) Makino, K., J. Hidaka et al.: *J. Japan Soc. of Powder and Powder Metallurgy*, **29**, 229-235 (1982).
- 6) Hidaka, J., S. Miwa et al.: The Preprint of 20th Discussions of Powders (1982).

Some Technical Views of Recent Drying Processes in Japan

Tetsuo Yoshida*

Chubu Institute of Technology

1. Introduction

Wet particulate materials processed in drying apparatus can be mainly classified into four forms; slurry, paste or sludge, powders under 100 mesh and particles over 100 mesh. There are several technical guidebooks or handbooks already published to simplify the task of selecting the dryer type more suitable for such above materials.

In this report, however, my discussion will be limited to the followings;

- The material must be organic sludge which is difficult to deal with.
- The technical bases and the dryer types will be shown in the practical operations for such material in Japan.
- Application to energy saving and anti-pollution will be also referred since they have been playing a more significant role in recent drying processes.

2. Dewatering and drying mechanism in the powder bed

When the whole pore spaces are saturated only with water, the powder bed will be in the capillary state from the viewpoint of so-called *packing structure*. Table 1¹⁾ shows the well-known packing structures of powders containing various amounts of liquid and air, which may be helpful to understand the present paper.

2. 1 Preliminary process for drying

It is difficult to dry completely an organic powder bed due to its poor capability of water removal as well as its high moisture content. Thus a preliminary moisture removal by mechanical dewatering method would be required to save energy consumed in succeeding drying process, as indicated in Fig. 1.²⁾

Dewatering from slurry state to capillary one

Filtration is an effective preliminary mechanical operation which can remove mobile liquid among particles from the slurry state to the capillary one. Materials in the capillary state are pasty and may feature thixotropic behavior like that of colloidal dispersion which can flow continuously during agitation but would present gel-like appearance in stationary condition.

Further dewatering from capillary state

Press or vacuum dewatering method is practically used to remove more water in the capillary state. As a result of slow press operation, the material will reach the equilibrium compressing condition where the whole weight of the powder bed would be supported by the solid particles alone. In this case the moisture content of inorganic sludge will represent about 30% (W.B.) with shear by screw squeezing. With respect to organic sludge, however, the moisture may be decreased to at most 50 to 60% (W.B.) using vacuum dewatering, remaining within capillary state. Therefore drying process involving evaporation must be required to obtain more moisture-free condition such as the funicular (F-1) or the pendular one (P).

2. 2 Case hardening

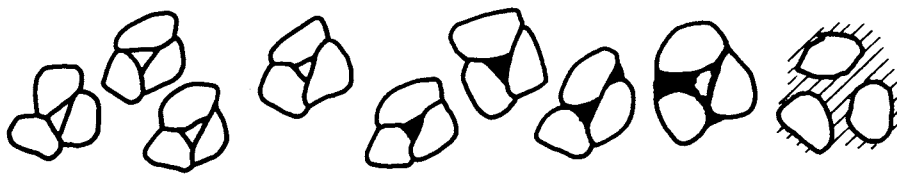
There is a surface evaporation period in an ordinary air drying process, where water evaporates on the surface of the material to which it is carried in liquid condition from the interior by the capillary suction pressure. With respect to organic sludge having the same size of colloid, on the other hand, it is peculiarly observed that the falling-rate drying will take place almost without the surface evaporation period. This is due to the phenomenon as follows:

When the drying operation begins, water in pore spaces among the particles near the sur-

* 1200 Matsumoto-cho Kasugai, Aichi, 487
TEL. 0568 (51) 1111

Received February 14, 1983

Table 1¹⁾ Packing character of powder-liquid systems

						
Particle (solid phase)	continuous	continuous	continuous	dis-continuous	dis-continuous	dis-continuous
Air (gaseous phase)	continuous	continuous	dis-continuous	—	—	—
Liquid hull (liquid phase I)	dis-continuous	continuous	continuous	continuous	continuous	dis-continuous
Free liquid (liquid phase II)				dis-continuous	continuous	continuous
Stage	Pendular P	Fenicular F-I F-II		Capillary C-I C-II		Slurry S
Critical point	C-1		C-2	C-3	C-4	C-5
In soil physics	P.L (plastic limit)				L.L (liquidus limit)	
Rheological system	Powder system		Mud system			Slurry system

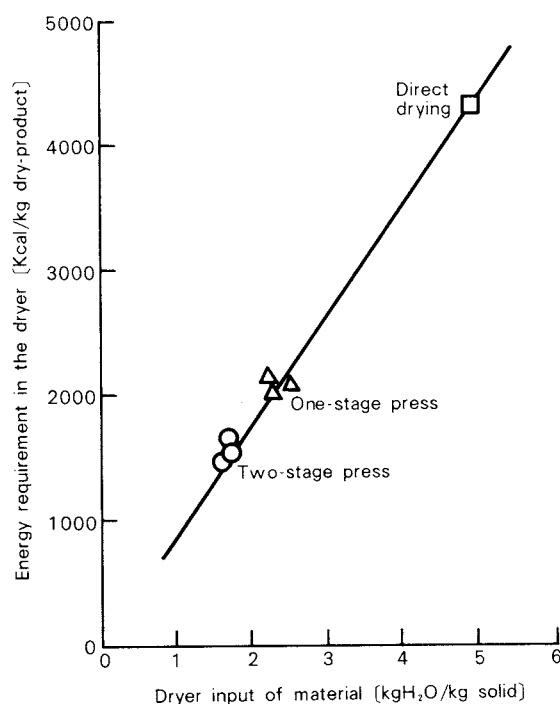


Fig. 1 Effect of mechanical dewatering on dryer heat load²⁾

face is carried by the osmotic suction pressure toward the outside. In the case of such a material as organic sludge, however, water evaporates more rapidly on the surface than the complement by water transferred from the inside

can be achieved, and then the funicular-water near the surface disappears suddenly and van-der-Waals force becomes dominant over the suction force. Accordingly particles near the surface would agglomerate by such a force to cause the case hardening. This so-called *surface skin* must require long drying period with a temperature difference of 2 to 5°C between the matter and the hot gas due to its envelopment of vapor generated inside.

2. 3 Granulation

Drying proceeds from the capillary state to the funicular one through the plastic limit condition (approximately 33% moisture content), where granulation takes place because of the favorable moisture content. Not only this granulation but the surface skin which encloses moisture within the interior must result in the elongation of drying period. When the sludge whose drying characteristic is given by Fig. 2³⁾ is to be dried, the drying process accompanied by disintegrating mechanism will offer great advantages as shown in Fig. 3.³⁾ It has been reported that the residence time in a rotary dryer of conduction type without a disintegration mechanism reaches to several hours, whereas that of a rapid dryer with a disintegrator at most 5 minutes.

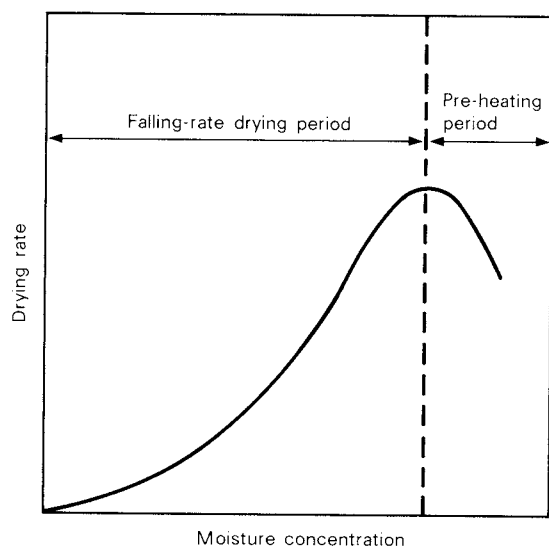


Fig. 2 Drying characteristic of sludge³⁾

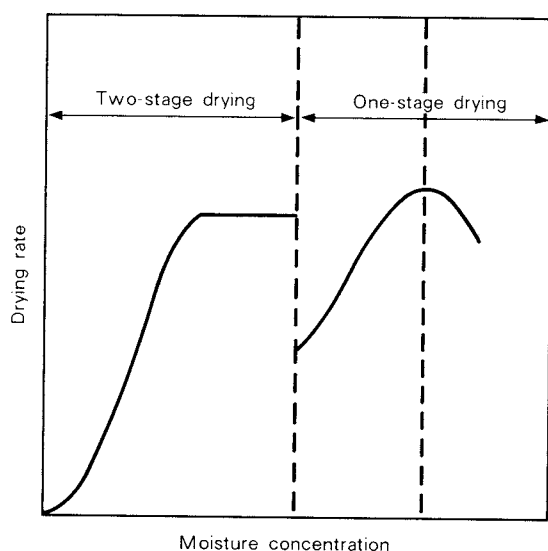


Fig. 3 Drying characteristic of sludge using two-stage method³⁾

3. Several methods for the promotion of drying rate

When colloidal matters are to be dried, the pre-operation such as extrusion or pre-forming have been practically used to develop the evaporation surface and shorten the time required for water transfer in the materials. In spite of such countermeasures the drying rate would tend to be decreased, if case hardening takes place to cause poor moisture transfer, as previously stated. The application of superheated vapor to several continuous processes can provide successfully improved drying rates as follows (which may be also adaptable for energy saving as stated later).

3. 1 Drying operation in superheated vapor

Boiling period

When wet materials enter superheated vapor, vapor condenses on them due to their lower temperature than the saturated one of the surrounding gas phase. A great deal of latent heat generated at this time causes rapid temperature increase of the materials up to near the boiling point. It makes the colloidal gel structure break easily and prevents the case hardening.

Evaporation period

In this period, as illustrated in Fig. 4⁴⁾, the drying rate can be very high, since the water moves from the center toward the surface by means of the pressure flow resulted from the vapor arising inside. For this reason, the critical moisture content would be lower than in the case of only air drying, and also the falling-rate curves become slightly convex.

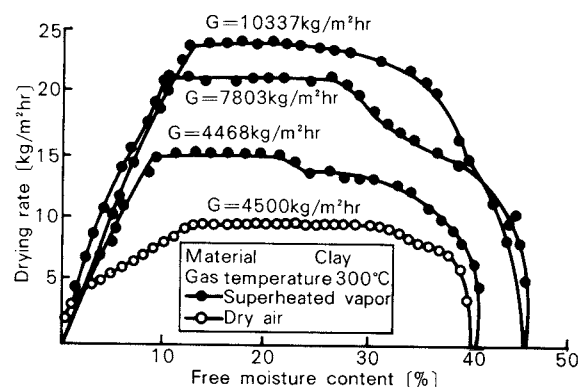


Fig. 4 Drying rate curve⁴⁾

The finish product has porous structure due to simultaneous vapor release from the surface and the interior. When this method is applied to the closed-circuit system, the air in the system will give place to the vapor in less than an hour. Therefore no boiler may be required and a self-inertizing effect will be achieved for materials which may be easily subject to oxidation.

3. 2 Drying gel-like materials and solvent recovery

In case of drying homogeneous gel formed from colloidal sol, the drying rate drops greatly since the vapor pressure of material reduces rapidly after a certain drying condition proceeds, and as a result the shrinkage continues to the end of the process. If such a material will be dried within an atmosphere vapor made by the

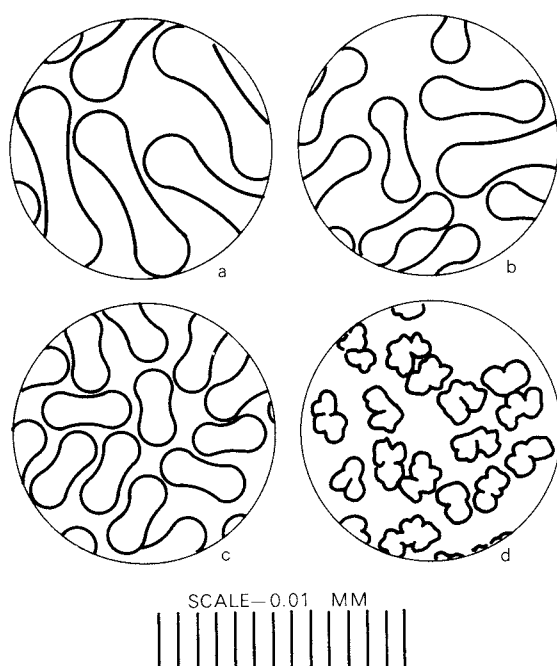


Fig. 5 Microscopic observations⁵⁾

a, b, c. Fiber dried with superheated vapor. d. Air-dried fiber

	Temp. of spinning chamber, °C	Stretch (in spinning chamber)	Denier	Strength, grams/denier	Elongation, %
a	148	1.25	18.3	0.80	44.0
b	119	2.66	9.85	1.04	41.3
c	84	6.74	4.35	1.19	38.8

solvent contained in the sol, the drying behavior of material may be differ from that of drying in the atmosphere of air.

Fig. 5⁵⁾ photographically shows cross sectional features of fibers obtained by dry spinning method from spinning dope solved in acetone. The cross sections of them shown in a to c of these pictures are for superheated vapor drying, on the other hand, one shown in d is for air drying. The former presents homogeneous product dried instantaneously without forming surface skin. The latter, on the contrary, offers shrunken product resulted from the surface skin which might take place in the early period to curb the vapor transfer from the inside to the surface.

Fig. 6⁵⁾ illustrates the solvent recovery process in the superheated vapor spinning system. This process requires neither absorption plant nor rectifying column for solvent recovery which is necessary to air drying spinning process, since only superheated acetone vapor is reused by circulation and its excess vapor is condensed.

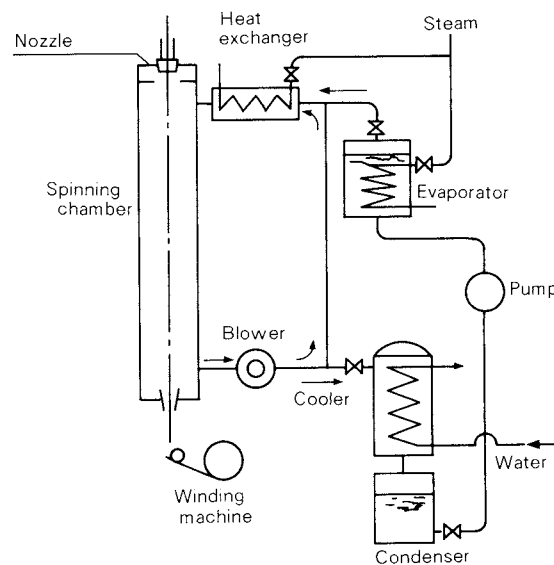


Fig. 6 Spinning with superheated vapor as scaled up to mass production⁵⁾

3. 3 Combination with vacuum drying

A combination of superheated vapor and vacuum drying will successfully prevent superheating of the material and the influence of oxygen. In general the pressure of a conventional vacuum dryer ranges from 3 to 50 mm Hg of absolute vacuum. However the drying process of chopped material using superheated vapor can be operated at 350 mm Hg abs. and around the saturated temperature of 80°C. Such a process produces powdery product with high quality when drying is rapidly completed and bubbles are kept stable.

3. 4 Direct heating by combustion gas

It has been experimentally confirmed that a drying rate would not depend on air content in the superheated vapor which is limited to at most 15%. Excellent results of drying sludge have been reported using semi-closed circuit dryer with high humidity and temperature, as illustrated in Fig. 7.⁶⁾ It is well known that the

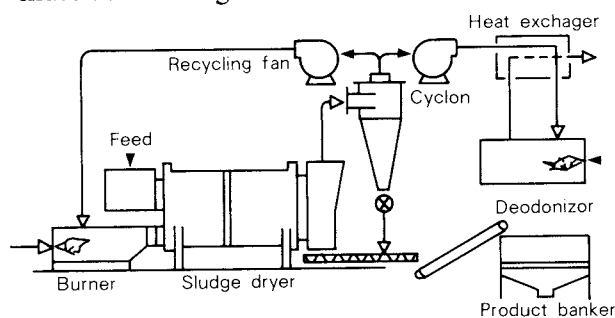


Fig. 7 Semi-closed circuit dryer⁶⁾

elevated inlet temperature or hot gas recycling system may enable the heat efficiency of the dryer to increase.

In the sludge dryer as shown in this figure, the material is heated by direct heating method generating hot gas at 700 to 800°C, which discharges out of the dryer at 150 to 200°C and is sent to cyclone. The gas within the dryer consists of the combustion gas and air (14%) and superheated vapor (86%). This process, using only a little gas with high humidity, can achieve easier anti-pollution treatment of exhaust gas and higher heat efficiency (approximately 80%) than a conventional one using a large volume of gas with high temperature. The sludge containing 70 to 80% water (W.B.), which is fed into the dryer in the same direction with hot gas, is dried so as to achieve the surface renewal and development using inner-rotating breaker. Then it becomes a spherical particle of 1 to 4 mm in diameter to be discharged as a finish product containing 13% water (W.B.) at 70 to 80°C. It is also reported that last exhaust gas contains dust load of 0.05 to 0.2 g/Nm³.

4. Application to energy saving and anti-pollution

It is well known that drying operations used in various industrial processes have been requiring considerable amounts of the whole fuel consumption. Recent sudden rise of energy cost has been needing more active counter-measure for energy saving as well as anti-pollution (which often necessitates energy). It was already pointed out in Fig. 1 how advantageous

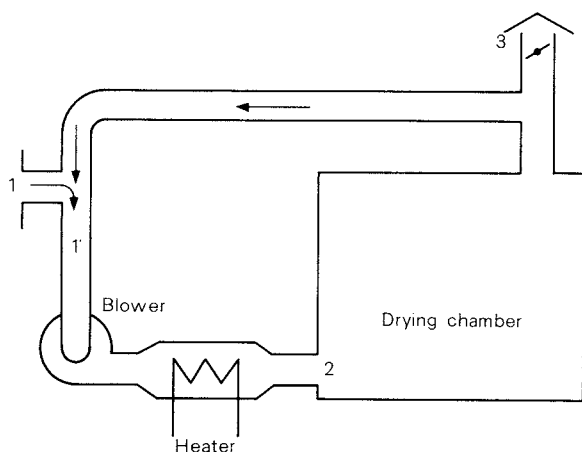


Fig. 8 Closed circuit dryer

it is to remove as much water as possible in the preliminary mechanical method to save energy in the drying process. Improved heat efficiency, on the other hand, can be provided by next other favorable methods for such a purpose.

4. 1 Hot gas recycling

The heat efficiency of hot gas dryers is calculated by the following equation:

$$\eta_T = \frac{t_2 - t_3}{R(t_2 - t_3) + (1 - R)(t_2 - t_1)} \times 100$$

where t_1 : surrounding air temperature
 t_2 : inlet air temperature
 t_3 : outlet air temperature
 R : ratio of recycling air flow rate to that of air flow through the dryer

Judging from this equation and also Fig. 8, η_T increases with an increase in temperature at the point 2 when the point 1' is kept hot, or η_T becomes 100% infinitely as R reaches to a unit. The elevated value of R , however, causes poor drying rate due to increased humidity in the dryer. Therefore if R can be increased without causing a drying rate reduction, an excellent drying process can be expected. The author and his co-worker identified that a rate of hot gas drying would increase as humidity rises, if the gas within the system is kept hotter than a certain temperature.⁷⁾

This is schematically shown in Fig. 9⁷⁾ where H denotes absolute air humidity. If a temperature remains above the inversion point, the evaporation rate increases with increasing humidity. Furthermore the evaporation rate will

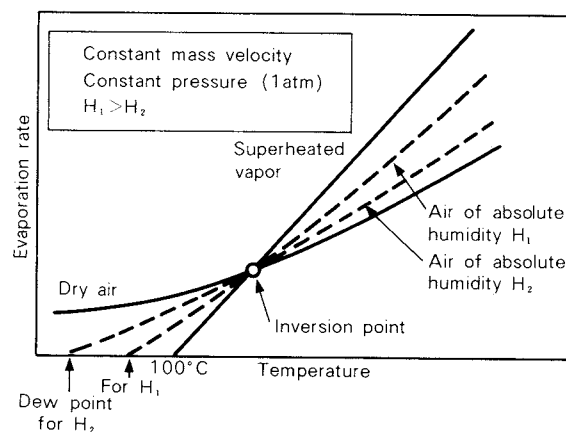


Fig. 9 Relation between evaporation rate and gas temperature⁷⁾

Table 2⁸⁾ Pneumatic drying of slurry in a mining refinery

Parameter		Closed circuit type	Total rejection type
Evaporation rate	[kg/h]	566	566
Inlet moisture content of material	[%]	85	85
Outlet moisture content of material	[%]	10	10
Feed rate	[kg/hr]	680	680
Inlet air temperature	[°C]	500	350
Outlet air temperature	[°C]	150	120
Exhaust gas rate	[kg/h]	620	7,430
Recycle ratio (R)	[%]	9.17	—
Exhausted heat	[kcal/h]	20,200	188,000
Heat loss	[kcal/h]	30,300	37,800
Total heat input	[kcal/h]	428,000	597,000
Heat efficiency	[%]	87.9	62.4
Efficiency promotion	[%]	41	41

reach to the maximum when nothing but superheated vapor exists in the system. The temperature of the inversion point ranges from 170 to 200°C, depending on the mass flow rate. Accordingly the higher temperature is advantageous so as to increase R when it is above the inversion point.

Table 2⁸⁾ shows two different systems of drying the slurry in a sinkpond of a mining refinery. The closed circuit system with the recycling ratio R of about 92% could provide higher efficiency by about 40%, as compared with the total rejection one. It could also produce a self-inertizing effect. The dryer type used there might be guessed to be a self-inertizing pneumatic one including a direct burner, as shown in Fig. 10.⁸⁾ It has another advantage in the decreased emission problems, since the amount of exhaust gas occupies only 8% within the whole system.

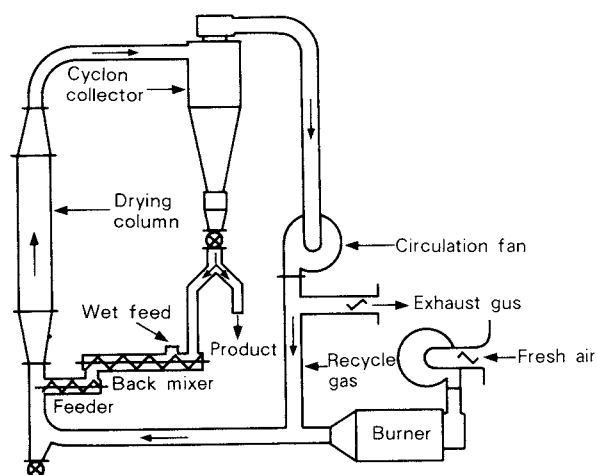


Fig. 10 Self-inertizing pneumatic dryer⁸⁾

4. 2 Utilization of latent heat existing in the exhaust gas

4.2.1 Hybrid dryer with evaporator

After juice extraction, citrus fruits decrease volume by 1/3 or weight by half. Their wastes including flesh and pericarp require a good deal of energy for the use as fodder. Therefore the efficiency improvement has proven to be a serious problem in the drying processes among the citrus fruit industries.

The author and his co-worker previously suggested how advantageous the use of hot and humid air is for such a drying process, as shown in the reference.⁷⁾ The new drying system technically based on the paper, where vast latent heat of exhaust gas out of the semi-closed circuit hot gas dryer was utilized for the evaporation concentrator, was constructed and worked successfully. In these days, this type of system has been adopted at the some citrus processing industries in Florida as well as those in Ehime and Wakayama of Japan.

Fig. 11⁹⁾ shows an outline of such a system where the finish product (fodder) containing the moisture of 10% can be obtained from the waste containing 85%. In the steady condition, the vapor occupying 80% in the recycle gas condenses in the heating stage of the first evaporator (natural convection and long column type), where its latent heat concentrates the waste liquid (8% citrus molasses) from a press. This process exhausts the excess uncondensed gas of 5000Nm³/h, which may be no more than 1/3 compared with a conventional type, as indicated in Table 3.¹⁰⁾ The heat efficiency of

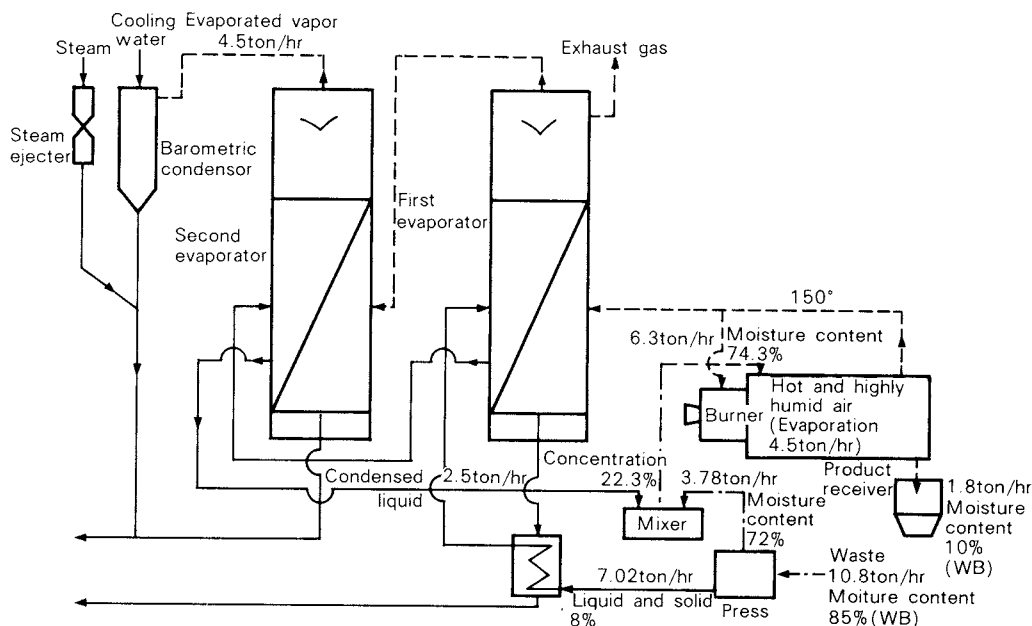


Fig. 11 An example of latent heat utilization combining dryer with evaporator in citrus-fruit processing system in Japan⁹⁾

the advanced process can reach to 160% because of better utilization of latent heat in the exhaust gas, though the heat-exchanging surface of the evaporator requires twice as wide area as that of conventional vapor heating type.

Table 4²⁾ shows the test result performed in

Florida which indicates that particulate emission can be sufficiently reduced by half with recycling 30% vapor and further more reduced by less than 1/10 using a triple effect evaporator with a single-stage press.

Table 3 Economical comparison with conventional type¹⁰⁾

Parameter	Conventional type A	Hybrid type with evaporator B	Saving	Ratio of B to A
Evaporation rate	9.0 ton/h	9.0 ton/h		100%
Production rate	1.8 ton/h	1.8 ton/h		100%
Fuel consumption	0.9 ton/h	0.35 ton/h	0.55 ton/h	39%
Heat efficiency	62 %	160 %		
Power consumption	140 KWh	170 KWh	-30 KWh	-120%
Dry exhaust air flow rate	25,000 Nm ³ /h	5,000 Nm ³ /h	20,000 Nm ³ /h	20%

Table 4 Dust concentration in stack gas from citrus plup and peel dehydrators²⁾

	Feed* [ton/h]	Exhaust dust [kg/h]	
		permission**	measured value
Dryer and scrubber			
without vapor recycle	8.4	6.1	34.2
with 30% vapor recycle	8.6	6.3	17.3
using improved scrubber	8.9	6.4	3.9
Triple effect evaporator with single press			
using dryer only	18.2	9.8	11.7
using both dryer and evaporator	41.2	14.2	2.8
Double effect evaporator with two stage press and flash evaporation			
dryer, flash evaporation, and evaporator	21.4	10.8	6.5

*) This value is a net one of all the material fed into the process without air, liquid, gas fuel and water.

**) This is based on the act of Florida State

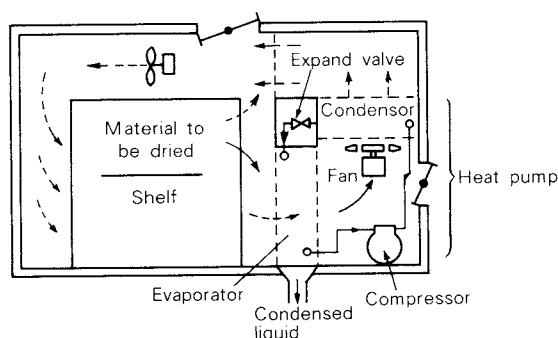


Fig. 12 Dryer using heat pump¹¹⁾

4.2.2 Utilization of heat pump system¹¹⁾

Heat pump is a practical equipment based on thermodynamic consideration for the purpose of heating instead of refrigeration. In such a system, mechanical work by a compressor W [KJ] draws heat Q_2 [KJ] from the cooler side (evaporator) to the hotter one (condenser), where total heat $Q_1 (= Q_2 + W)$ is discharged. Fig. 12 illustrates a direct, batch dryer where the heat pump system can be successfully applied to save energy as well as to dry efficiently as follows; when humid air enters such a heat pump system, most of water vapor from wet materials is condensed on the evaporator where latent heat of the vapor Q_2 is absorbed. Then the dehumidified air is carried by fan to the condenser where it gives heat Q_1 . After leaving this system, this hot and dehumid air is sent to the trays to dry materials. This may be a kind of drying methods recovering the latent heat of dryer exhaust gas, which results in high efficient operation.

The dryer like this has been mainly prevalent in wood industry using dry air at the maximum temperature of 50°C (the ratio of dehumidification rate $C_e = 2.0 - 2.5$ kg/KWh). Another utilization is to dehumidify materials sensitive to humidity such as sugar, grain for cake and ceramic, or materials which must be kept in low humid condition.

Recently new processes operated at the maximum temperature of 97°C was developed in chemical pharmaceutical industries so as to dry powdery materials using as little energy as possible.

4.2.3 Freeze drying with LNG¹²⁾

Imported LNG occupies about 70% in gas fuel which is used in large cities such as Tokyo,

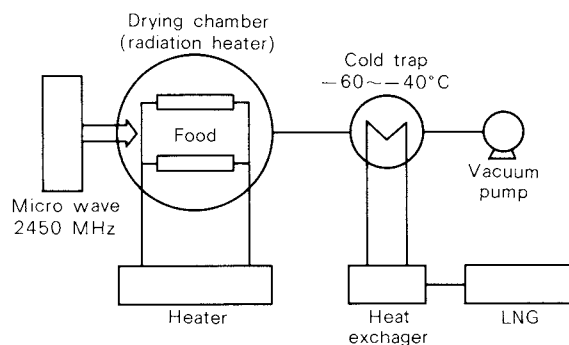


Fig. 13 Freeze dryer (Hybrid heating)¹¹⁾

Osaka, Nagoya and so on. From the viewpoint of energy saving, utilization of the cold heat of the fuel having the boiling point of ca. -160°C has been tried for various industrial purposes.

Freeze drying is one of the results obtained from such trials. It has an advantage of not only drying colloidal material which is difficult to dry completely, but also drying food with the following excellent features;

- no change in taste or nutritive value
- achievement of low moisture content
- easy restoration to the original state

Fig. 13¹²⁾ illustrates new freeze drying process where LNG cold is utilized for preliminary freezing and ice is sublimated by a micro wave heating as well as a conventional radiation heating. This process can provide energy saving effect with the utilization of LNG, sterilization effect using micro wave heating and productivity improvement which may shorten operation time by 20 to 50%.

The present paper is concerned with several advanced drying processes in Japan, emphasizing drying wet materials such as organic sludge which is impossible to dry so much efficiently as ordinary materials. It also refers the application of such processes to anti-pollution as well as energy saving that has been a serious problem in this country due to the recent rise of energy cost.

References

- 1) Umeya, K.: Proceeding of U.S. - Japan Seminar on Mech. of Granular Material 222-240 (1978).
- 2) Byran, W.L.: *AIChE Symp. Series*, 73, 163 (1977).
- 3) The Soc. Chem. Eng. (Japan): "Technology and apparatus for sludge treatment (Environment conservation services)" p.142 (1978).

- 4) Hyodō, T.: Ph.D. Thesis, Osaka City University
p.53 (1971)
- 5) Yoshida, T. and T. Hyōdō: I.E.C., *Process Design
and Develop.*, **2**, 52 (1963).
- 6) Kawai, S.: The preprint of the 13th technical dis-
cussion in the Society of Powder Technology,
Japan (1978).
- 7) Yoshida, T. and T. Hyōdō: *I.E.C., Process Design
and Develop.*, **9**, 207 (1970).
- 8) Noden, D: *Processing*, **20**, No.12 (1974).
- 9) Kawai, S.: *Kagaku Kōgaku*, **42**, No.2 (1978).
- 10) Hot and high humid dryer, Brochure of Okawara
Manufacturing Co., Ltd.
- 11) Hodgett, D.L.: *The Chem. Engineers*, July 1 August
(1976).
Nishino, H.: *J. Japan. Soc. Mech. Eng.*, **18**, No.67
(1952).
- 12) Ishida, Y. and T. Matsubara (Osaka Gas Ltd.):
Energy and Resources, **3**, No.4 Japan (1982).

Survey of Recent Advances in Research on Powder Mixing in Japan

Munetake Satoh* and Keijiro Terashita*

*Department of Chemical Engineering
University of Osaka Prefecture*

1. Introduction

Mixing or blending of solid particles is one of the most important unit operations widely used in many industries to control the raw materials or to homogenize the final products. According to various requirements in many processes, various kinds of mixing equipments have been developed and a lot of technical devices have been applied to solve the practical problems. Numerous studies on the mixing of solid particles have been done by means of theoretical and experimental methods. Research on the solid mixing involves very comprehensive subjects such as the expressing method of the mixing state and the mixing process on the basis of mathematical model, mechanisms of mixing and segregation caused by the difference in the physical properties of solid particles, effect of the physical properties of powders and operating conditions on the performance of the mixers, design and scale up of mixers, power requirement of mixers, computer simulation of mixing processes and so on.

In this review, recent works on the mixing of solid particles published in academic journals from the last review³⁶⁾ in 1975 to today are introduced.

2. Fundamental studies on the mixing processes

2. 1 Degree of mixing

Various kinds of index to express the mixing state of solid particles have been proposed and used by many researchers. Most of the available definitions of the mixing index, which specifies

homogeneity or distribution of the composition in a solids mixture, are based on the variance of the concentration of a certain component among spot samples. This statistical definition cannot provide a sufficiently deep insight into the microscopic and geometric nature of a mixture. A new definition of the degree of mixing was proposed based on the mean contact number from a microscopic and geometric viewpoint. Usually, it is difficult to measure the contact number around the key particles in a mixture. The determination of the concentration of particles by spot sampling, instead of direct counting of the contact number, as a practical method of estimating the mean contact number was examined for the regular packing of binary component system¹⁾. It was shown that the concepts of the coordination number and contact number could be applied to the expression of the mixing state for the regular packing arrangements with irregular patterns²⁾ and for the multicomponent solids mixture in the completely mixed state⁵⁾. The knowledge of the structure of a mixture which is the final product of the mixing operation is essential in understanding sintering and packing characteristics, and reactivity of the mixture. From this viewpoint, clarifying the microscopic arrangement of particles comes to be of great importance.

2. 2 Mechanisms of mixing

The solids mixing process has been regarded as a probabilistic phenomenon which involves basic three mechanisms: convective, diffusive and shearing mixing. The mixers have been classified into the various types according to the ways to work the mechanical forces which promote the mixing of solid particles. Rotary vessel type mixers have been adopted in many researches for the observation of flow patterns

* 4-804 Mozu-Umemachi, Sakai, Osaka, 591
TEL. 0722 (52) 1161

Received May 13, 1983

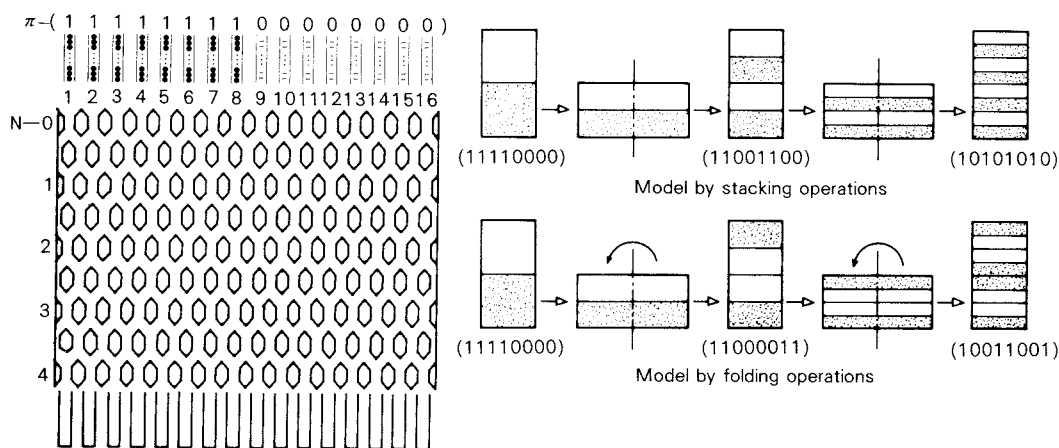


Fig. 1(a) Diffusive mixing model
(Probabilistic branching model)

Fig. 1(b) Convective mixing models
(Strata forming model)

and the application of mathematical models. Steady state Markov chain model was applied for describing the main flow patterns of particles in the V-shaped type mixer and circulation time distribution along the flow was obtained by the transition probability¹²⁾. Furthermore, as the application of this model, the segregation of solid particles in the mixer was simulated with the aid of a digital computer^{9,10,11)}.

In the actual mixers, it is difficult to distinguish or separate basic three mechanisms. A new approach called “the synthesis of a mixing system” was proposed to describe the complicated mixing processes. It was assumed that the mixing process consisted of two basic mechanisms, diffusive and convective mixing. The diffusive mixing is described by a probabilistic branching model where the particles flow down between hexagonal obstacles which are located in zigzag lines on a plane as shown in Fig. 1(a). On the other hand, for the convective mixing, the mixing process is attempted to describe using the models by stacking and folding operation as shown in Fig. 1(b). The optimum feeding strata to achieve the completely mixed state in the shortest time was discussed by the combination of these two elemental models³⁾.

2. 3 Segregation of de-mixing models

It is well known that solid particles tend to segregate when the particles in the mixture have different physical properties such as size, density, internal friction coefficient, shape, surface conditions and so on. A number of mechanisms have been proposed as responsible ones for the segregation effect, including vibrational

segregation in which larger particles tend to rise to the surface, percolating segregation in which the top layer of particles acts as a screen through which all except the larger particles are able to pass and reach the stationary region below, puring segregation in which larger particles tumble further down the free surface of a growing pile, free flight segregation which results from particles having different trajectories and so on. The axial segregation profile of binary solid mixtures during the mixing and segregation processes in a horizontal rotary conical vessel was studied by using several kinds of combination of particles. The segregation characteristics profiles based on the concentration distribution of concerned particles with time were measured as shown in Fig. 2 (a) and (b) and it was confirmed that the demixing potential, proposed in the Rose's equation, related to the axial arrangement of the particles in the vessel^{27,35)}. Furthermore, the radial and axial segregation in a rotary vessel type mixers were closely related to the permeation effect measured in a moving bed²⁵⁾. The cascading angle difference between particles of the mixture was found to be one of the important factors for the segregation in the mixer²⁶⁾. The rotary conical vessel can be used as a continuous separator of the mixture applying the characteristics of segregation of which larger particles tend to move toward the narrower end of the vessel and smaller particles toward the wider end²⁸⁾. The segregation of particles with different density in both the axial and radial direction was measured by counting the tracer particles according to the mixing time.

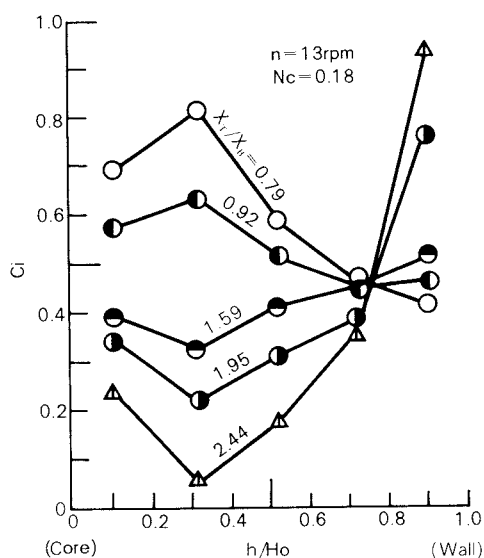


Fig. 2(a) Experimental results of radial distribution of B-particle concentration. Concentration (bulk volume fraction) C_i vs. radial depth of the bed (h/H_o) in a cylinder was plotted with permeation effect (x_T/x_B) obtained in a moving bed.

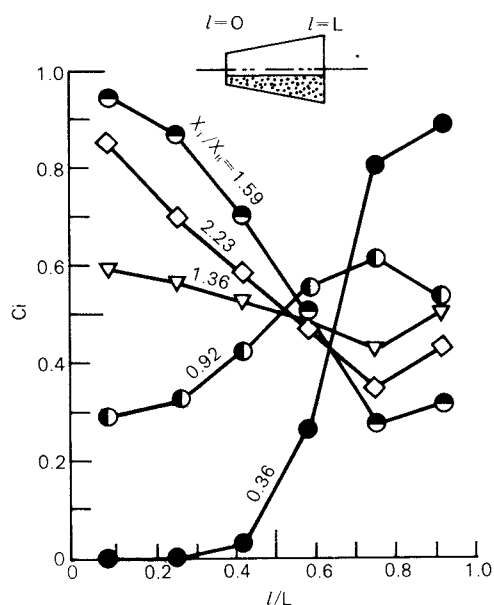


Fig. 2(b) Experimental results of axial distribution of B-particle concentration C_i in a horizontal rotating conical vessel, differing in (x_T/x_B). (l/L) is axial distance from the end of of the minimum diameter in a conical vessel at $n = 15$ rpm.

The statistic characteristics of the motion of each particles depend upon the variation of concentration profiles. It has been shown, in such a case, the theory of Semi-Markov process model can be extended by means of the experi-

ments and the computer simulations^{8,9,10} On the other hand, as a macroscopic treatment for the mixing and segregation phenomena, apparent diffusive coefficients of particles of different density in the cylindrical vessel were measured and the effect of the end walls on mixing was discussed^{11,34}.

3. Mixing operations

There are a number of problems to be solved in the actual mixing operations such as selection of the mixing equipment, determination of the optimum operating conditions, improvement of the physical properties of solid particles and so on. Segregation caused by the difference of particles size is remarkable when the particles have spherical shape and good flowability. The degree of segregation based on the standard deviation of the tracer concentration was measured using radioactive tracer method, after mixing of atomized powder metal mixture having widely dispersed size distribution. Two different types of mixers, a ball mill and a static (or motionless) mixer, were examined in the mixing performance. It was shown that using the static mixer as a secondary mixer after mixing with the ball mill was rather effective than using each mixer respectively. It was also noticed, however, that some segregation took place at the declining part of the mixer where the free flowing layer was observed at the same time²⁹. To obtain homogeneous mixture of fine and irregular shape powders, the static mixer was attempted to apply to the mixing system³⁰.

It was pointed out that the internal friction coefficient was one of the important factors to affect mixing characteristics³³. Internal friction coefficients have been measured by a direct shear tester for a number of powders having different particle diameters and densities, and for their binary mixtures. The mixing performances of the mixers have been correlated much better with the internal friction coefficient than with the change in particle diameter or density. Fig. 3 shows the relationship between the final degree of mixing $M_\infty(1 - \sigma/\sigma_0)$ and difference of the internal friction coefficient $\Delta\mu_s$ of each powder component before mixing. While the final degree of mixing in the rotary vessel type mixers decreases as $\Delta\mu_s$ increases, those in the fixed type ones are hardly influenced by the

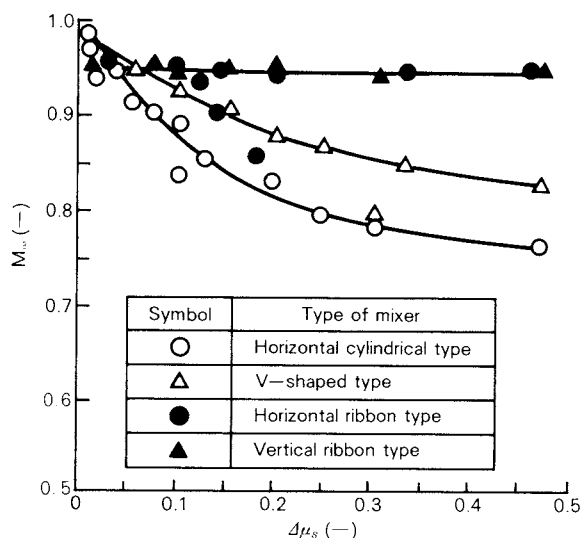


Fig. 3 Relationship between terminal degree of mixing $M_{\infty} = 1 - \sigma_{\infty}/\sigma_0$ and difference of internal friction coefficients $\Delta\mu_s$.

friction coefficient.

Fine powders under $10\mu\text{m}$ in diameter are difficult to achieve the complete mixing state because of their high adhesiveness, tendency to agglomeration and poor flowability. Mixing of these materials requires some mechanisms to homogenize them disintegrating their agglomerates by strong shearing force and some additional device to prevent adhesion of the materials on to the mixing equipment and coagulation each other.

Experimental studies on the continuous mixing of fine particles have been done by using a vertical cylindrical mixer with a variety of impellers. It has been found that the principle of designing an effective impeller for continuous mixing is to give intensive radial mixing without increasing axial mixing. On the basis of this principle, the new types of impellers suitable for continuous mixing of fine and cohesive powders have been developed and their performance has been evaluated by means of the tracer response technique¹³⁾. It has also been shown that a properly designed vibratory feeder with a suitable feedback control system can be used to keep the feed rate of fine and cohesive powders into a continuous mixer at a constant value¹⁶⁾.

A high speed pulverizer was applied to the mixing of coarse binary particles with a simultaneous size reduction instead of the direct mixing of fine and cohesive powders. After coarse binary particles were directly fed to the

pulverizer, the degree of mixing of products was measured. When each component of the binary particles had nearly the same hardness, even though they showed tendency of segregation before grinding, segregation did not take place during the operation and high degree of mixing was obtained³¹⁾. One of the advantages of this grind mixing is the prevention of segregation of mixture owing to reduction of flowability of the fine products.

On the contrary, some attempts have been done to improve the physical properties of powders and the uniformity of the mixture. Coarser particles such as crystals or granulates were mixed with other fine powders in order to make the powders suitable for dispensing and to improve its flowability. With increasing fraction of coarser particles in the mixture, angle of repose of the mixture decreases. The final degree of mixing was affected by the ratio and size of the coarser particles⁷⁾. Another report gave experimental results that in case of mixing fine and coarse materials, sufficient agitation of the coarser one is essential for effective mixing of the finer at the beginning of mixing and that adhesion of the finer particles on the surface of the dispersed coarser ones has a great effect on the final mixing state. In this case, the cohesive fine powder decreases the tendency of segregation by means of coagulation by itself and agglomeration with the coarser particles⁶⁾.

These results suggest the possibility of controlling the physical properties of solid particles according to the mixing purposes.

Fluidized bed or pneumatic type mixers are suitable for mixing of solid particles having almost equal physical properties and good flowability. On the other hand, injection of gas into the particle bed tends to segregate the component having different physical properties. Mixing and/or segregation processes of particles by succeeded single bubble were observed in a two dimensional fluidized bed, containing particles of different size and density. It was found that the local convective mixing of particles was influenced by the bubble diameter and the frequency of bubble formation. Even if there exists difference of physical properties between the component in a binary mixture, the motion of the particles of less amount of component was restrained by the motion of bulk component, i.e. segregation of different particles

from the mixture bed was controlled by the mass flow¹⁴⁾.

The mixing characteristics of positive and negative air mixers were investigated under the unsteady fluidizing conditions. Using both methods of injecting gas into the powder bed by compression and suction, the degree of mixing, mixing time and the power requirement were measured and these results were compared with the results of a V-shaped mixer. It was shown that the mixing performance of the air mixer was better than that of the other types when the particles to be mixed had little difference in the physical properties, and that the power requirement in suction fluidized mixer was less than pressurized one⁴⁾.

4. Power requirement of mixer

For design or selection of suitable mixing equipments of solid particles and for decision of optimal operational conditions, the mixing performances should be evaluated taking account of the power requirement of mixers as well as the rate of mixing and the final degree of mixing. Power requirement of mixers is markedly influenced in a complicated manner by various factors, such as the structure and dimension of mixing equipment, the physical properties of solid particles, the operational conditions and so on.

4. 1 Rotary vessel type mixers

Power requirement of horizontal cylindrical mixers has been measured with a variety of solid particles²⁰⁾. The total force exerted on the mixer shaft by the charged solid particles was assumed to be the sum of ; (i) the gravitational force by the powder bed, (ii) the inertia force for accelerating the powder mass, and (iii) the frictional force acting between the powder bed and the inside wall of the mixer. A dimensional analysis of the basic force balance equations has been made to obtain useful correlation of the power data in terms of the operating conditions, the dimensions of the mixers and the physical properties of the solid particles, specifically the bulk density and the friction factor between the vessel wall and the powder bed.

The Newton number, Ne , and the Froude number, Fr , both non-dimensional terms have been found important for the estimation of power requirement for this type of mixer. They can be correlated by the following equation²¹⁾:

$$\frac{T \cdot g_c}{R^3 \cdot L \cdot \rho_a g} = A + B \frac{N^2 \cdot R}{g} \quad (1)$$

where T : torque (kg·m), R : radius of cylinder (m), L : length of cylinder (m), and N : rotary speed (rpm), respectively. The left hand of the

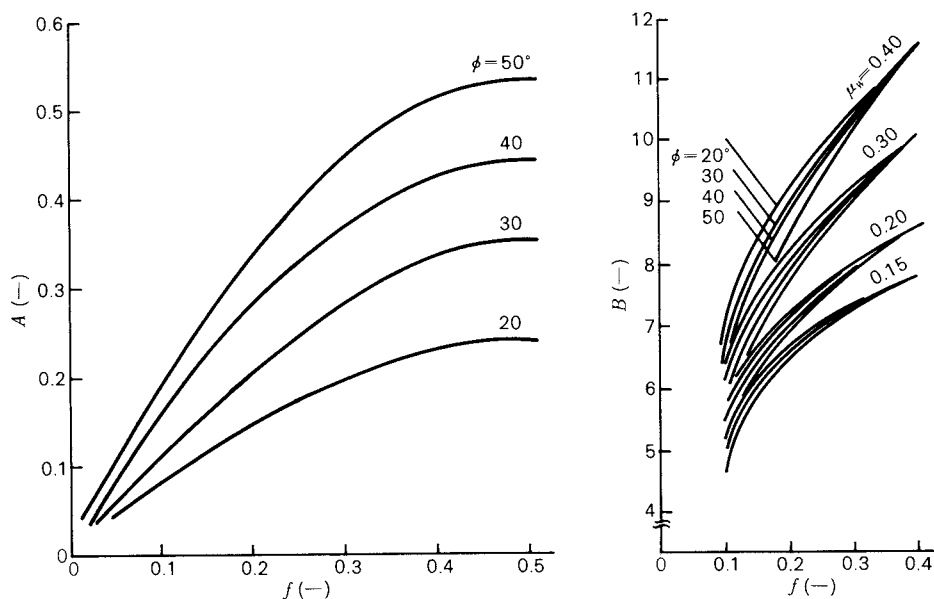


Fig. 4 Computed values of coefficients A and B in Eq. (1) for horizontal cylindrical mixers

equation (1) represents Newton number and the second term on the right hand side corresponds to Froude number. The value of A and B are function of the charge ratio $f(-)$, angle of repose ϕ (deg) and the friction coefficient of vessel wall $\mu_w(-)$. Fig. 4(a) and (b) show the calculated values of A and B as the function of the charge ratio. Using these figures, the power requirement of horizontal cylindrical mixers can be estimated. For the V-shaped and double cone type mixers, equation (1) is still admitted fundamentally, though the torque varies periodically with the revolution of the mixer's vessel.

4. 2 Fixed type mixers

The fixed type mixers consist of various shapes of vessel and agitator (mixing paddle, screw, pin or rod, ribbon, scraper etc.). It is very difficult to obtain the general relationship among the power requirement, the shape and dimension of mixer, the physical properties of solid particles and the operating conditions, because the flow pattern and mixing mechanism are more complicated than those in the rotary vessel type mixers. This situation is probably related with the fact that still very little is known about the rheological behaviour of solid particles.

The relationship among the mixing torque for the horizontal ribbon mixers and various factors has been studied. The torque increases with the charge ratio f , the bulk density ρ_a , the internal friction coefficient μ_i , and the dimension of the ribbon blade. On the other hand, the torque is not influenced by the rotary speed N in the range of $30 \leq N \leq 200$ (rpm). The shear force has been found to be a dominant factor in the total power requirement of the mixer. The power data P were well correlated with the experimental conditions by the relation¹⁷⁾:

$$P \cdot g_c = K \mu_i \cdot \rho_a \cdot g \cdot f(\pi D_0^2 L) d_e N \quad (2)$$

where, D_0 : diameter, L : length, d_e : characteristic length of ribbon and K : experimental constant.

For the vertical ribbon mixer, the effects of various operating condition on the mixing torque have been studied experimentally¹⁸⁾ and the power requirement for agitation of the powder bed has been analyzed by introducing a simplified model¹⁹⁾. The total force exerted on

the ribbon blades by the powder bed was assumed to be the sum of : (i) the pressure force by the powder bed in the passive Rankin state, (ii) the shear force acting on the circumscribing cylindrical surfaces around the ribbon blades, and (iii) the inertia force for accelerating the powder mass surrounded by the cylindrical surfaces. The ratio of the total force to the inertia force and the ratio of the inertia force to the shear force were calculated. Further experimental correction would be necessary for this kind of power equation and besides it becomes important to evaluate the dynamic physical properties of solid particles and flow patterns.

The tensiling process curves for powders with various moisture contents have been obtained experimentally in order to correlate the mixing torque with the tensile strength. From the trend between the breakup displacement and the moisture content, the powders were able to be classified into three stages according to the region of moisture content. Characteristics curves of torque were discussed based on the stage of powders and the tensile stress. The mixing torque for moist powders was excellently correlated with the tensile strength obtained by the tensile tests for the powders with the void fraction identical to that for the torque measurement³²⁾.

4. 3 Fluidized bed and moving bed type mixers

In the fluidized or moving bed with mixing devices, the fluidization of solid particles is promoted by the injection of air or gas into the powder bed and the mechanical agitation. It is well known that the packing state of powder bed becomes looser and both the bulk density and the internal friction coefficient decrease, once the powder bed is set to motion in the mixing equipments.

Relationship between the optimum condition of mixing and the total power requirement was investigated using a model of fluidized bed with plate paddles¹⁵⁾. The total energy (defined as the sum of power requirement for mechanical agitation and aeration) taking account of the time required to reach the final degree of mixing became minimum in the region where the air velocity was about 1.4 to 2 times as high as the minimum fluidization velocity. The resistance force for agitating the powder bed depends much upon the pressure drop when

the air velocity is under the minimum fluidization velocity. The pressure drop in a moving bed with a double herical ribbon was measured changing the shape of ribbon blades, operating conditions and physical properties of solid particles. The relationship among the dimensionless pressure drop Δp^* and various parameters was expressed in the following equation²²⁾,

$$\Delta p^* = K_{gas} R_p^{0.5} R_b^{-1} \exp(-N/5) u^* \quad (3)$$

where, $\Delta p^* = \Delta p / \Delta p_{mf}$, Δp : pressure drop, Δp_{mf} : pressure drop at the minimum fluidizing point, R_p : ratio of ribbon pitch to ribbon diameter, R_b : ratio of width of ribbon blade to ribbon diameter, N : rotary speed, $U^* = U / U_{mf}$, U : air velocity, U_{mf} : minimum fluidization velocity and K_{gas} : experimental constant.

On the other hand, the amount of decrease in torque due to the blowing air into the powder bed has been well interpreted in terms of a dimensionless pressure drop Δp^* as shown in Fig. 5. The general correlation equation for agitating torque with aeration has been provided as follow²³⁾,

$$T_G = T_0 (1 - 0.93 \Delta p^*) \quad (4)$$

where T_G and T_0 are mixing torque with and without aeration. The power requirement for the moving bed with mechanical agitation has been well correlated by the various experimental parameters within an accuracy of $\pm 30\%$. Additionally, the starting torque for moving bed type mixer was measured under the various

operating conditions and the relation between the initial void fraction of the powder bed and starting torque was discussed. The starting torque decreases almost exponentially with increasing initial void fraction. The reduction of the torque due to increase in void fraction has been correlated by an experimental equation²⁴⁾.

5. Conclusion

The recent advances in research on the mixing of solid particles were introduced in this review. For modeling of mixing mechanisms and mixing processes in the actual mixing equipments, effects of the physical properties of solid particles both in the state of static and dynamic on the behaviour of powder bed should be considered in the basic models. Research on the mixing processes under the condition of gravity free state or under different force field such as magnetic, electric, sonic etc, becomes more important item for designing mixers based on new mixing mechanisms. Furthermore, controlling the characteristics of powders for each purpose or designing the physical properties of solid particles (diameter, shape, density, void fraction, pore size, surface conditions, activity, flowability, etc.) using chemical and physical treatment is another interesting future subject of research.

References

- 1) Akao Y., H. Shindo, N. Yagi, L.T. Fan, R.H. Wang and F.S. Lai: *Powder Technology*, **15**, 207-214 (1976).
- 2) Akao Y., H. Kunisawa, L.T. Fan and R.H. Wang: *Powder Technology*, **15**, 267-277 (1976).
- 3) Akao Y., H. Shindo and H. Angel: *Journal of the Society of Powder Technology, Japan*, **19**, 639-645 (1982).
- 4) Akiyama T., T. Kano, K. Matsubara, M. Kono and J. Meio: *Journal of the Society of Powder Technology, Japan*, **20**, 135-141 (1983).
- 5) Fan L.T., J.R. Too, F.S. Lai and Y. Akao: *Powder Technology*, **22**, 205-213 (1979).
- 6) Fukuda T., Y. Fukumori and Y. Takeuchi: *Journal of the Society of Powder Technology, Japan*, **18**, 926-931 (1981).
- 7) Hayashi H., T. Kasano and K. Suhara: *Journal of the Society of Powder Technology, Japan*, **20**, 22-27 (1983).
- 8) Koga J., K. Yamaguchi and I. Inoue: *Kagaku Kogaku Ronbunshu*, **4**, 413-418 (1978).

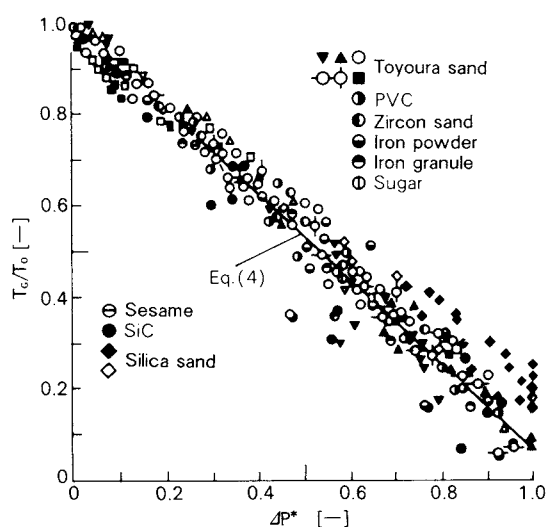


Fig. 5 Relationship between torque ratio T_G/T_0 and pressure loss ratio ΔP^*

- 9) Koga J., K. Yamaguchi and I. Inoue: *Journal of the Society of Powder Technology, Japan*, **15**, 595-603 (1978).
- 10) Koga J., K. Yamaguchi and I. Inoue: *Kagaku Kogaku Ronbunshu*, **5**, 26-33 (1979).
- 11) Koga J., K. Yamaguchi and I. Inoue: *Powder Technology*, **26**, 127-130 (1980).
- 12) Koga J., I. Inoue, K. Yamaguchi and Y. Kuga: *Kagaku Kogaku Ronbunshu*, **6**, 217-219 (1980).
- 13) Miyanami K., M. Satoh and T. Yano: *Journal of Powder & Bulk Solids Technology*, **2**, 47-52 (1978).
- 14) Sano Y., K. Inotsume and I. Akiba: *Funsai (The Micromeritics)*, No.20, 49-55 (1975).
- 15) Sano Y. and Y. Motoyama: *Funsai (The Micromeritics)*, No. 21, 4-9 (1976).
- 16) Satoh M. and T. Yano: *Funsai (The Micromeritics)*, No.20, 91-98 (1975).
- 17) Satoh M., Y. Abe, K. Ishii and T. Yano: *Journal of the Society of Powder Technology, Japan*, **14**, 441-447 (1977).
- 18) Satoh M., Y. Abe, K. Ishii, K. Yoshikawa and T. Yano: *Journal of the Society of Powder Technology, Japan*, **14**, 448-453 (1977).
- 19) Satoh M., Y. Abe, K. Ishii and T. Yano: *Journal of the Society of Powder Technology, Japan*, **14**, 454-460 (1977).
- 20) Satoh M., K. Yoshikawa, N. Okuyama and T. Yano: *Journal of the Society of Powder Technology, Japan*, **14**, 669-680 (1977).
- 21) Satoh M., K. Miyanami and T. Yano: *Journal of the Society of Powder Technology, Japan*, **16**, 3-7 (1979).
- 22) Satoh M., Y. Hirata, Y. Kitada, K. Miyanami and T. Yano: *Journal of the Society of Powder Technology, Japan*, **18**, 881-817 (1981).
- 23) Satoh M., Y. Hirata, M. Ashida, K. Miyanami and T. Yano: *Journal of the Society of Powder Technology, Japan*, **19**, 3-9 (1982).
- 24) Satoh M.: *Funsai (The Micromeritics)*, No.26, 6-11 (1982).
- 25) Sugimoto M. and K. Yamamoto: *Journal of the Society of Materials Science, Japan*, **25**, 684-689 (1976).
- 26) Sugimoto M. and K. Yamamoto: *Journal of the Society of Materials Science, Japan*, **26**, 844-849 (1977).
- 27) Sugimoto M. and K. Yamamoto: *Kagaku Kogaku Ronbunshu*, **5**, 335-340 (1979).
- 28) Sugimoto M., T. Matsui and K. Yamamoto: *Kagaku Kogaku Ronbunshu*, **7**, 512-516 (1981).
- 29) Takeuchi H. and N. Sakurai: *Journal of the Research Association of Powder Technology, Japan*, **14**, 503-507 (1977).
- 30) Takeuchi H. and M. Yamamoto: *Journal of the Research Association of Powder Technology, Japan*, **14**, 572-575 (1977).
- 31) Terashita K., T. Yano, K. Mori and M. Hashimoto: *Funsai (The Micromeritics)* **24**, 4-11 (1979).
- 32) Terashita K., K. Miyanami, T. Konishi and J. Yoshida: *Journal of the Society of Materials Science, Japan*, **30**, 873-877 (1981).
- 33) Terashita K., H. Ohmura and K. Miyanami: *Journal of the Society of Materials Science, Japan*, **31**, 883-887 (1982).
- 34) Yamaguchi K., J. Koga and I. Inoue: *Kagaku Kogaku Ronbunshu*, **5**, 532-534 (1979).
- 35) Yamamoto K. and M. Sugimoto: *Journal of the Society of Materials Science, Japan*, **29**, 892-897 (1980).
- 36) Yano T., M. Satoh and K. Terashita: *Powder Technology*, **20**, 9-14 (1978).

Present Status of Bulk-Solids Transportation in Japan

Takeshi Kano*

Department of Chemical Engineering,
Shizuoka University

1. Introduction

Japan depends on foreign countries for many kinds of industrial raw materials and cereals, so that there are many apparatus used for bulk-solids handling which includes the landing of the material on our islands. Besides, Japan depends on the import from foreign countries for oil which is the energy source for her industries. It is very important for the Japanese industries to save energy by improving the equipment efficiency. Bulk-solids transport systems are no exception. In this review the present status of the domestic freight in Japan are introduced generally, and then reference will be made to bulk-solids transportation and pneumatic conveyor which have been mainly concerned by the author.

2. Status of domestic freight and bulk-solids transportation

The items of the freight transportation in Japan are shown in Fig. 1. Freight cars trans-

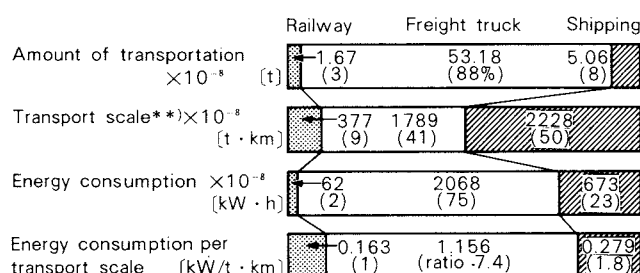


Fig. 1 Status of domestic freights in Japan (JNR report, 1980)

* 3-5-1 Johoku, Hamamatsu, Shizuoka, 432
TEL. 0534 (71) 1171

Received March 7, 1983

** Transport scale: This term is defined as a product of the weight (ton) and the distance (km) of the transport in this report.

port 88% of the whole domestic freights. Transportation by the car needs energy 7.4 times as much per transport scale** as that by the freight train does and the freight cars spend 3/4 of the whole energy.

In Japan, the weight of the whole domestic freights amounts to about 6 billion metric tons per year, in which the amount of dealing bulk-solids reaches to 620 million tons as shown in Table 1, which is about 10% of the whole freight weight.

The items of bulk-solids handling shown in Table 1 state that a Japanese has handled 5.38 tons of particulate materials in a year. Fig. 2 shows the proportion of the means of transport for typical bulk-solids in terms of the transport scale.

Table 1 Amount of bulk-solids handling in a year in Japan (1980)

Material		Amount × 10 ⁻³ tons	
Food and Feed	Rice	14,920	49,872
	Wheat	6,142	
	Soybean	4,574	
	Corn	12,833	
	Sugar	3,025	
	Salt	8,378	
Fertilizer		14,573	
Ore	Iron ore	134,200	145,453
	Bauxite	5,708	
	others	5,545	
Rock	Limestone	184,780	296,773
	Ballast, Sand	21,187	
	Coal	90,806	
Ceramic	Cement	87,960	98,116
	Dolomite, Clay	6,937	
	Alumina	1,863	
	others	1,356	
Wood chip		9,302	
Petrochemicals		9,505	
Sum		623,565	

$$\frac{623,565 \times 10^3 \text{ tons/year}}{115,870 \times 10^3 \text{ persons}} = 5.38 \text{ t/p} \cdot \text{y}$$

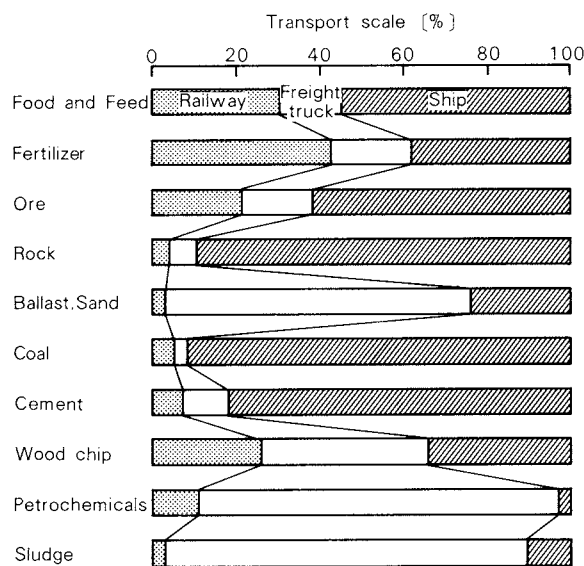


Fig. 2 Proportion of the means of transport in terms of transport scale ratio for typical bulk-solids (1980)

3. Types and features of bulk-solids transportation system

There are many kinds of equipment for bulk-solids transportation, each of which has its own optimal capacity and distance of transportation as shown in Table 2. The factors to be considered for the design of the transportation system are as follows; (1) the best selection of the equipment meeting the required transport conditions, (2) making up for equipment demerits to prevent some troubles, (3) consideration for circumstances, (4) rationalization of the investment cost in a plant and equipment, and (5) saving the running cost, especially saving energy. The energy consumption per transport scale depends upon the means of transportation and also the amount of the materials for each transportation as shown in Fig. 3. It is evident that the shipping suits a large scale transportation and it is rational making use of the railway for the middle scale transportation.

Concerning bulk-solids conveyance in factories, the energy consumption ratios of several conveyor types are shown in Fig. 4. These are the result of the investigation of about 250 Japanese companies conducted by the Association of Powder Process Industry & Engineering in Japan. The energy consumption ratio decreases as the transport scale increases regardless of type of the conveyor. The pneumatic conveyor system requires the largest energy

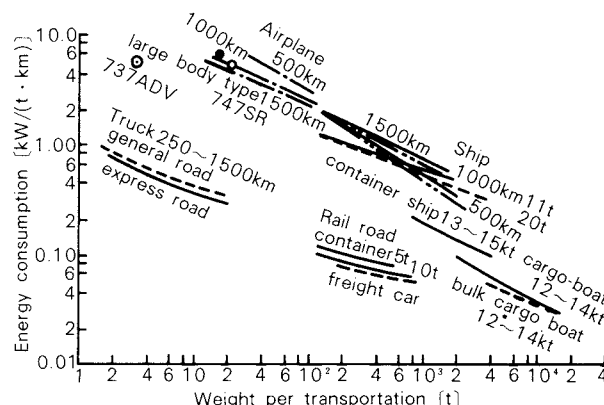


Fig. 3 The relations between the weight per transportation and the energy consumption. (Nippon no shigenzusesetsu; the Science and Technology Agency, 1982)

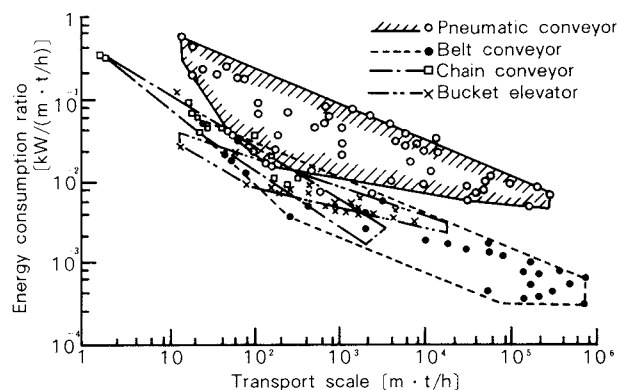


Fig. 4 The relations between the transport scale and the energy consumption ratio of several conveyor types. (1977)

consumption ratio which is from 10 to 15 times as large as the belt conveyor. The belt conveyor is used for coal, iron ore, limestone, etc., and it is able to transport the material for the distance of 20 km with the capacity of 5,000 t/h.

For the belt conveyor, chain conveyor and bucket conveyor, the technique for the system design is nearly completed, and then the conveyor makers standardize their equipment for easy selection by their users. On the other hand, they design the different pneumatic conveyor system according to each specification of their users depending on their empirical data, though these are described with mathematical forms and calculated by the computer.

4. Pneumatic conveyors


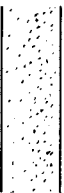



Pneumatic conveying systems are divided generally into two types; vacuum system and pressure system. On the other hand, according

Table 2 Types and features of typical transportation systems

Styles	Conveyor types	Range of application				Choice of route				Trouble			Maintenance	Power requirements†
		Distance [m]	Capacity [t/h]	Max. size lump [mm]	Max. temp. [°C]	Horizontal	Vertical	Bend	Branch	Residue	Dispersion	Abrasion		
Continuous conveying	Trough type	0.5~10 2~15	2~300 0.4~200	30 30	300 *	○	△	×	×	B	C	C	overall	M
	Belt-conveyor	5~2,000	5~6,000	—	*	○	×	×	△	C	A	A	roller, bearing	S
	Chain-conveyor	2~200	1~300	50	300	○	○	○	×	A	C	B	chain, bearing	M
	Bucket-elevator	10~60	1~600	100	80	×	○	×	×	A	C	B	chain, bearing	S
Batch conveying	Pneumatic-conveyor	20~1,500	0.5~600	30	600	○	○	○	○	C	C	C	bend, valve	L
	Fluidizing-slide	1~200	5~300	1	80	☆	☆	○	○	C	C	B	damper	S
	Hydraulic-conveyor	50~10,000	10~200	30	80	○	○	○	○	C	C	C	bend, valve	L
	Railroad car	—	††10~30	—	80	○	×	○	×	C	④	④	④	S
	Tank lorry	—	5~15	30	80	○	×	○	×	C	C	C	packing, valve	S
	Container	—	1~3	50	80	○	○	○	×	B	A	A	inlet, outlet	S
	Ship	—	~150,000	—	80	○	×	○	×	B	B	B	—	S

* ; The equipment using rubber is able to be applied up to 80°C, and the one using steel, up to 300°C ○, △, × ; These mean the applicability in order.
 ④ ; Troubles and maintenance parts are quite different depending on construction A, B, C ; These show the trouble happening frequency in order.
 † ; Power requirements are compared per unit conveying weight. †† ; Capacities are shown as per one unit. ☆ ; downslope 4~10 deg.
 L ; large, M ; middle, S ; small

Table 3 Flow patterns of pneumatic conveyor

Description		Flow pattern	Power source	Pressure [N/m ²]	Air velocity [m/s]	Material/Air
Suction or Low pressure	Suspension flow		Fan Roots blower	0.5 ~ 1.4 × 10 ⁵	15 ~ 30	0.1 ~ 5
						
High pressure	Dense-phase slugging flow		Roots blower Screw-compressor Reciprocal-compressor	0.5 ~ 1.5 1.4 ~ 4 2.5 ~ 7	15 ~ 30	5 ~ 15 7 ~ 50 40 ~ 150
						
						

to the flow patterns in the ducts they are classified into two categories; (1) suspension flow type that is a turbulent flow of sufficiently high velocity to keep the material distributed in the duct at low material concentration. (In this case the influence of gravity is scarcely noticeable.), (2) dense-phase slugging flow type that is a slugging flow at sufficiently high pressure to transfer the material dune or the intermittent material plugs at a high concentration. These flow patterns with typical conditions are given in **Table 3**.

Power requirements are calculated by the following equation for the pneumatic conveyor system.

$$E_L = \frac{Q \cdot P}{60 \cdot 1000 \cdot \eta} \quad (\text{kW})$$

Q is the air volume rate (m^3/min), P is the pressure loss in all pneumatic line (N/m^2), η is the efficiency of the blower and some other power sources which is usually about 0.6 ~ 0.75.***

In usual design of pneumatic conveyors, first of all, the pressure losses are estimated at each part of the conveying line such as a feeder, pipes and a collector. These are usually calculated by a computer which has some fundamental functions of fluid dynamics and empirical data in its memories. The empirically designed values based merely on the pressure loss, however, do not always minimize the total required energy and the cost of equipment. There is a risk of designing a too wasteful system placing excessive emphasis on safety transportation. The design of an economical pneumatic conveyor requires optimization of the whole system taking account of the total cost as well as exacter estimation of the pressure loss.

5. Suspension flow type - vacuum unloading system

The schematic diagram of a typical vacuum unloading system is shown in **Fig. 5**. This system is used to unload the imported grains, alumina, etc., and more than 200 systems are

*** P is a total pressure loss in the pneumatic line and Q is determined at the atmospheric pressure in the pressure systems. But in the vacuum systems, Q is determined at the pressure subtracting the pressure loss from the atmospheric pressure.

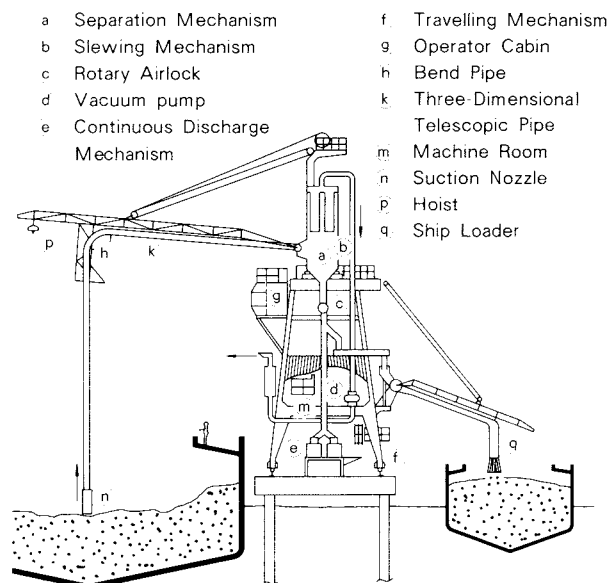


Fig. 5 Typical ship unloading system with a telescopic pipe

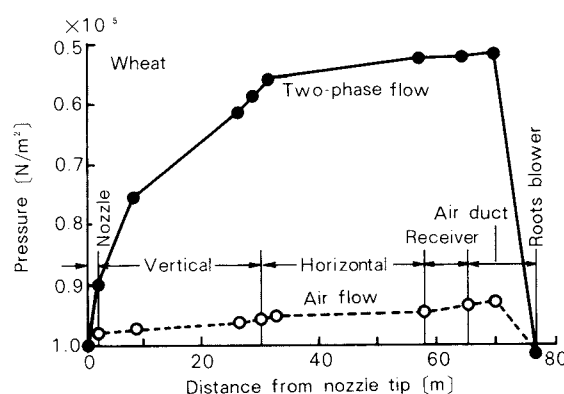


Fig. 6 Pressure curve of a ship unloading system

operated in Japan. The Roots blower of which suction pressure is about $0.5 \times 10^5 \text{ N/m}^2$ is available for these unloader. The typical pressure changes along the conveying line are shown in **Fig. 6**.

To design the transportation system requiring less energy, the pipe diameter should be increased step by step in the down-stream direction as the pressure loss increases, namely as the air expands, so that the pressure changes would become smoother as shown in **Fig. 6**. For instance, the air density is 0.66 kg/m^3 at the suction pressure of $0.5 \times 10^5 \text{ N/m}^2$. When the diameter of the pipe is uniform through the entire conveying line, the air velocity at the end of conveying line is twice of the starting point, the pressure loss increases 2.05 times supposing it is proportional to the dynamic

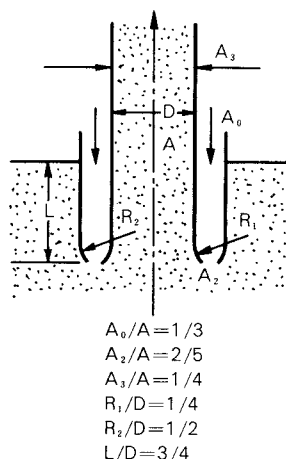


Fig. 7 Optimal dimensions of the suction nozzle (the cross sectional area is indicated with character A.)

pressure, and the abrasion of pipes and valves increases 8 times as much as the initial one supposing it is proportional to the cubed air velocity. In this way these factors accelerate wasting energy, wear and damages of the equipment and breakage of the transported materials. In the vacuum unloading systems, the pressure loss at the suction nozzle should not be ignored. The conventional suction nozzle has spent 25% of the total energy consumed by the system with the pressure loss of $0.125 \times 10^5 \text{ N/m}^2$. The improved nozzle based on the analytical and experimental research in aerodynamics shown in Fig. 7 reduces the pressure loss to $0.085 \times 10^5 \text{ N/m}^2$ corresponding to about 2/3 of the conventional value. By means of the suitable selection of the diameter of the conveying pipe according to the pressure loss and the improved suction nozzle, the material/air mass ratio increased from 16 to 25 ~ 26.

The vacuum unloading systems with a capacity of 200 ~ 300 t/h per nozzle and a material ratio of 25 ~ 26 work for the wheat conveying in Japan.

6. Dense-phase flow type - blow tank system

A typical dual blow tank system is shown in Fig. 8. In this system, a reciprocal or screw-type compressor with the maximum exhaust pressure of $5 \sim 8 \times 10^5 \text{ N/m}^2$ is usually used as the power source. Charging of the materials to the tank and discharging from it are repeated automatically, and the materials are conveyed alternately by the two tanks in this system. Several tank sizes are standardized by manu-

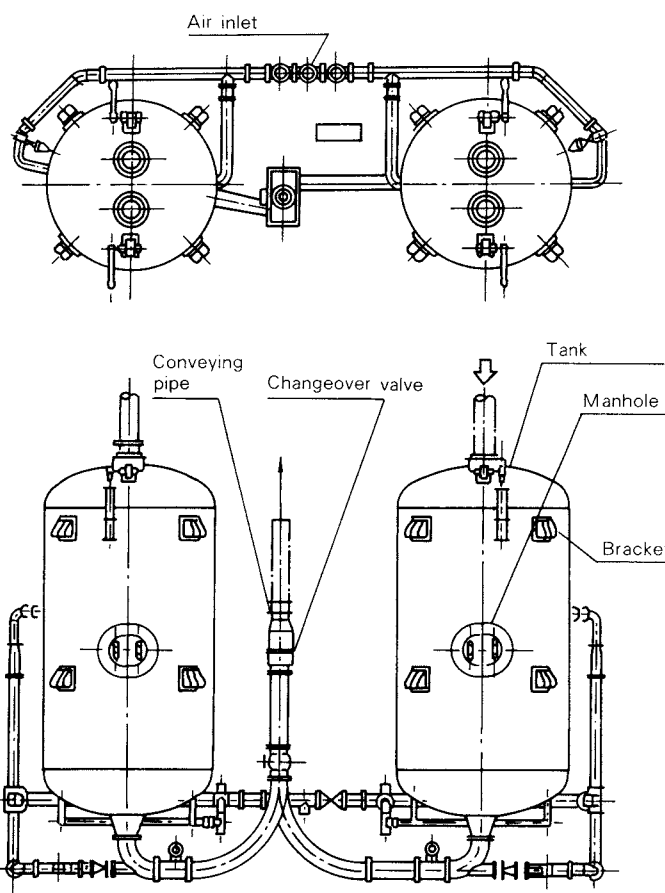


Fig. 8 Dual type blow tank system

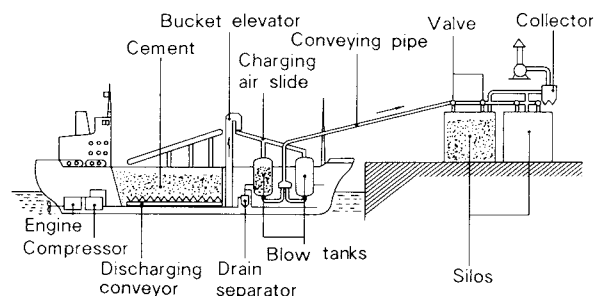


Fig. 9 The schematic diagram of a dual blow tank system on a bulk cargo ship for conveying cement

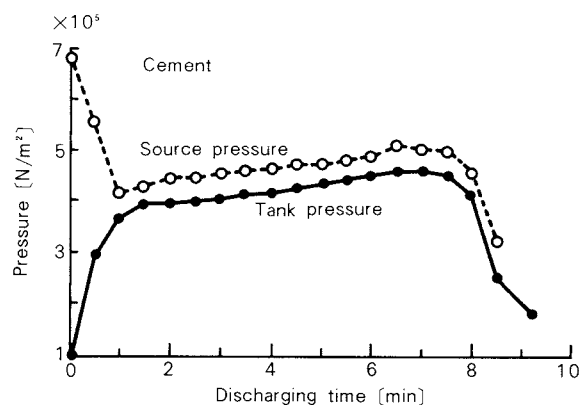
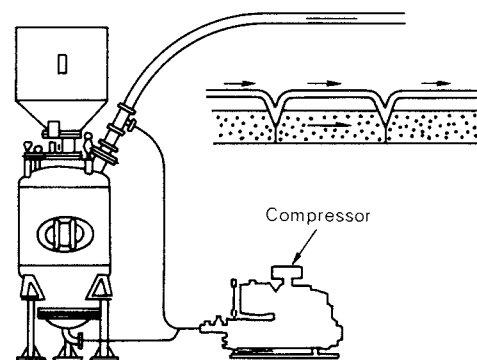


Fig. 10 The pressure curve in a blow tank

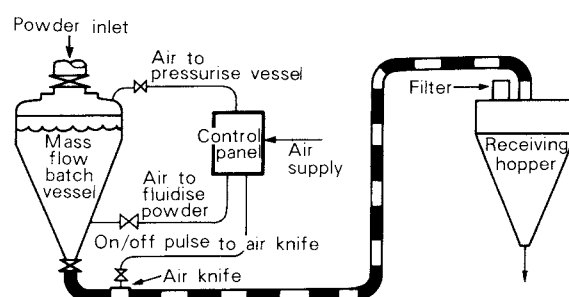
facturers having diameters up to 5.3m and volumes up to 80 m³ for the larger capacity and longer distance conveying.

The schematic flow of the cement landed from the tanks on a bulk cargo ship to the silos is illustrated in **Fig. 9**. Typical pressure curves of the blow tank to convey cement for a distance of 600 m are shown in **Fig. 10**. In this system, a conveying capacity of 550 t/h and a material ratio of 60 are realized taking the reduction of energy loss into consideration for its design. In the middle scale unloading system for cement, the material ratio is about 136 in a pilot test system with a length of 120 m and about 100 in actual unloading systems.

In the plug flow conveying system, which has been improved as an application of the blow tank system, the material plugs having a length of a few meters shift continuously in pipes. Several different systems shown in **Figs. 11-(a), (b), (c)** belong to this plug flow type. **Fig. 11-(a)** indicates that the diaphragm plate at the bottom of the blow tank feeds the materials intermittently to the conveying pipe in which plugs are conveyed at a relatively slow speed. In **Fig. 11-(b)**, the pressurized air is injected through the nozzle inserted in the pipe with a constant interval to prevent wasting too high pressurized air, namely the energy requirements. The system shown in **Fig. 11-(c)** functions by the alternate introduction of a pressurized air on the top of materials contained in the tank and in the pipe inlet at the bottom of the tank. In another case, the transportation of materials is performed with the help of the



(b) (Bühler Co. - Sinto Kogyo Co.)



(c) (Sturtevant Co. - Nakashima Manu. Co.)

Fig. 11 Schematic diagrams of plug flow systems

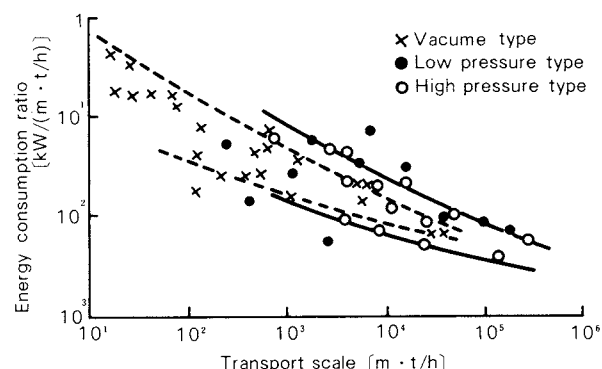


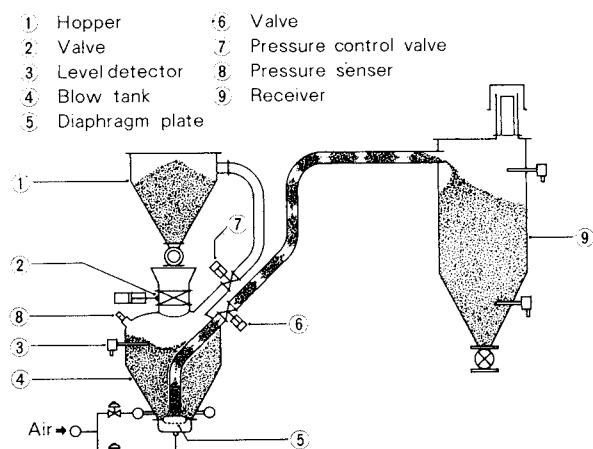
Fig. 12 The relations between the transport scale and the energy consumption ratio of the pneumatic conveyors (1977)

automatic injection of the pressurized air controlled with pressure sensors to detect the abnormally high partial static pressure in the conveying pipe because of the choking.

From results shown in **Fig. 12**, which is reported by the Association of Powder Process Industry & Engineering in Japan, the larger a conveying scale is, the less the energy consumption ratio is, but there is no considerable difference concerning the relationship among the pneumatic conveying types.

7. Problems in conveyors

The following subjects require further in-



(a) (Fuji Paudal Co.)

vestigation regarding the transportation by the conveyors:

- (1) Larger capacity transportation with saved energy.
- (2) Longer distance transportation with saved energy.
- (3) Transportation of three phase mixture.
- (4) Transportation combined with drying, humidification, cooling, mixing, reaction, etc.

The subjects of (1) and (2) are counter-measures to the expansion of the scale of industrial transportation. The 3rd subject where the mixed materials of solid, liquid and gas are conveyed in pipe line, is investigated in order to apply to the disposal of waste matters and the productive industry. The 4th subject has been investigated in chemical and foods industries. The progress of the theoretical investigations, applications and establishment of technique are expected.

8. Conclusions

In a number of process industries, the materials having the form of bulk-solids are handled frequently in the processes from the raw materials to the final products. From the viewpoint of rationalization of the process and of energy saving, it is important for projecting a transport system to select the best conveying type meeting the conditions and to select the best equipment with excellent efficiency and high reliability. Besides, it is necessary to conduct a harmonious management of the economics and the politics which have anything to do with materials imported from many foreign countries and the final products to be exported. In addition, it is essential to compile the techniques which are supported by science and engineering. It could not be realized without co-operation and appreciation of the whole world.

Informational Articles

Activity of *The Party of Powder Technology (Japan)*

The Party of Powder Technology (Japan), which publishes this journal 'KONA', has been holding *The Symposium on Powder Technology* at Osaka or Kyoto once a year since 1968. In each symposium, several lecturers have presented various topics concerning powder technology from fundamental science to prac-

tical application, and active discussions were conducted among about a hundred attendance mainly consisting of users having strong interest in powder technology. The following list of the symposium previously held will help readers to recognize the drift and the aim of the party.

(*The Symposium on Powder Technology previously held*)

1	Size reduction, classification, dust collection and mixing	July 25th, 1968
2	Size reduction and dust collection	May 20th, 1969
3	Bulk handling (powder characteristics, storage and feeding)	Dec. 12th, 1969
4	Size reduction and anti-pollution, drying and mixing	Aug. 21th, 1970
5	Countermeasure for fine dust in a factory	Aug. 19th, 1971
6	International conversation on powder technology (Speaker: H. Rumpf, A. W. Nienow and C. E. Lapple)	Oct. 16th, 1972
7	Measurement of powder characteristics and its automation	Aug. 21th, 1973
8	Unit operation and characteristics of powdery materials	Aug. 21th, 1974
9	Environmental problems	Aug. 8th, 1975
10	Approach to continuous processes	Aug. 20th, 1976
11	Estimation of powder characteristics applicable to technology and its practical operation	Aug. 5th, 1977
12	Symposium on solid – liquid system	Aug. 24th, 1978
13	Estimation of mechanical characteristics of powdery materials and its application to practical processes (I)	Aug. 8th, 1979
14	As above (II)	Aug. 6th, 1980
15	Advanced powder technology in the world (Speaker: S. Goren, H. Shubert and L. T. Fan)	Sept. 6th, 1981

The latest symposium was given at Hosokawa Micron Co. Ltd. in Osaka on August 20th, 1982 with the theme '*New Powder technology and characteristics*', which recently received con-

siderable attention in this country. After the following three lectures, there was an animated discussion especially over the process of new materials or the change in powder characteristics.

Lecturer	Lecture topic
Masafumi Arakawa (Institute for Chemical Research, Kyoto University)	New material and its powder characteristics
Sumio Sakka (Mie University)	New ceramics
Saburo Imoto (Kuraray Co., Ltd.)	Present state of polymer composite

The next symposium will be held with the theme 'Characteristics and application of ultra-fine particles' at Tokyo on September 8th, 1983.

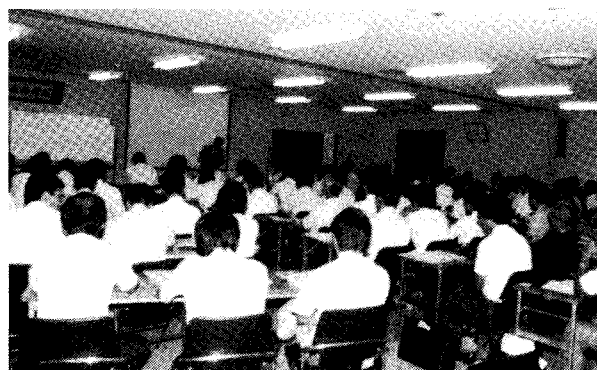


Photo:
The Symposium on Powder Technology in 1982.

Professional or business association and publication concerning powder technology in Japan

A great many industries involve powder and bulk-solids process in themselves. Most of them founded their own professional or business association to study their own field or to promote cooperation of their business world.

There are, on the other hand, two major associations concerning powder technology independent of a specified industry or an academic field. One is 'The Society of Powder Technology, Japan' which is an academic association founded in 1956. The other is 'The Association of Powder Process Industry and Engineering', which was founded 1971 with the support of manufacturers and closely related users. Both of them, which often act in co-operation, have been holding regular meetings,

seminars, training courses to promote enlightenment of powder technology. The latest activity was the summer seminar sponsored by the *Society of Powder Technology, Japan* which was held at Shizuoka on July 18th through 20th in 1983, where 20 papers on particle designs for powder treatment were presented.

With respect to regular publication carrying articles related with powder technology, there are many journals in each field in Japan. The following list indicates principal ones, the first three of which have been making a speciality of powder technology. The formers of them have been published by the above-mentioned associations, while the latter by Hosokawa Micromeritics Laboratory since 1957.

• Funtai Kōgakukaishi [Journal of the Society of Powder Technology, Japan] (in Japanese)	The Society of Powder Technology, Japan
• Funtai To Kōgyō [Solids Handling & Processing Industry] (in Japanese)	The Association of Powder Industry and Engineering, Japan
• Funsai [The Micromeritics] (in Japanese)	Hosokawa Micromeritics Laboratory
• Kagaku Kōgaku [Publication of the Society of Chemical Engineering, Japan] (in Japanese)	} The Society of Chemical Engineers, Japan
• Kagaku Kōgaku Ronbun-shū (in Japanese)	
• The Journal of Chemical Engineering of Japan (in English)	
• Zairyō [Journal of the Society of Materials Science, Japan] (in Japanese)	The Society of Materials Science, Japan
• Nippon Kikai Kōgaku Ronbun-shū [Journal of the Japan Society of Mechanical Engineering] (in Japanese)	The Japan Society of Mechanical Engineering
• Funtai Oyobi Funmatsuyakin [Journal of the Japan Society of Powder and Powder Metallurgy] (in Japanese)	The Japan Society of Powder and Powder Metallurgy

The following titles of research papers are selected from the above journals published in the latter half of 1982. Although they do not

cover the whole, readers can probably know the present trend of the study on powder technology in Japan.

Journal of the Society of Powder Technology, Japan Vol.19 (1982)

Title	Author(s)	Page
• Power Requirement of a Moving Bed with Mechanical Agitator	M. Satoh, Y. Hirata, M. Ahida, K. Miyanami and T. Yano	3–9
• A Study of Electrostatic Precipitation. Part III (Performance of Electrostatic Precipitators Using an Electro-Charged Water Column for Discharge Electrodes)	I. Aoki, M. Suzuki and T. Matsuyama	10–17
• Impact Test of Single Particle using a Drop Weight Type Apparatus, PART I (Relationship between Impact Energy and Impact Load Produced)	Y. Kuwahara, F. Saitoh and S. Yashima	157–164
• Fluidization of Large Char and Coal Particles	T. Hirama	164–170
• Impact Test of Single Particle using a Drop Weight Type Apparatus, PART II (Fracture Probability and Fracture Load of Particle)	Y. Kuwahara, F. Saitoh and S. Yashima	211–218
• Pressure Drop in a Horizontal Pneumatic Conveyance Transporting Solid Particles Consisting of Different Size	S. Sakamoto and Y. Morikawa	219–225
• The Effect of Filling Methods on Wall Pressure Distribution in a Bin	R. Moriyama, N. Hayano and T. Jotaki	225–231
• Hopper Slopes in Cargo Hold of Self-unloading Ships	H. Tsunakawa	273–276
• Characteristics of a Cascade Impactor Under Specific Conditions	H. Yoshida, H. Masuda and K. Iinoya	277–283
• Performance and Application to a High Temperature Test of a Direct Shear Tester with Parallel Plates	M. Hirota, T. Oshima and M. Naitoh	337–342
• The Operation of a Continuous Thickener and Two-paraeel Settling Tanks Using a Batch Settling Curve	E. Obata and H. Wanatabe	343–350
• Weakness of Pellet Strength in Pelletizing Municipal Inorganic Residues	K. Uchida, T. Ohtake, S. Tomizawa, K. Kamiya, F. Ikazaki and M. Kawamura	350–356
• Observations of Airborne Dust Particles by a Scanning Electron Microscope	H. Yamamoto and A. Suganuma	357–363

Funsai (The Micromeritics) No. 27 (1983)

Title	Author (s)	Page
• Effect of Grinding an X-ray Line Boarding of Silicon Nitride Powder	Y. Kuwahara and K. Suzuki	4–10
• The Effect of Temperature upon the Void Fraction and the Angle of Repose of Powder	E. Fujiwara, M. Suzuki M. Hirota and T. Oshima	11–15
• A New Method of Partial Classification Efficiency Measurement	A. Suganuma	16–20

Kagaku Kogaku Ronbun-shū Vol.8(1982)

Title	Author (s)	Page
• Behavior of a 1m Square Gas-Fluidized Bed – Jet and bubble characteristics	GOLFERS (Group of Larger Scale Fluidization Engineering Reseachers)	464–469
• Classification of Particle Shape by Principal Component Analysis Method	S. Endoh, Y. Kuga, J. Koga and K. Yamaguchi	476–480
• Dislodgement of Deposited Dust Layer on Fabric Filter by Normal Stress – Dislodgement by impaction acceleration	J. Tsubaki, M. Naito, H. Tagami, F. Kousaka and G. Jimbo	481–486
• Melting Behavior of Polyvinyl Chloride Resins	T. Nakayama and I. Yamada	507–509
• Prediction of Terminal Settling Velocities for Spherical Particles	Z. Tanaka, M. Fukushima and T. Takahashi	528–529
• An Experimental Study of Simultaneous Granulation and Separation in a Horizontal Rotating Conical Vessel	M. Sugimoto and T. Kawakami	530–532
• Collection Efficiency of a Polytetrafluoroethylene Membrane Filter for Aerosol Particles	T. Takahashi and A. Kanagawa	535–538
• Flow Control of Solid Particles Using a Throat and Gas Addition	S. Yoshioka, M. Hirato, Y. Satomi and H. Ozaki	618–623
• Collection and Re-entrainment of Mist Particles from a Fibrous Filter	C. Kanaoka, H. Emi, N. Fujii and M. Yamaguchi	624–628
• Effect of Filter Charge on Aerosol Filtration by Nuclepore Filters	T. Takahashi and A. Kanagawa	629–634
• Method for Prediction of Drying Characteristics of Coarse Granular Bed by Using Relationship between Capillary Suction Pressure and Moisture Content	M. Kuramae	671–676
• Single Fracture of Irregular Shaped Particle under Impact Loading	S. Yashima, F. Saito and Y. Masuko	710–716
• Classification Performance of Two-Stage Virtual Impactor	H. Masuda and T. Motooka	717–721
• Particle Size Distribution of Product of a Screen Mill	J. Koga, Y. Kuga and K. Yamaguchi	750–752
• Classification Efficiency of a New Classifier with Cut Size Smaller than 10 μ m	H. Yamamoto and A. Suganuma	753–756

Journal of Chemical Engineering of Japan Vol. 15 (1982)

Title	Author (s)	Page
• Performance of a Droplet Separator with Multistage Rows of Flat Blades	K. Ushiki, E. Nishizawa, T. Banikona and K. Iinoya	292–298
• Continuous Separation of Particles According to Shape on an Inclined Vibrating Plate	E. Abe and H. Hirose	323–326
• Effect of Water on Bending Strength of Glass	Y. Kanda, M. Hasegawa and T. Honma	402–404

Title	Author (s)	Page
• Fluidity and Other Characteristics of Powders in a Vibrating Field	M. Arakawa	878-882
• Effects of Internal Friction Coefficient on Performance of Various Solid Mixers	K. Terashita, H. Ohmura and K. Miyanami	883-887
• Simultaneous Operation of Granulation and Separation in a Horizontal Rotating Conical Vessel (The Effect of the Feed Ratio of Binder to Powder on the Sizes of Products)	M. Sugimoto, T. Kawakami and S. Nakamura	888-892
• Triaxial Compression and Extension Properties of Polystyrene Powder Compact	R. Hara and K. Umeya	929-932

Exhibitions displaying powder and bulk-solids apparatuses in Japan

A wide variety of powder and bulk handling apparatuses have been designed and manufactured to meet extensive user's needs. The newly developed facilities, are on display in two big shows with the related conferences in Japan every year.

One of them is 'Chemical Plant Show'; the other 'Powdertec Japan'. They are held alternately every year, inviting about 60,000 visitors from almost fields of industries in this country. The former displays various kinds of apparatuses for chemical process industries including powder treatment, while the latter is the only exhibition showing powder and bulk-solids equipment. Today, many industries pay more attention to powder and bulk-solids treatment than before, because they recently recognized its significance in their own processes.

'Powdertec Japan' is seven years old and it has grown in size. The latest one was 'Powdertec Japan '82' held at Harumi in Tokyo in 1982 in the following. In this exhibition, more than 400 apparatuses from 125 exhibitors were displayed, such as pulverizer (42), air classifier (10), sieve or separator (24), feeder (24), transport apparatus (36), mixer (37), granulator (27), dust collector (16), dryer (24), process unit (29), system parts (33), controller/measuring device (107).

Term : September 27 through October 1 in 1982

Location : Tokyo international trading center (Harumi, Tokyo)

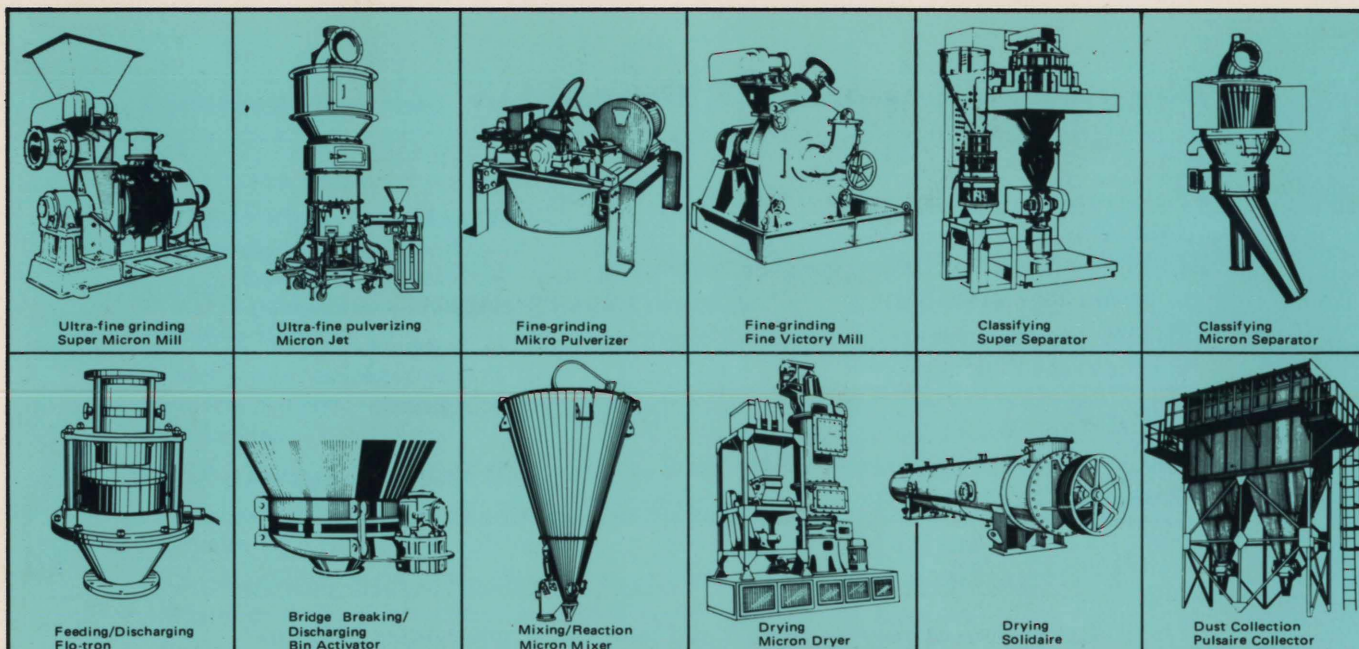
Displaying area : 8513 m²

Number of exhibitors : 125 companies

Number of attendance : 63647 visitors



Photos: Powdertec Japan '82



CONTRIBUTING TO THE RAPID PROGRESS OF INDUSTRIES

**From
the traditions
of
yesterday.....
quality
for
tomorrow**

Hosokawa has specialized in powder processing technology for over 65 years. Today, Hosokawa makes a complete line of advanced equipment for fine-grinding, classifying, drying, mixing, dust collection, measurement and so on. Yet, Hosokawa's most distinguished feature is

its capability of the system engineering that will satisfy a wide variety of industries needs. Whenever you have a problem, planning, or project relating to powders, first consult with Hosokawa.

HOSOKAWA MICRON CORPORATION

Hosokawa Products are available from:

In Europe (Continent)
Hosokawa-Nauta Europa B.V.
2003 RT Haarlem, Holland,
P.O. Box 773, Nijverheidsweg 25
Telephone: (023) 31 9073
Telex: 41167

In the U.S.A.
Vibra Screw Incorporated
755 Union Boulevard,
Totowa, N.J. 07511
Telephone: (201) 256-7410
Telex: 130-448

In the U.K.
Hosokawa-Nauta (UK) Ltd.
Hughenden Road, High Wycombe
Buckinghamshire, England.
Telephone: (0494) 443866
Telex: 837208

Other Areas
Hosokawa International Inc.
No. 10, 2-chome, Minami-Kyutaro
Machi, Higashi-ku, Osaka 541, Japan
Telephone: (06) 261-5141
Telex: J63837